Copyright Warning & Restrictions

The copyright law of the United States (Title 17, United States Code) governs the making of photocopies or other reproductions of copyrighted material.

Under certain conditions specified in the law, libraries and archives are authorized to furnish a photocopy or other reproduction. One of these specified conditions is that the photocopy or reproduction is not to be "used for any purpose other than private study, scholarship, or research." If a, user makes a request for, or later uses, a photocopy or reproduction for purposes in excess of "fair use" that user may be liable for copyright infringement,

This institution reserves the right to refuse to accept a copying order if, in its judgment, fulfillment of the order would involve violation of copyright law.

Please Note: The author retains the copyright while the New Jersey Institute of Technology reserves the right to distribute this thesis or dissertation

Printing note: If you do not wish to print this page, then select "Pages from: first page # to: last page #" on the print dialog screen

ABSTRACT

Fracture of Cementitious Composites

by
Sira Tindukasiri

Studies in fracture mechanics of concrete use a testing setup which tends to include unacceptably large errors in deflection measurements. Recent work reported by Kim [3] has proposed a new testing setup to eliminate these errors and consequently produce better determinations of fracture parameters.

The error which occurs most frequently is in the measurement of the load-line deflection. Until recently, the way this measurement has been made, using a dial gauge or LVDT (Linear Variable Differential Transformer) to measure the deformation between the center of the specimen and the frame, includes the crushing of the concrete surface at the supports and other extraneous deformations. The crushing overstates the deflection measurement which leads to an overestimate of the energy absorbed by the specimen and consequently, the predicted fracture toughness of concrete. Rather than the load-line deflection the CMOD (Crack Mouth Opening Displacement) is another measurement which can be used to determine the fracture energy the tested concrete specimen absorbed.

Since there is a bilinear relationship between CMOD and load-line deflection, it can be shown that the load vs. CMOD relationship yields the same fracture toughness value as that determined by the actual load-line deflection. Previous research studied only plain concrete with different specimen sizes and notch depths. To extend the idea, the same experiment has been done for fiber reinforced concrete beams.

The results show another kind of error which may be due to large beam deformations found when testing fiber reinforced concrete beams. This error is very small in plain concrete but more pronounced in fiber reinforced concrete. To correct this error, a new testing setup is recommended.

Test results based on CMOD measurements indicate that the bilinear relationship between the load vs. CMOD exists for cementitious composites. For fiber reinforced concrete, the initial slope (S1) is 3.6 with the second slope (S2) equals 0.986. These values are larger than those reported for plain concrete. Experiments show that fiber reinforced concrete beams can resist more load with increased fiber length and volume fraction. Different types of fiber did not give significantly different results, except for hooked end fibers which gave higher strength. Determination of fracture parameters based on CMOD seems to eliminate errors due to crushing at contact surface between concrete and supports which results in extraneous deformations. Fracture energy computed based on CMOD should be smaller than those calculated based on the erroneous deflection

measured with reference to the frame since extraneous deformations are eliminated. Furthermore, research conducted using measurements of deflection with reference to machine base should be reconsidered. It is recommended that this testing procedure be used as the standard for toughness testing of cementitious composites.

FRACTURE OF CEMENTITIOUS COMPOSITES

by

Sira Tindukasiri

A Thesis
Submitted to the Faculty of
New Jersey Institute of Technology
in Partial Fulfillment of the Requirements for the Degree of
Master of Science in Civil Engineering

Department of Civil and Environmental Engineering

May 1993

APPROVAL PAGE

Fracture of Cementitious Composites

Sira Tindukasiri

Dr. Methi Wecharatana, Thesis Advisor
Professor of Civil and Environmental Engineering, NJIT

Dr. Dorairaja Raghu, Committee Member
Professor of Civil and Environmental Engineering, NJIT

Dr. C. T. Thomas Hsu, Committee Member
Professor of Civil and Environmental Engineering, NJIT

BIOGRAPHICAL SKETCH

Author: Sira Tindukasiri

Degree: Master of Science in Civil Engineering

Date: May 1993

Date of Birth:

Place of Birth:

Undergraduate and Graduate Education:

- Master of Science in Civil Engineering,
  New Jersey Institute of Technology, Newark, NJ, 1993

- Bachelor of Engineering (C.E.), Chulalongkorn
  University, Bangkok, Thailand, 1991

Major: Civil Engineering

Presentations and Publications:

Tindukasiri, Sira and Wecharatana, Methi. "Fracture of Cementitious Composites." Presented in Bangkok, Thailand, November, 1992, at the Annual Meeting of the Engineering Institute of Thailand'1992, Bangkok,Thailand: p.p., 1235-1252.

TABLE OF CONTENTS

LIST OF TABLES

LIST OF FIGURES

CHAPTER 1

INTRODUCTION

In fracture mechanics of concrete composites, many reported fracture parameters such as fracture toughness or the stress intensity factor (K_{IC}), critical strain energy release rate (G_{IC}) and, fracture energy(G_F) are highly contradictory and inconsistent. These variations were first attributed to the non-linear and inelastic behavior of cementitious composites. It is now believed to be largely due to the amount of microcracking in the vicinity of the crack tip.

To incorporate the effect of the microcracked or fracture process zone into the linear elastic fracture mechanics concept, many researchers have proposed non-linear fracture models by representing the process zone as a fictitious crack on which traction forces apply. The traction force is theoretically related to the extent of damage or debonding of the concrete composites. Depending on the assumption of the failure mode at the vicinity of the crack tip, that is Mode I-direct opening or Mode II-shear failure, the force pull-out displacement relationship is essentially derived from the assumed failure condition. For Mode I failure which is commonly assumed, the stress (Force)-displacement relationship is obtained from a uniaxial direct tensile test. Since concrete is a brittle material and very weak in tension, conducting a uniaxial direct tension test to obtain the complete stress-displacement curve is extremely difficult, particularly in the post-peak region. To avoid the direct tension test, many researchers proposed use of a notched beam specimen as an indirect method to measure the stress-displacement relationship of concrete. The test setup and testing procedure are simple and can be easily conducted. Although the failure mode is in tension, due to the compression zone in the top portion of the beam many investigators have been concerned about the accuracy of the measured fracture energy. Nonetheless, the method has been adopted and recommended by RILEM Committee on Fracture Mechanics and is commonly used to measure the fracture toughness of concrete and other cementitious composites.

The most important parameter obtained from the standard notched beam test is fracture energy (G_F). It is generally referred to as the amount of energy needed to fracture a unit area of concrete. Such a fracture process should normally take place in a uniaxial tensile test. For the sake of simplicity, the fracture energy is measured using a standard notched beam specimen. The beam test is also used to predict the toughness index of fiber reinforced concrete.

Recently a series of round-robin tests was conducted by a group of inter-university researchers to evaluate the validity and consistency of "toughness index" of fiber reinforced concrete. It was found that the results obtained from a notched beam test were inaccurate since they incorporated extraneous deformations at the load point and supports. The task force recommended that the standard ASTM testing setup be modified to

eliminate these extraneous deformation. Kim [3] has developed a new testing setup. By measuring the load-line deflection with reference to the neutral axis of the notched beam rather than the conventional measurement from the machine base, he was able to confirm the presence of extraneous deformations and eliminate them. He conducted a series of notched beam tests on plain concrete and mortar and established that the extraneous deformation due to support crushing was of the same order of magnitude as the actual beam deflection. Kim also suggested that the CMOD, which is another fracture parameter. Previously used for pacing the test, was not affected by the test setup and could be used to determine fracture energy provided that certain relationships exists between load-line deflection and CMOD. Kim reported that for concrete and mortar there was a bilinear relationship between deflection and CMOD.

The objective of this study is to verify whether the testing setup developed by Kim applies also to fiber reinforced concrete and whether the bilinear relationship between CMOD and deflection exists for other cementitious composites like fiber reinforced concrete. A series of experiments on fiber reinforced concrete notched beam specimens will be run and it is anticipated that a standard testing setup for cementitious composites can be recommended as a result of this investigation.

CHAPTER 2

FRACTURE MECHANICS MODELS FOR CONCRETE

Three of the most well known nonlinear fracture models for concrete are the Fictitious Crack Model (FCM) by A.E.Hillerborg, the Crack Band Model (CBM) by Z. B. Bazant and the Two-Parameter Fracture Model (TPFM) by Jenq and Shah. [5]. These models are all intended to incorporate the nonlinear behavior of concrete into the analysis of fracture process of concrete.

2.1 Fictitious Crack Model (FCM)

Hillerborg, et al. proposed the FCM for predicting crack growth behavior in concrete. Fig.2.1 shows a typical crack tip stress distribution based on the proposed model. The stress-crack width (σ-ω) relationship, considered a material property, defines the post-peak behavior of the material. The pre-peak behavior of the material is assumed to be linear elastic and is defined through a stress-strain (σ-ε) relation. Pre-peak non linearity is often neglected for mathematical convenience and is, in practice, very small compared to the post-peak inelastic behavior (Fig. 2.2). The fracture energy in the FCM is given by

$$G_F = \int \sigma(\omega) d\omega. \qquad (1)$$

G_F is one of the key parameters needed to implement the FCM. To determine G_F, a notched beam specimen is tested until it is completely fractured. The amount of total energy absorbed during the fracture process divided by the fracture area will be the fracture energy of the concrete material. Although the actual G_F should be determined from the uniaxial direct tension test, due to the degree of difficulty in conducting the direct tension test most researchers seem to accept the indirect method of the notched beam specimen. The standard notched beam specimen has a given specific dimension since it was shown that the fracture parameters measured from notched beam specimens was specimen size dependent. Therefore, the dimension of the test specimen must strictly adhere to the recommended requirements.

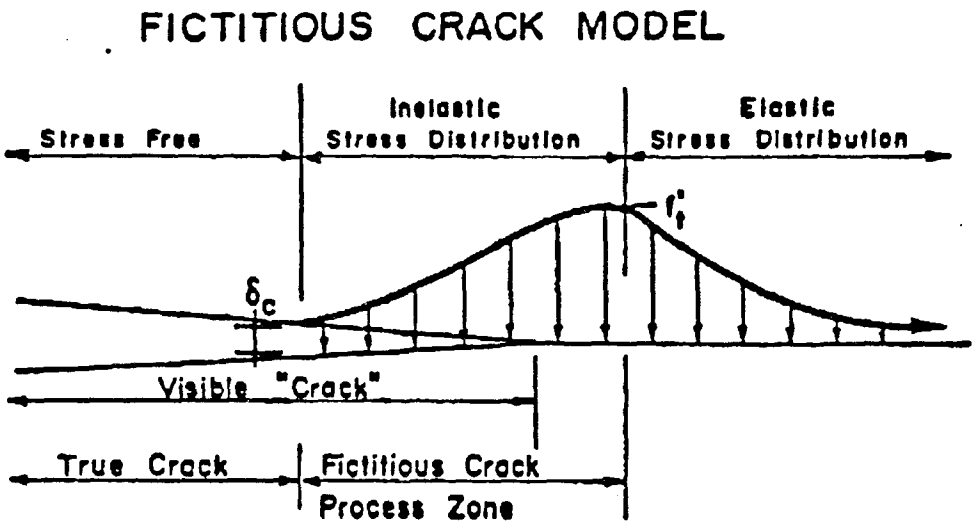

Figure 2.1 Crack Tip Stress of Fictitious Crack Model

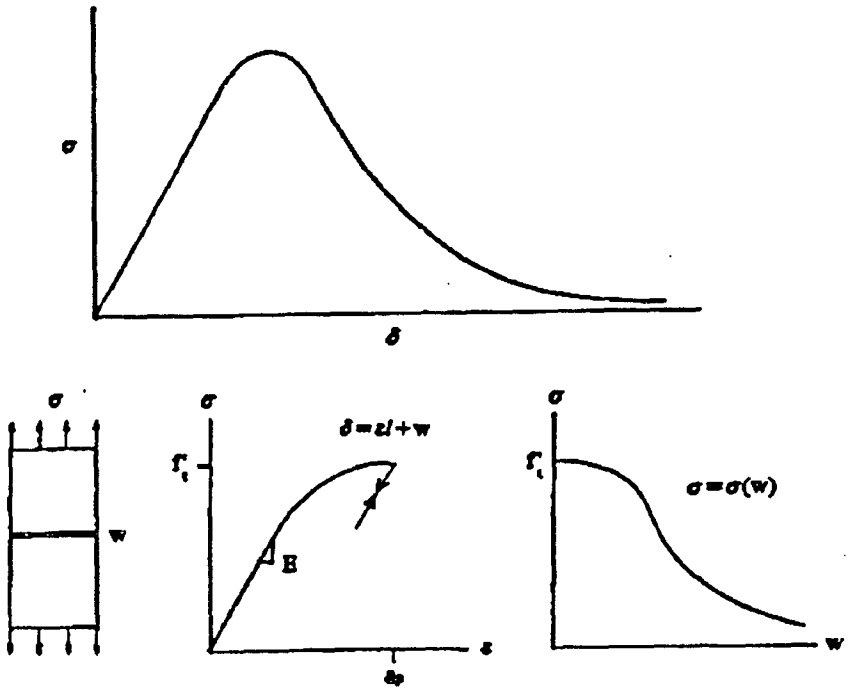

Figure 2.2 Stress-Displacement Relationship

Finite element analysis is also necessary to implement the model. The model has been shown to correctly predict the experimentally observed size effects for notched and unnotched beam specimens. However, it has been pointed out that the experimentally observed values of fracture energy (G_F) are dependent on the specimen size. The values obtained by the model are quite sensitive to the uniaxial tensile strength which is not easy to determine. Furthermore, to obtain the peak load of the specimen, the whole load deflection curve should be numerically calculated, which requires considerable computational time.

2.2 Crack Band Model (CBM)

Arguing that energy cannot be dissipated in the fracture process of concrete , Bazant and Cedolin, and Bazant and Oh [6] have proposed the crack band model which treats the localization as bands of distributed cracks. The pre-peak and post-peak behavior are both described by a stress-strain relationship (pre-peak modulus E_1 and post-peak modulus E_2, Fig. 2.3). The width of the crack-band W_c can be used to relate the stress-strain response to the fracture energy.

$$G_F = W_o \int \sigma d\varepsilon \tag{2}$$

$$G_F = \frac{W_o^2}{2} f_t \left(\frac{1}{E1} - \frac{1}{E2}\right)$$

The results are similar to those obtained from fictitious crack model if the same values of G_F and f_t are used in the crack band model. The major difference between the FCM and the CBM models is that the FCM uses a discrete crack concept while the CBM approach is based on the smeared crack principle. In some cases, these two models provided similar results while in some other instances, their predictions were completely different. Nonetheless, the results predicted using both models were claimed to be in good agreement with the observed experimental data which obtained from testing a standard notched beam specimens.

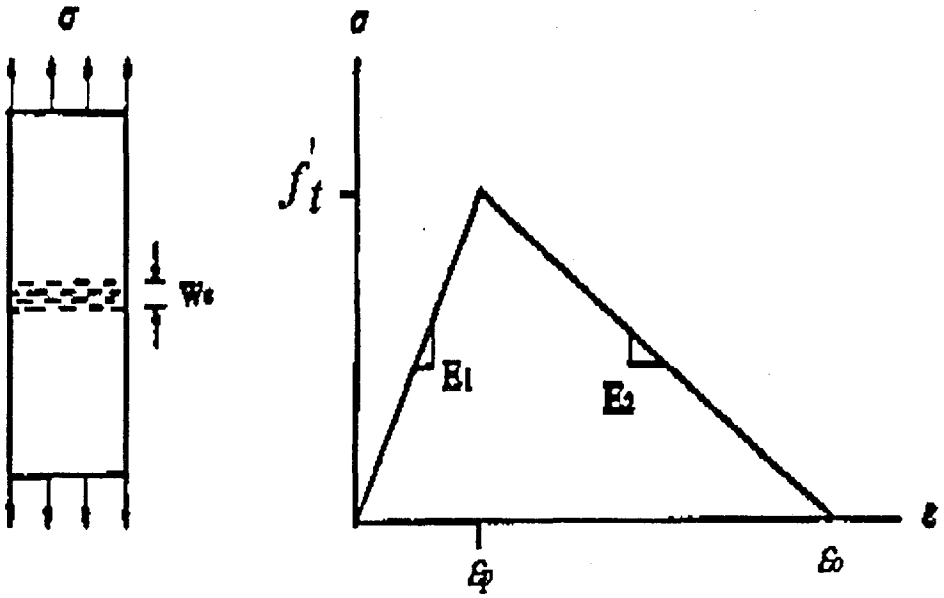

Figure 2.3 Crack Band Model

2.3. Two-Parameter Fracture Model (TPFM)

Realizing the tediousness involved in implementation of the FCM, Jenq and Shah[7] proposed a two-parameter fracture model which does not require the post-peak constitutive relation. The stress intensity factor calculated at the tip of the effective crack is determined in such a way that the measured elastic crack-mouth-opening displacement ($CMOD_e$) is equal to the one calculated using the LEFM. By either assuming the crack profile or directly using the LEFM formula, the elastic critical crack tip opening displacement ($CTOD_e$) can be obtained. Based on Three Point Bend tests on different beam sizes and mix-proportions, they concluded that both K_{IC} and $CTOD_e$ are specimen size independent. Since both fracture parameters are directly determined from LEFM formula. Crack tip singularity is automatically incorporated in the model. This was claimed to be the major difference between the TPFM and the two previous finite element models (FCM and CBM) since both models neglected the singularity at the crack tip. Fig.2.4 shows the typical Load-CMOD response with the two critical fracture parameters.

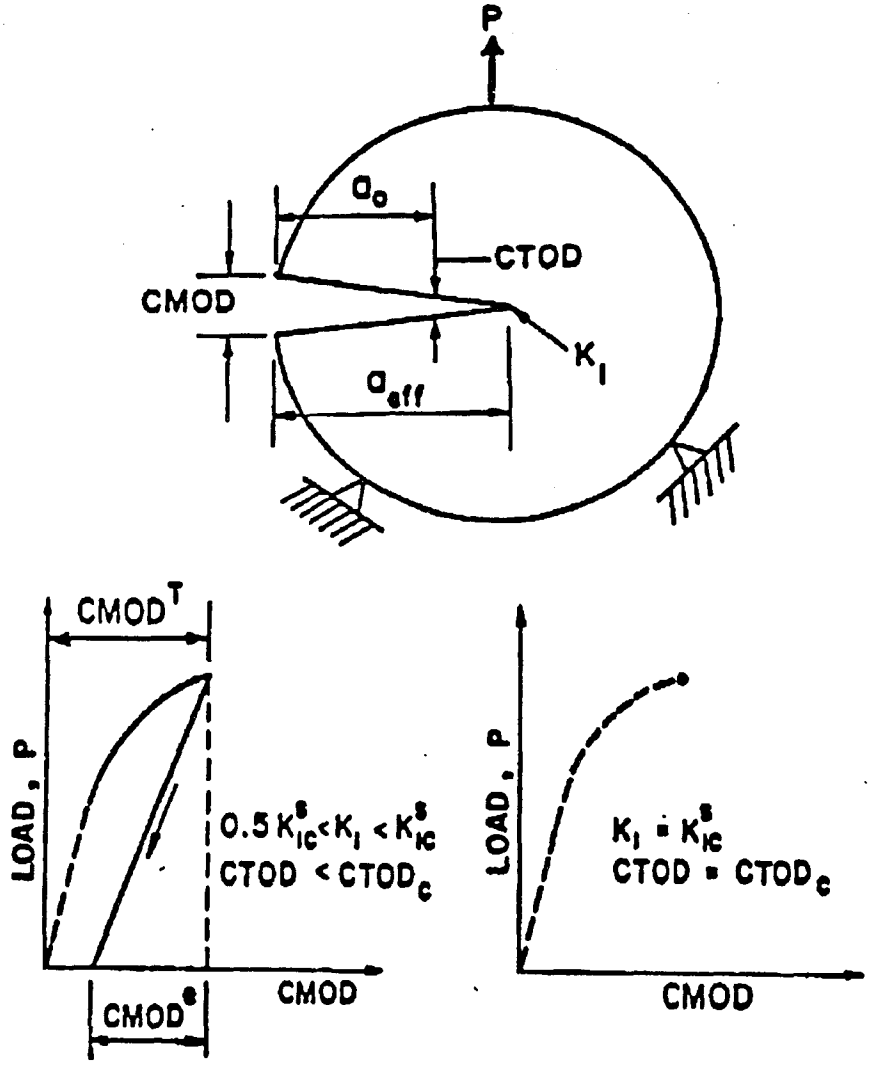

Figure 2.4 Two-Parameter Fracture Model

As proposed in the TPFM, the initial crack growth, the maximum applied load and the corresponding elastic $CMOD_e$ are all directly obtained from the experiment. With the known specimen geometry and the Young's modulus, the effective elastic crack length (a_{eff}) can be calculated from the LEFM formula using measured $CMOD_e$ and the measured maximum load. The task to calculate a_{eff} using the LEFM formula is not simple since iteration or trial and error is needed to obtain an a_{eff}. With the calculated effective crack length, K_{IC} and $CTOD_e$ can be obtained using the available LEFM formula. It should be noted that the results predicted from all three proposed non-linear fracture models were reported to be in good agreement with experimental data obtained from testing the notched beam specimens.

2.4 Proposed Model (Constant Fracture Angle Model)

The validity of the FCM models was evaluated by Ratanalert and Wecharatana [5] and found to have problems in predicting Load-deflection and Load-CMOD relationships simultaneously using the same set of input variables for a given notched beam tested. No justified explanation was provided at time. The inter-university round-robin test on the determination of toughness index of fiber reinforced concrete conducted by six universities[4] reported problems associated with the testing setup where extraneous deformation could be mistakenly incorporated into the measured load-line deflection. To overcome this problem, Kim proposed a new testing setup and a Constant Fracture Angle Model [3]. The concept of his model is as follow:

2.4.1 Phenomenological Aspects

The phenomenological aspect of a Mode I fracture may be described by considering a specimen loaded in tension with prescribed displacement increments. Preexisting microcracks, mostly located on the aggregate-matrix interface, after initial settling, assume an equilibrium position with respect to the load. As loading increases, bond cracks grow, and, after a point, microcracks in the matrix start developing from existing voids and bridging between bond cracks. Even at and after peak load, crack surfaces are not completely separated, but still resist some tensile stress, probably because of aggregate interlocking effects and traction between surfaces. Slowly, with increasing displacements, stress transfer across the micro cracked region drops to zero, and specimen fails.

A load-displacement (or stress-strain) curve obtained under a displacement controlled test up to failure has two distinct regions; an ascending branch before, and a descending, softening, branch after the peak load (Fig. 2.5). The Modulus of Elasticity is usually used to characterize the stress-strain relation in the elastic domain, and the peak stress characterizes the tensile strength of an elastic material. However, in the process zone, it has been postulated, after analysis of the softening branch of uniaxial tension test results, that stress and the process zone displacements are functionally dependent through a local process zone softening constitutive relation. The material in the process zone supports stresses after the peak load which is proportional to the displacement in the process zone. One constitutive relation holds between stress-strain in the elastic domain, e.g., Modulus of Elasticity and another holds between stress and process zone displacements locally in the process zone.

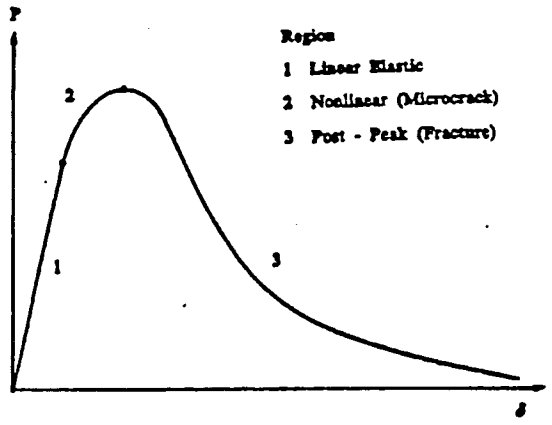

Fig. 2.5 Typical Load-Deformation Curve of Concrete

2.4.2 Modeling

In proposing the Constant Fracture Angle Model, the relationship between CMOD and load-line deflection was developed based on the LEFM concept. CMOD measurement is used because it is more reliable than the load-line deflection measurement since CMOD is not affected by support crushing, and all support crushing occurs before peak load.

2.4.2.1. Linear Elastic Range

For the initial portion, the linear elastic range, the LEFM concept can be used to obtain a CMOD-load line deflection relationship. Crack Mouth Opening Displacement (CMOD) is

$$\text{CMOD} = \frac{6PSa}{Ebd^2} V1(A) \qquad (3)$$

where P is the load, S, the span of the beam, b, the beam width, d, the beam height, a, the initial notch depth, A, is the ratio of the initial notch length to beam depth, and V1(A) is a size effect factor depending on the loading type and the ratio of the span to the beam depth. In the case of the three point bend test specimen for S/d = 4, V1(A) is

$$V1(A) = 0.76 - 2.28A + 3.87A^2 - 2.04A^3 + \frac{0.66}{(1-A)^2} \qquad (4)$$

The total load-line deflection of beam can be expressed as

$$\delta_p = \delta_c + \delta_n = \delta_c + (\delta_b + \delta_s) \qquad (5)$$

where δ_c is the deflection due to the crack, δ_n the deflection of the uncracked beam, δ_b the deflection due to bending and δ_s the deflection due to shear.

$$\delta_b = \frac{PS^3}{4Ebd^3} \tag{6.1}$$

$$\delta_s = \frac{3(1+\upsilon)PS}{5EA} \tag{6.2}$$

$$\delta_c = \frac{3PS^2}{2Ebd^2} V2(A) \tag{6.3}$$

where

$$V2(A) = (\frac{A}{1-A})^2 (5.58 - 19.57A + 36.82A^2 - 34.94A^3 + 12.77A^4) \tag{7}$$

substituting Eq.(6) into Eq. (5) and dividing by Eq. (3) gives:

$$\frac{\delta_p}{CMOD} = \frac{30dSV2(A) + 5S^2 + 12(1+\upsilon)d^2}{120daV1(A)} \tag{8}$$

The value of υ=0.2 is commonly used for concrete and other cementitious materials. The derived formula should leave S/d as a variable but substitute the value of $\upsilon = 0.2$. Hence

$$\frac{\delta_p}{CMOD} = \frac{30(S/d)V2(A) + 5(S/d)^2 + 14.4}{120AV1(A)} \tag{9}$$

If S/d = 4 as recommended by ASTM standard, Eq, (9) is

$$\frac{\delta_p}{CMOD} = \frac{V2(A)}{AV1(A)} + \frac{23.6}{30AV1(A)} \tag{10}$$

Based on the Eq. (8), load-line deflection can be expressed as follows:

$$\delta_P = S1\ CMOD \tag{11}$$

where S1 is a constant determined by loading type and specimen geometry.

2.4.2.2 Post Peak Range (Crack Propagation Range)

In the post-peak range where cracks start to propagate, the relation between CMOD and load-line deflection can be derived using the following assumptions:

1. Fracture energy, G_F, is a material property.
2. Microcracks are fully developed at the peak load, and when a crack propagates the size of fracture process zone does not change.
3. The ratio of the change of CMOD to the change in crack length is constant. (Fig. 2.6)

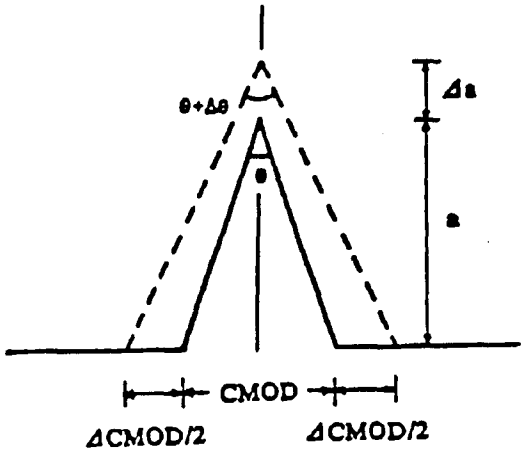

Figure 2.6 Relation Between CMOD and Crack Length a

The incremental ratio of load-point deflection to CMOD, $\Delta\delta_p/\Delta$CMOD, can be expressed using chain rule as

$$\frac{\Delta\delta}{\Delta\text{CMOD}} = \frac{\Delta a}{\Delta\text{CMOD}} \frac{\Delta\delta_p}{\Delta a} \tag{12}$$

The energy due to small increment of load-line deflection, ΔU, is

$$\Delta U = P\Delta\delta_p \tag{13}$$

Substituting Eq. (13) into Eq. (12) gives

$$\frac{\Delta\delta_p}{\Delta\text{CMOD}} = \frac{\Delta a}{\Delta\text{CMOD}} \frac{\Delta U}{P\Delta a} \tag{14}$$

Since $\Delta U / b\Delta a$ is the fracture energy G_F with b as the beam width, Eq. (14) changes to Eq. (15)

$$\frac{\Delta \delta_P}{\Delta CMOD} = \frac{G_F}{bP} \frac{\Delta a}{\Delta CMOD} \tag{15}$$

The right side of the above equation is a constant because G_F is a material property and $\Delta a/\Delta CMOD$ is a constant (refers to assumption 3). Therefore, $\Delta \delta_p/\Delta CMOD$ is a constant.

$$\frac{\Delta \delta P}{\Delta CMOD} = S2 \tag{16}$$

S2 is a material property, independent of size, and can be determined by experiments.

2.4.2.3 Microcracked Process Zone

In the microcracked process zone, microcracks start and fully develop at the peak load. Near the peak load, the coalescence of microcracks produces a traction-free surface (l_e) in the process zone. This traction-free surface continuously changes causing a continuous slope change from S1 to S2 (Fig.2.7).

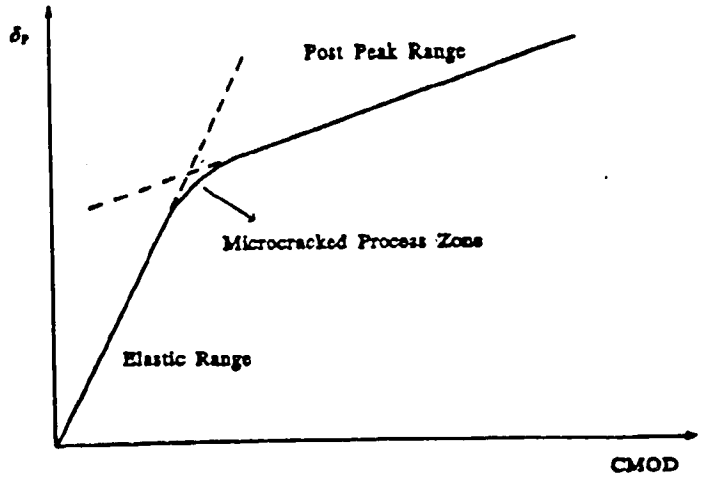

Figure 2.7 δ_p-CMOD Curve

The change of slope, ΔS , due to increment of load ΔP is

$$\Delta S = \frac{\Delta \delta_p}{\Delta CMOD} = \frac{\frac{\partial \delta P}{\partial a} \Delta a + \frac{\partial \delta P}{\partial P} \Delta P}{\frac{\Delta CMOD}{\partial a} \Delta a + \frac{\Delta CMOD}{\partial P} \Delta P} \tag{17}$$

Using LEFM the above equation can be expressed as

$$P = \frac{P_{max}}{(1+K)} \tag{18}$$

where

$$K = \frac{K1\frac{3s^2}{2Ebd^3} - K2\frac{6s}{Ebd^2}\Delta s}{\frac{\partial CMOD}{\partial P}\Delta s - \frac{\partial \delta_p}{\partial P}} - \Delta a \tag{19}$$

$$K1 = 2\frac{A}{(1-A)^3}(5.58 - 19.57A + 36.82A^2 - 34.94A^3 + 12.77A^4) + \frac{A}{(1-A)^2}(-19.57 + 73.64A - 104.82A^2 + 51.08A^2) \tag{20}$$

where $A = \frac{a}{d}$

$$K2 = V1(A) + A(-2.28 + 7.74A - 6.12A^2 + \frac{1.32}{(1-A)^3}) \tag{21}$$

Δa in Eq.(19) is calculated from the CMOD value at the peak load using Eq. (3). Eq. (3) is a polynomial function of A requiring a numerical method for the determination of A. Since $a = a_0 + \Delta a$, Δa can be found. So, Eq.(18) can be used to solve for P, which is the proportional limit in this case.

What the constant fracture model suggested is that if the size of fracture process zone is fully developed at the peak load and simply shifted forward when crack propagates, the nonlinearity due to the process zone will remain constant through out the whole crack propagation process. Thus, post-peak fracture can be considered based on LEFM. To evaluate the validity of this model, Kim conducted series of experiment on mortar and concrete beams and reported that the bilinear relationship between CMOD and load-line deflection existed provided that the load-line deflection was measured from the neutral axis of the notched beam rather than from conventional machine base. The study conducted here is to further extend this concept into fiber reinforced concrete materials where large beam deformation occurs. Details of this investigation will be discussed next.

CHAPTER 3

EXPERIMENTAL PROGRAM

3.1 Experimental Program I

The experimental program in this study can be divided into two parts. The first used the same testing setup as proposed by Kim [3]. The results indicated some potential problems associated with the testing setup. The setup was then modified and tested in the second program.

According to Kim [3], the size of the notched beam specimen which provided the most consistent results is the 3×6×27 in. beam with 1.2 in. notch depth on a 24 in. span length. Thirty fiber reinforced concrete beams were cast in plywood molds and tested. Standard 3×6 in. cylinders were cast to be tested for the compressive strength and Young's modulus of the composites. All specimens, both beams and cylinders, were cured in a lime-saturated water until one day before testing when they were taken out. All specimens were tested at the age of 28 days.

After being removed from the curing tank, the beams were notched using an electrical saw cutting on the 3 in. width side to a 1.2 in. depth. In this case, the notch-depth ratio, A, is 0.2 in which previous research indicated to be the optimum value for toughness testing. Prior to testing, clip gage holders and reference frame holders were glued to the specimen at approximately the neutral axis of the beam which was at half the uncracked ligament.

All samples were tested on an **MTS** system closed-loop servo-controlled hydraulic testing machine calibreated to NIST standards. The closed-loop system enabled the use of CMOD control under which the CMOD was increased at a rate of 0.002 in. per minute. This control mode provides a stable beam failure which then allows all values of interest to be measured. Raw data was recorded in a PC data acquisition system with a sampling rate of 2 Hz. using a software called Unkelscope.

Four measurements were made and electronically recorded by the data acquisition system. The load was measured by the load cell, traceable to NIST just prior to the start of the testing, attached to the MTS. Two measurements of the load line deflection were made. The first, LVDT1, was made using a Linear Variable Differential Transformer (LVDT), resolving 0.05 in. into ten volts, measuring between the beam and a reference frame attached at the level of one half the unnotched depth, as seen in Fig. 3.1. The reference frame was hinged above one support and free to move laterally above the other. The second measurement, LVDT2, was a conventional measurement, also using an LVDT with the same range characteristics of LVDT1, between the beam and a fixture attached to the test stand. The last measurement was of the CMOD, made with an MTS clip-on gauge which resolved 0.02 in. into ten volts.

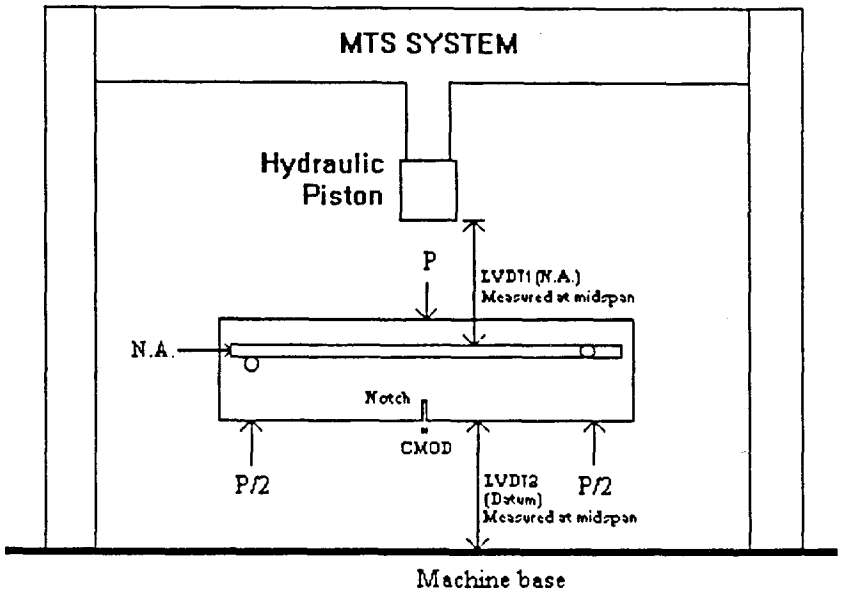

Figure 3.1 Testing Setup Using CMOD

3.1.1 Materials Composition and Properties

Type I portland cement was used with siliceous sand passing sieve #4 and coarse basalt aggregate of 3/8 in. maximum size. The standard mix-proportion used are 35 lbs of cement to 80 lbs of sand and 80 lbs of coarse aggregate with 16 lbs of water or 1 : 2.29 : 2.29 : 0.46 of Cement : Sand : Aggregate : Water.

Only steel fibers were used in this study with the percent fiber volume fraction (V_f) of 0.5, 1.0, and 1.5%. Three types of steel fiber, hooked-end, crimped, and milled were studied. Most fibers used have a length of 1 in. with an aspect ratio (l/d) of 60. The amount of fibers added in each mix is summarized in Table 3.1.

The compressive strength of and modulus of elasticity of fiber reinforced concrete (FRC) were determined in accordance with ASTM standards (ASTM C-39 and C-46a). A typical complete stress-strain curve of 0.5% V_f FRC is shown in Fig. 3.2. The FRC in this study has a compressive strength about 10,000 psi and the modulus of elasticity of 3×10^6 psi.

All specimens were tested using the same testing setup as proposed by Kim [3]. The results, to be discussed later, indicated problems associated with the selected location for the deflection measurements. As a result, the test setup was modified and all tests were repeated in the second experimental program.

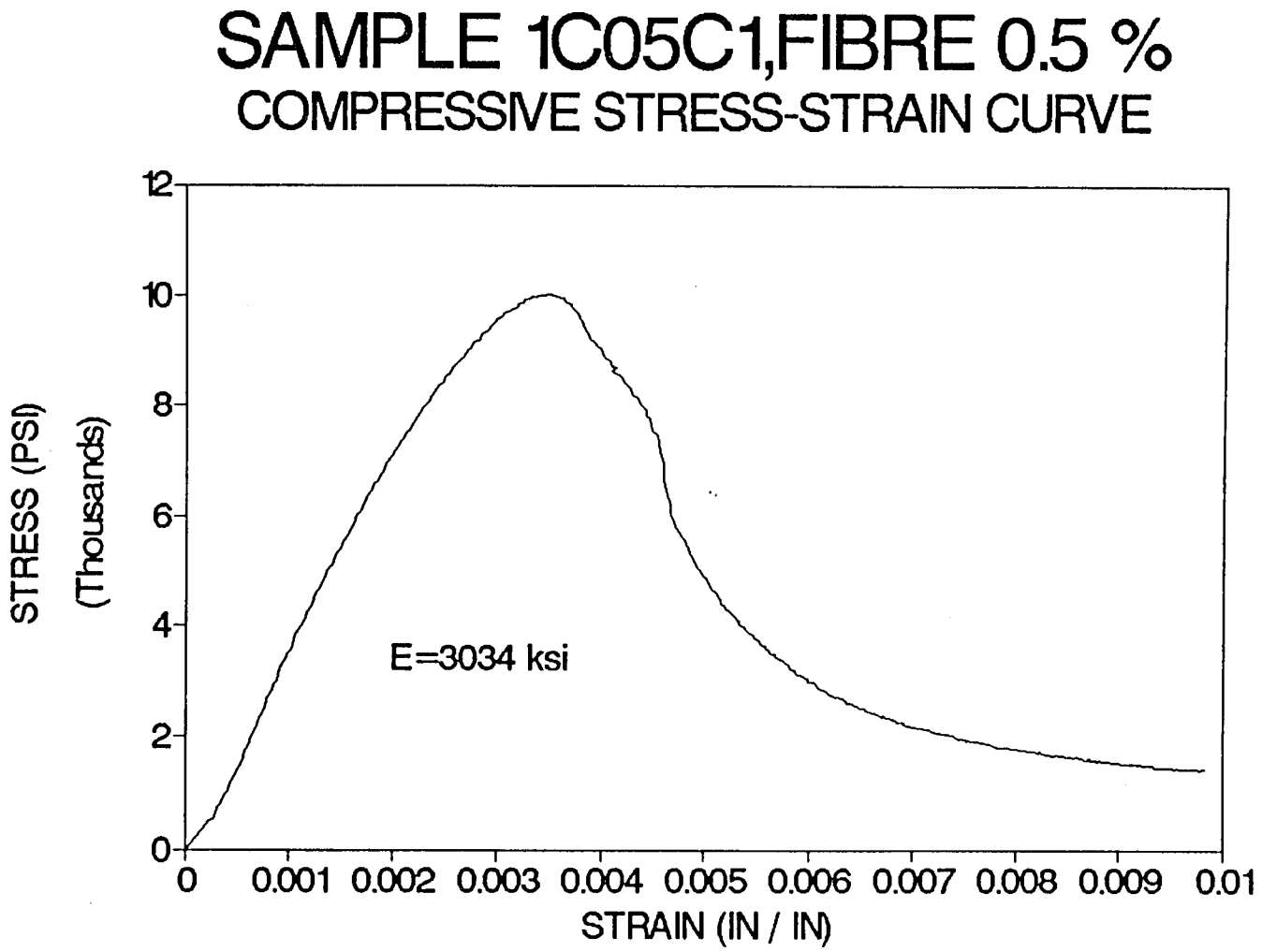

Figure 3.2 Stress-Strain Curve

Table 3.1 Mixed Proportion of Beam and Cylinder Specimens.

Specimen	Fiber type	Wt. of Fiber (lb)
D05B1	0.5%,1 in.	3.43
C05B1	0.5%,1 in.	3.43
H05B1	0.5%,1 in.	3.43
D10B2	1.0%,2 in.	6.86
D10B1	1.0%,1 in.	6.86
C10B1	1.0%,1 in.	6.86
H10B1	1.0%,1 in.	6.86
D15B1	1.5%,1 in.	10.29
C15B1	1.5%,1 in.	10.29
H15B1	1.5%,1 in	10.29

3.2 Experimental Program II

All specimens were prepared and tested in the same way as in the first experimental program I except that the setup was modified. Fig. 3.3 shows the new testing setup. The difference between the new setup and the previous one is the location at which the two LVDT's contact with the reference legs. LVDT2 (with reference to the datum) was removed and placed to measure at the same location as LVDT1 (with reference to the N.A.) in order to correct the error occurred in experimental program I.

The modification is necessary since during testing the beam specimen may rotate about its longitudinal axis which is a result of section irregularity from casting. In addition, large deformation which often occurs in fiber reinforced concrete beam tends to yield different deformation profile than plain concrete. It is then critical to measure the two deflections, as referenced from datum and neutral axis, from the same location on the beam. This is different from the first testing setup which allows to measure the same two deflections from different locations. The results obtained using the new test setup seem to eliminate problems due to extraneous deformation induced in the first setup. Details of these studies will be discussed in the next section.

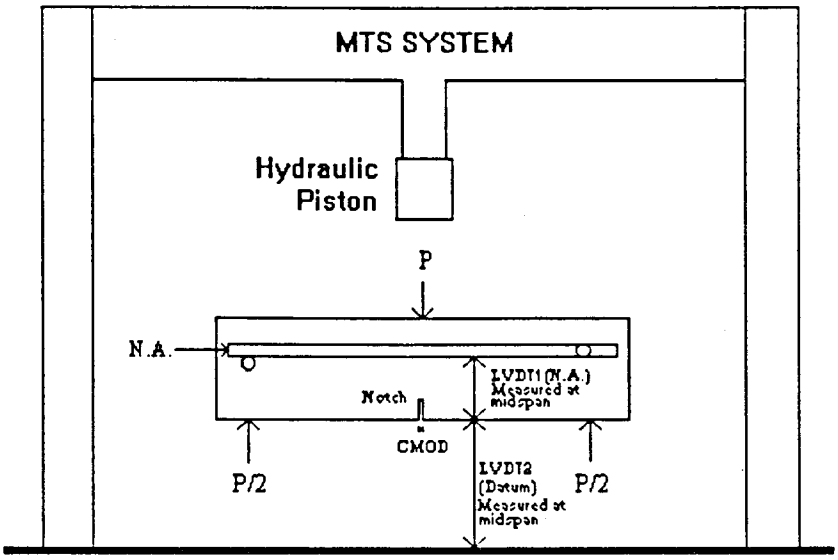

Figure 3.3 New Testing Setup

CHAPTER 4

RESULTS AND DISCUSSION

4.1 Load-CMOD-Deflection Relationships.

The results obtained from experiments are usually in terms of load, CMOD and deflection. In this study, two deflections were measured, one with reference to the machine base and the other measured from the neutral axis of the beam. Fig. 4.1 shows a typical load-deflection (LVDT1) curve for a 0.5 % fiber reinforced concrete beam. The deflection in this figure designated as LVDT1 was measured with reference to the neutral axis of the notched beam. Fig. 4.2 shows the corresponding load-deflection (LVDT2) curve of the same beam as in Fig. 4.1 except that the deflection designated as LVDT2 was measured with reference to machine base. From the figures shown both curves are rather similar and one can never tell the difference between them. Both curves show the elastic region prior to peak load and a long tail of softening response thereafter.

To compare the difference of the two observed deflections, Fig. 4.3 was prepared by plotting load versus CMOD and the two deflections. The load-CMOD relationship shows a similar pattern as the load-deflection curve with the elastic range and a post-peak softening. The other two relationships are plots of CMOD versus each of the measured deflections (Datum and N.A.). It should be noted that CMOD-deflection curves are bilinear in nature and the deflection measured with reference to N.A. is higher than those measured with reference to datum or machine base. This is in contradiction with those reported for mortar and plain concrete by Kim [3] which had the deflection measured from N.A. lower than these from machine base. Kim justified his results reasoning that since extraneous deformations were incorporated into the deflection measured with reference to machine base and not included with those measured from the neutral axis, the deflection measured from Datum must always be bigger. It should be noted that Kim's experiment was conducted only on mortar and concrete which had small deformation at failure. However, for fiber reinforced concrete, large deformation (Fig. 4.4) occurs as a result of fiber reinforcement bridging across the crack. Therefore, the FRC beam tends to deform with an elastic curve while for plain concrete specimen the beam breaks in half with each portion on both sides totally separated and remains straight. The difference in the deformation profile of these two materials indicates that the selected location for measuring each deflection is very critical to the observed result. If the two deflections are to be compared, both must be measured from the same point. Therefore, the testing setup was then modified and all tests were repeated over which will be discussed later.

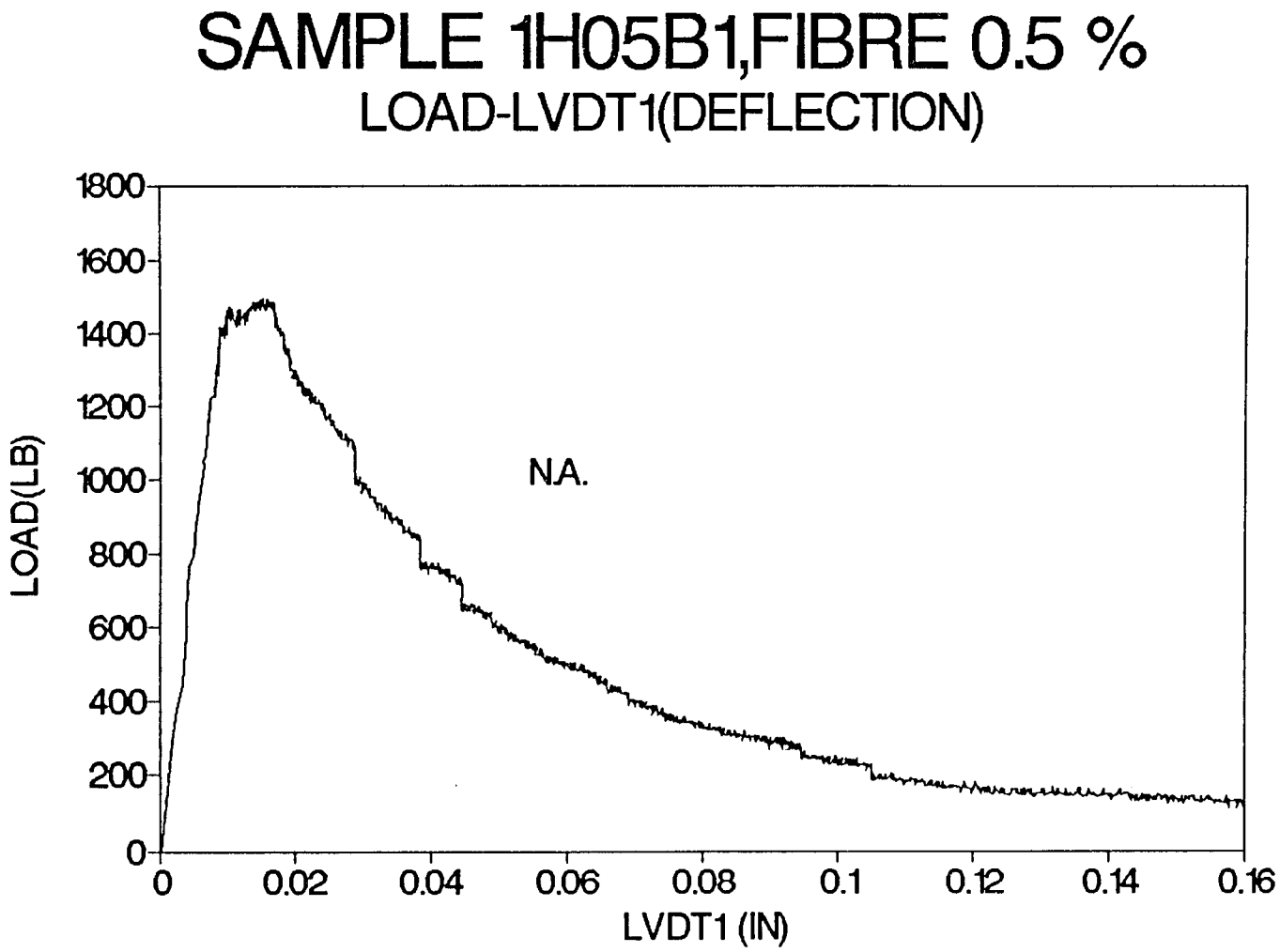

Figure 4.1 Load-Deflection (N.A.) Relationship from Experiment I of 0.5% Fiber Reinforced Concrete Beam

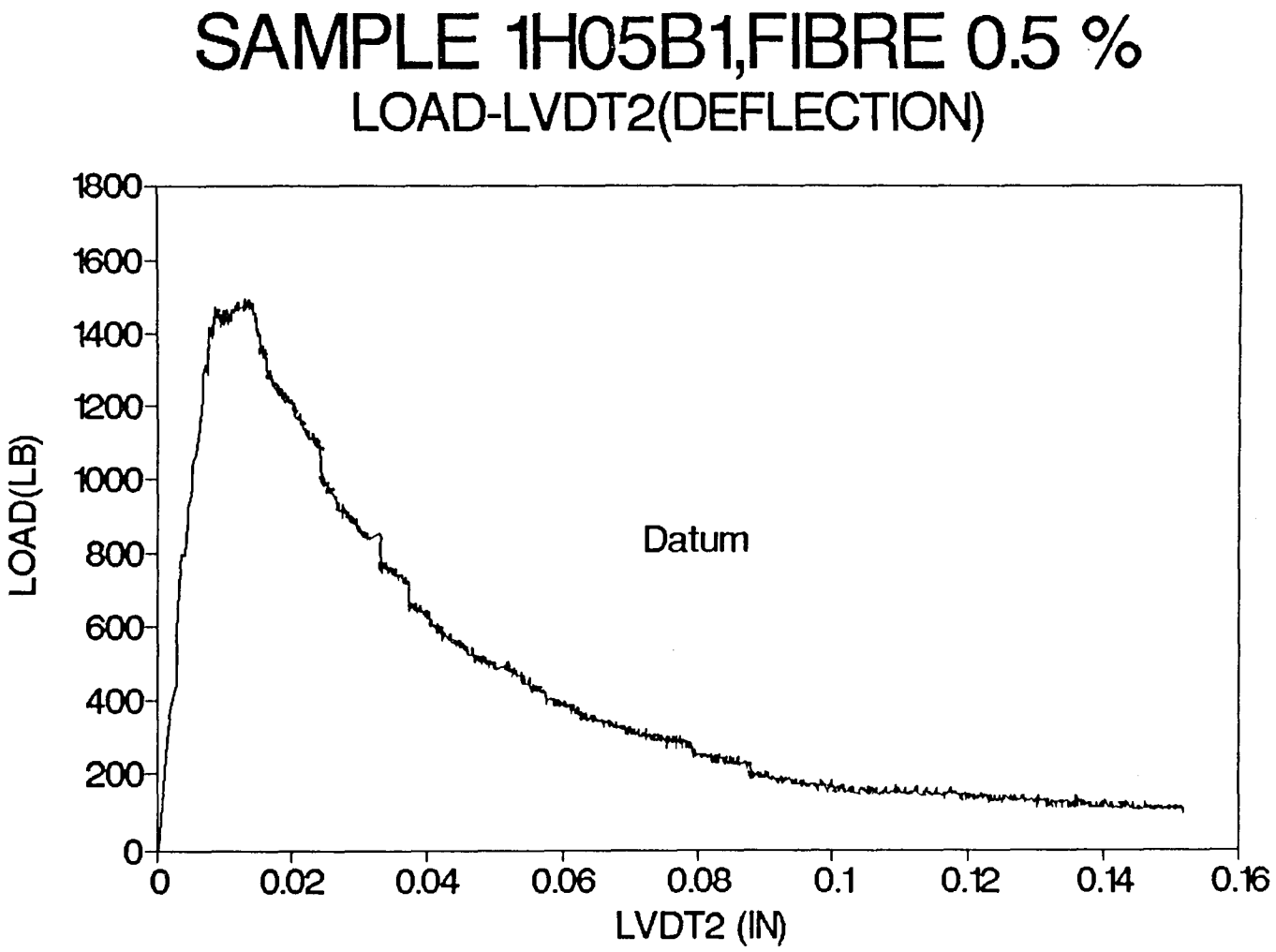

Figure 4.2 Load-Deflection (Datum) Relationship from Experiment I of 0.5% Fiber Reinforced Concrete Beam

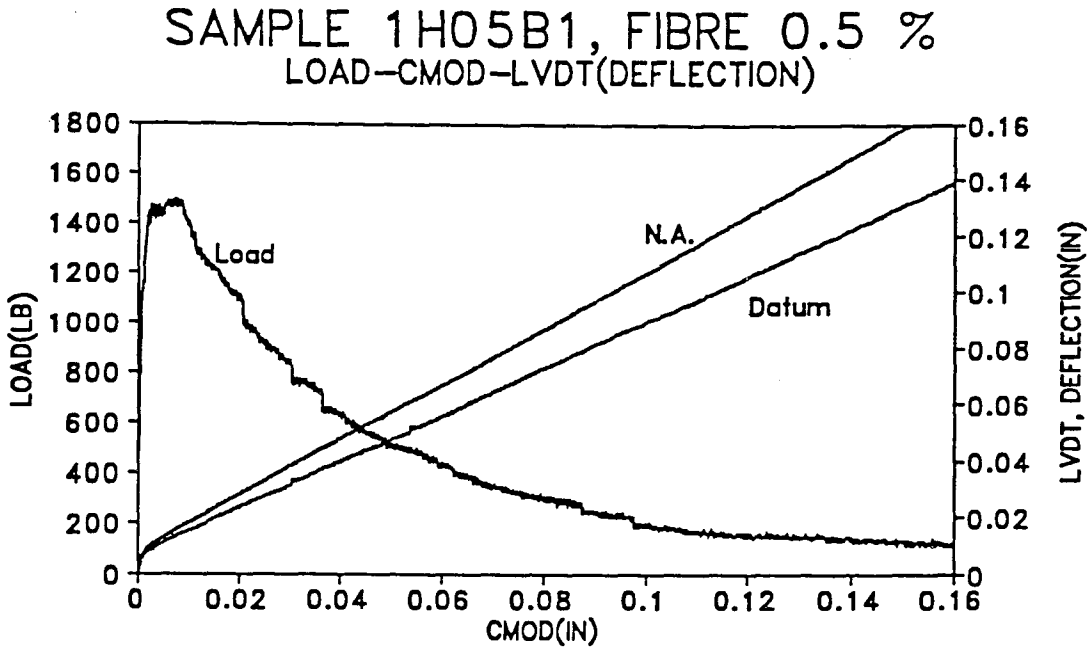

Figure 4.3 Load-Deflection-CMOD Relationship

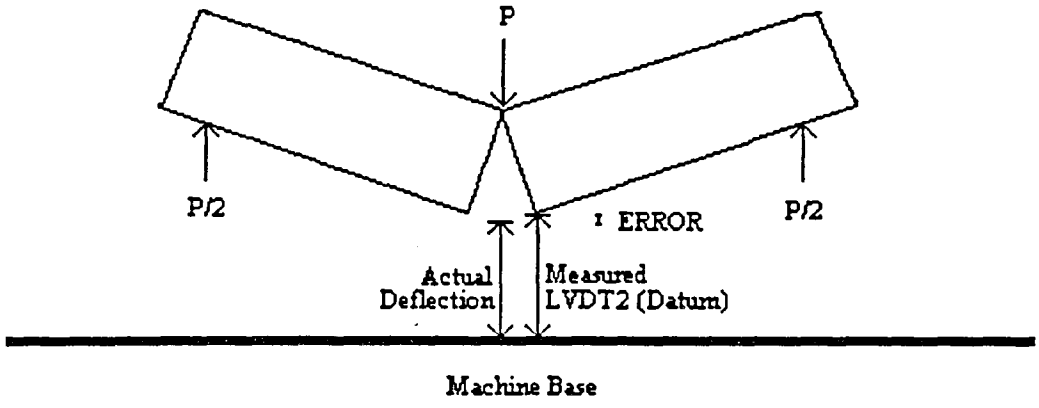

Figure 4.4 Error in Measurement
of Deflection in Experiment I

4.2 Bilinear CMOD-Deflections Relationship

Experimental results presented in Fig. 4.3 clearly shows that there is bilinear relationship between CMOD and deflection. The point that slope changing from S1 to S2 seems to coincide with the location around peak load citing the effect of fully-developed fracture process zone. The decrease of slope or stiffness of the whole system undoubtedly relates to the progressive microcracking. Once the microcracked zone is fully-developed, overall stiffness of the system depends solely on crack propagation which results to a linear relation between CMOD and deflection. Fig. 4.5 shows a plot of deflection versus CMOD of the 0.5% FRC beam. The initial slope S1 equals to 3.47 is determined using equations developed in Chapter 2 whereas the second slope S2 is directly obtained from Fig. 4.3 using the deflection measured from N.A. The curves presented here so far are results obtained from the 0.5% FRC series. The same curves for other fiber volume fraction of FRC are provided in the Appendix.

4.3 Results from the New Test Setup

When deflections were measured from the same location as described in the new test setup, the observed results are shown in Fig. 4.6. Both CMOD-deflection curves remain bilinear as in the first setup. However, the results from the new setup show that deflection measured from N.A. is smaller than these measured from Datum. This finding agrees with Kim's conclusion that extraneous deformation due to support crushing is usually incorporated in the deflection measured from machine base. The two bands on the CMOD-deflection curve shown in Fig. 4.6 were results of noise interference during testing. Nonetheless, the trends of these two curves are clearly bilinear. Fig. 4.7 shows the computed bilinear relationship for the second test setup. It can be seen that the variation of S1 is about 5% whereas for S2 the variation increases by 16%. These numbers imply that the effect of extraneous deformation is not as critical in the elastic range as to the post-peak region. This is primarily due to the fact that the extent of support crushing is pronounced around the peak load region where microcracking is fully-developed. The effect is cumulative in the system and reflected in a weaker overall stiffness. The results shown in Fig. 4.6 and Fig. 4.7 are only for a 0.5% FRC beam specimen. Details of these same behavior for other percentage of fiber volume fraction and type of fibers can be found in the Appendix.

It is clear from this study that selection of location for measuring deflection of cementitious composites is of particular importance to the final outcome of the observed results. If load-line deflection is to be used as key parameter for fracture study, it is critical that extraneous deformation be eliminated. Otherwise, the amount of measured fracture energy will be over estimated.

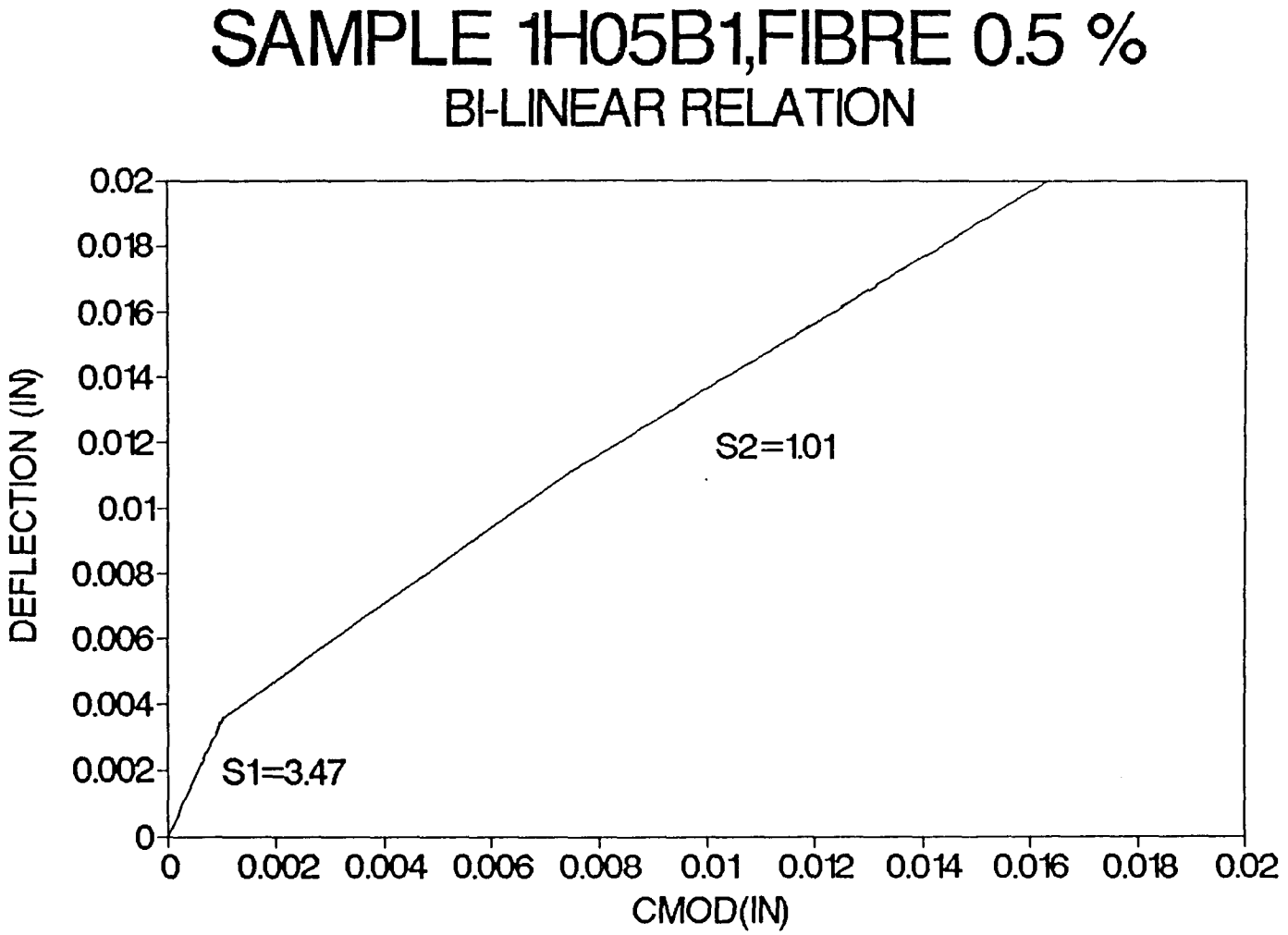

Figure 4.5 Bilinear CMOD-Deflection Relationahip

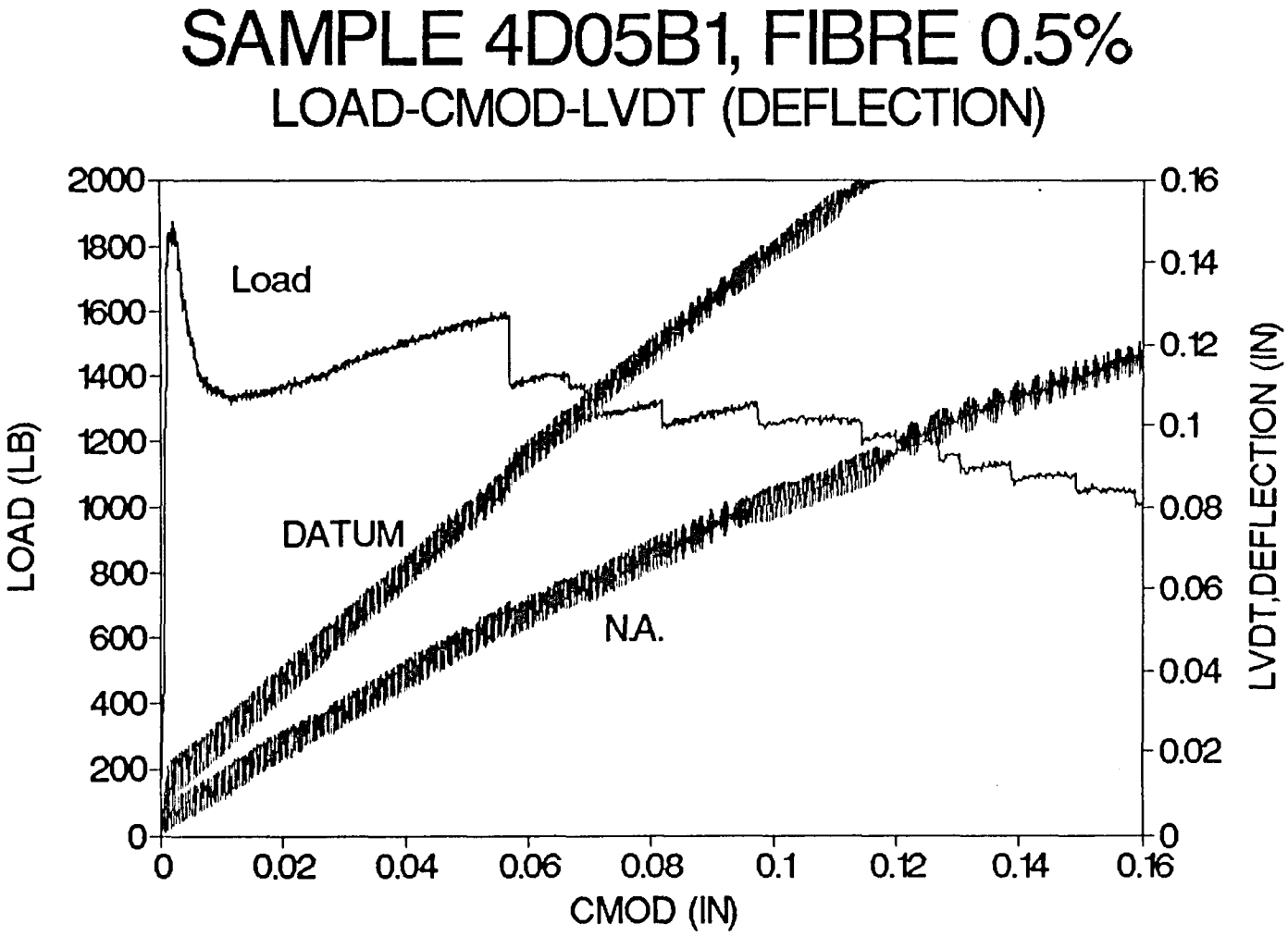

Figure 4.6 Load-Deflection-CMOD Relationship

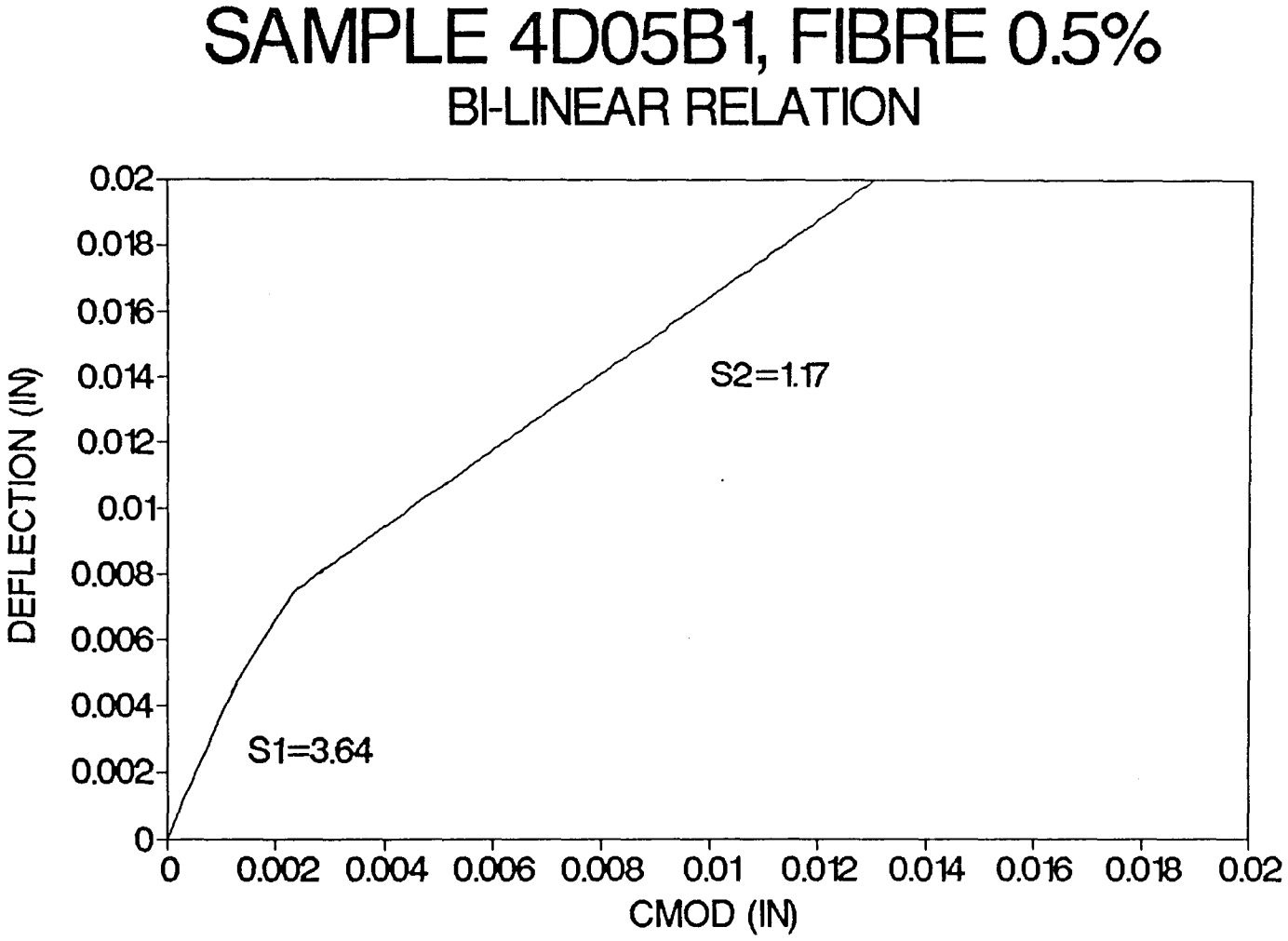

Figure 4.7 Bilinear CMOD-Deflection Relationship

4.4 Load-CMOD Relationship

To avoid potential errors due to extraneous deformation and selected location for deflection measurement, Kim [3] suggested that CMOD responses shown in Fig. 4.3 and 4.6 were not in any way affected by the testing setup. However, in order to use load-CMOD response with the applied energy of the load-deflection behavior. Such a relationship can be obtained through the bilinear relationship between load-line deflection and the CMOD.

The fracture energy is usually taken as the area under the load-deflection curve. However, there have been many discrepancies determining the fracture energy for cementitious composites, now known to result from the difficulties encountered making exact measurements of the load-line deflection. These problems can be eliminated using the bilinear concept because the CMOD value is used to calculate the fracture energy. The fracture energy can be computed using the following expressions:

$$U = \int P \, d\delta \tag{22}$$

$$U = K\int P \, dCMOD \tag{23}$$

Where K is equal to S1 in the elastic range and S2 in the post peak region if S1 and S2 are constant. However, if S1 and S2 are nonlinear relations, Equation (23) can still be used to determine fracture energy by simply incorporated the nonlinear relation K into the integral. The study reported for mortar and concrete by Kim [3] and for fiber reinforced concrete in this study confirm that S1 and S2 for these cementitious composites are linear. Therefore, CMOD can easily be used to determine fracture energy of concrete and fiber reinforced concrete.

CHAPTER 5

CONCLUSIONS

From this investigation, the following conclusions can be drawn:

1. When the amount of fiber increases, the maximum load increases while the Modulus of Elasticity remains essentially.

2. Short and long fibers have different maximum loads. The longer fiber produces a much higher maximum load even though they have about the same Modulus of Elasticity.

3. The results of this experiment do not show any significant differences due to fiber type, except for hook-end fiber which provides slightly higher load carrying capacity.

4. The actual load-line deflection to be used to determine fracture energy must be measured with reference to the neutral axis rather than from machine base, as usually done, since this will eliminate any potential extraneous deformations due to support crushing.

5. For materials with large deformations or extensive nonlinear behavior due to fiber bridging or aggregate interlocking, the location for measurement of the load-line deflection must be carefully selected since potential errors can be incorporated in the measured deflection as a result of beam rotation, which can be large especially in the case of Fiber Reinforced Concrete.

6. To avoid the complexity of the testing setup required to accurately measure the load-line deflection, CMOD, which is unaffected by the testing setup, support crushing or large beam rotations, is a more reliable parameter for use predicting the fracture energy of cementitious composites.

7. A bilinear relationship between CMOD and deflection exists for cementitious composites. For fiber reinforced concrete, the initial slope (S1) is about 3.6 with the second slope (S2) equals approximately 1.0. These values are larger than those reported for mortar and plain concrete. The results of S1 and S2 for different types of fiber and volume fraction of FRC are summarized in Table 5.1.

Table 5.1 Conclusion of Data Results

Specimen	Fiber type	Wt. of Fiber(lb)	Max. Load(lb)	E ksi	S1	S2
D05B1	0.5%,1 in.	3.43	1420.90	2963.95	3.61	1.04
C05B1	0.5%,1 in.	3.43	1640.63	3079.91	3.58	1.05
H05B1	0.5%,1 in.	3.43	1494.14	2933.90	3.54	0.94
D10B2	1.0%,2 in.	6.86	4165.04	3031.31	3.54	0.98
D10B1	1.0%,1 in.	6.86	1469.73	3044.80	3.57	0.98
C10B1	1.0%,1 in.	6.86	2036.13	3241.10	3.54	1.00
H10B1	1.0%,1 in.	6.86	2187.50	3084.98	3.64	0.88
D15B1	1.5%,1 in.	10.29	4155.27	3210.21	3.71	1.06
C15B1	1.5%,1 in.	10.29	2646.48	3210.21	3.67	0.97
H15B1	1.5%,1 in	10.29	2778.32	3202.59	3.62	0.96

APPENDIX A

RESULTS FROM EXPERIMENTAL PROGRAM I

Figure A 1.1a to A 1.9d are results from Experimental Program I. Nine samples are shown here. Each sample has four figures and has a cover page which shows the dimension and other information of the sample.

BEAM CODE	1H10B1	
CAST DATE	9-4-91	
TEST DATE	11-26-91	
LENGTH	27.2	inch
DEPTH	5.9	inch
WIDTH	3.0	inch
KNOTCH DEPTH	1.1	inch
SPAN LENGTH	24	inch
LEG SPAN	23.2	inch
FIBRE TYPE	HAREX	
length	1.0	inch
%	1.0	%
wt. (fibre)	6.9	lbs
MIX P CEMENT TYPEI	34.7	lbs
SAND PASSED #4 SIE	80.6	lbs
#3/8 inch AGGREGAT	80.6	lbs
WATER	16.0	lbs
MAXIMUM LOAD	2187.5	lbs
A	0.178	
V1(A)	1.44206	
V2(A)	0.144376	
S/D	4.064	
E	3084975	psi
S1	3.627154	
S2	0.441212	

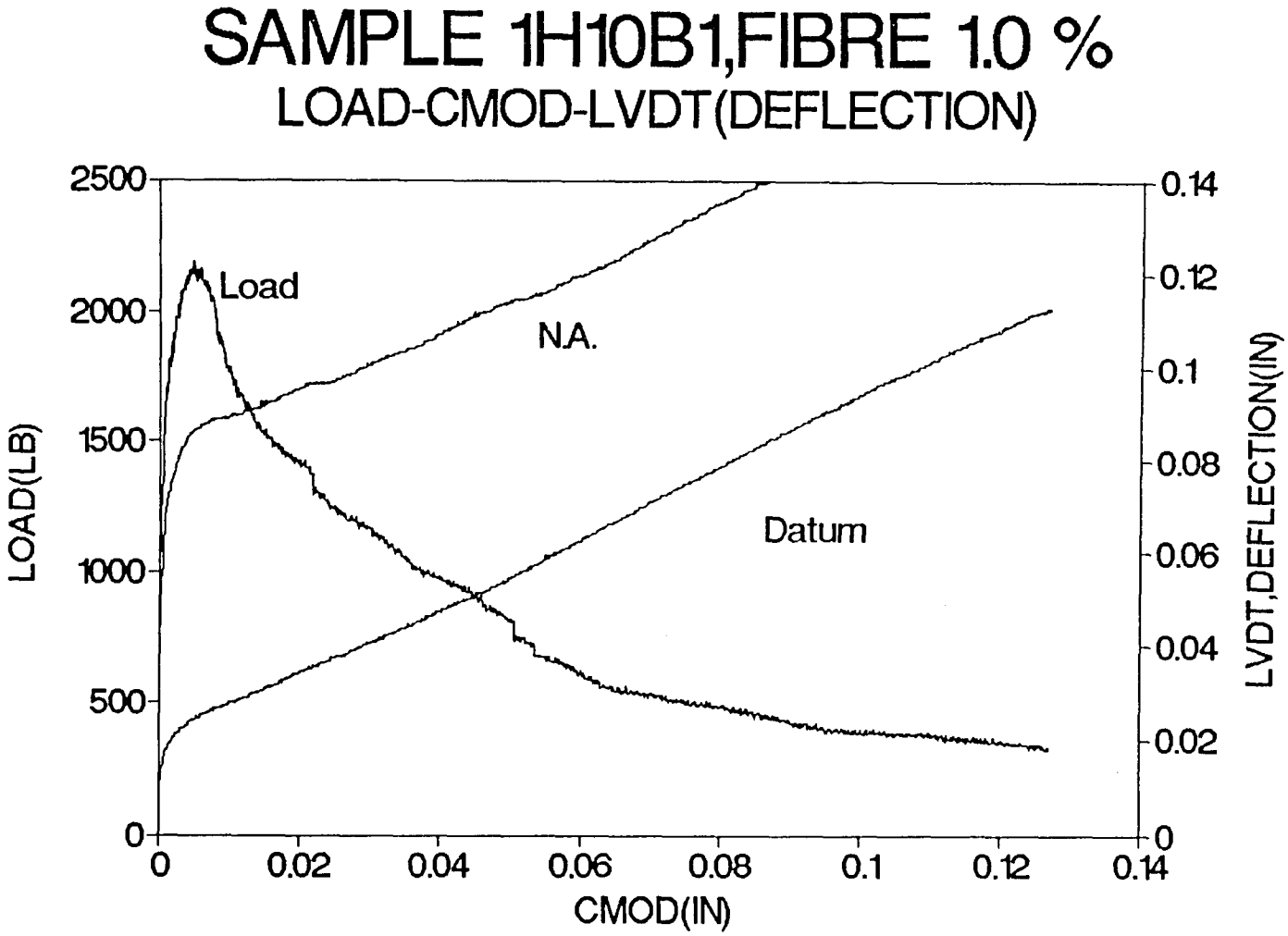

Figure A 1.1a Load-CMOD-Deflection Relationship

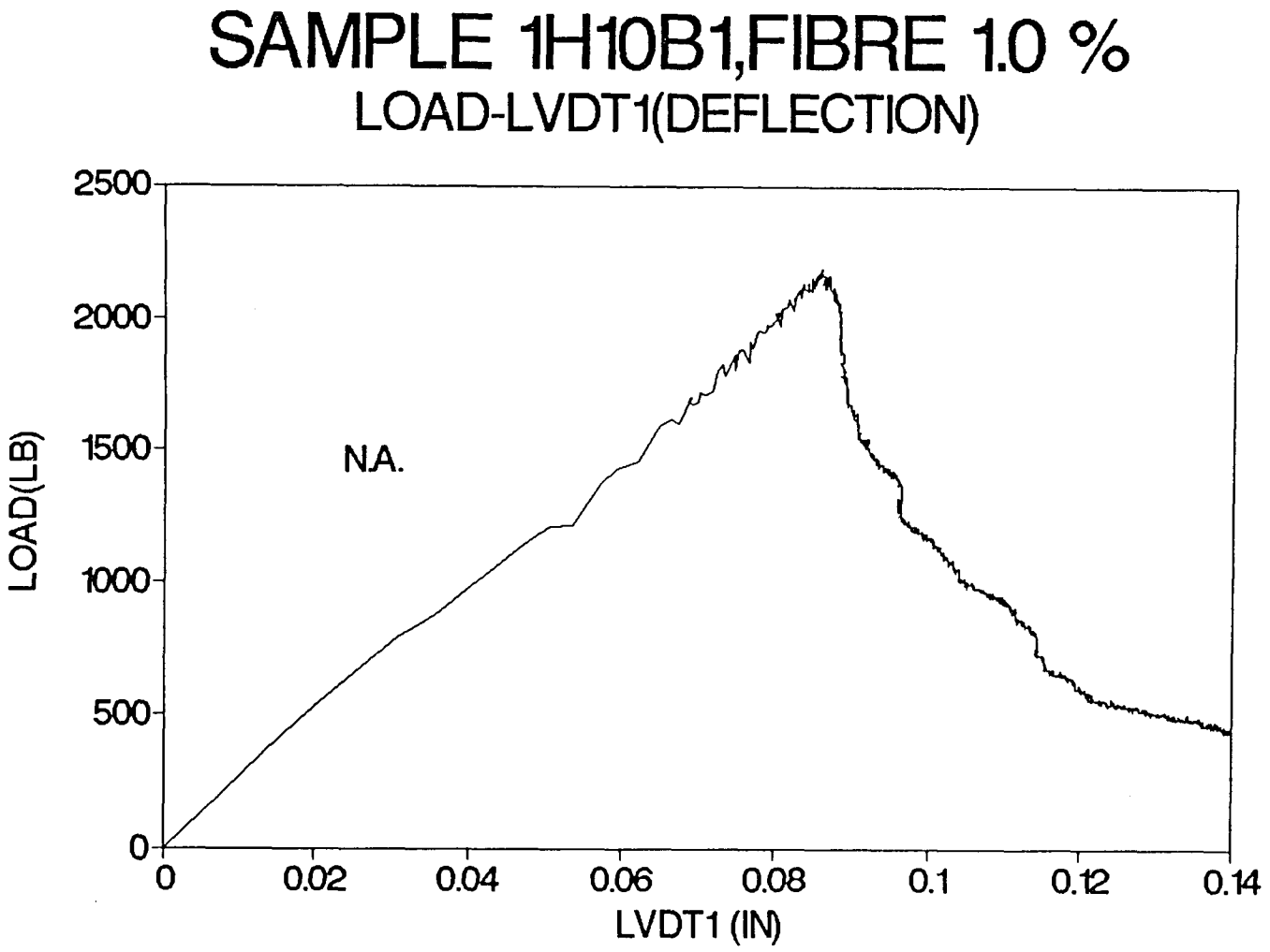

Figure A 1.1b Load-Deflection (N.A.) Relationship

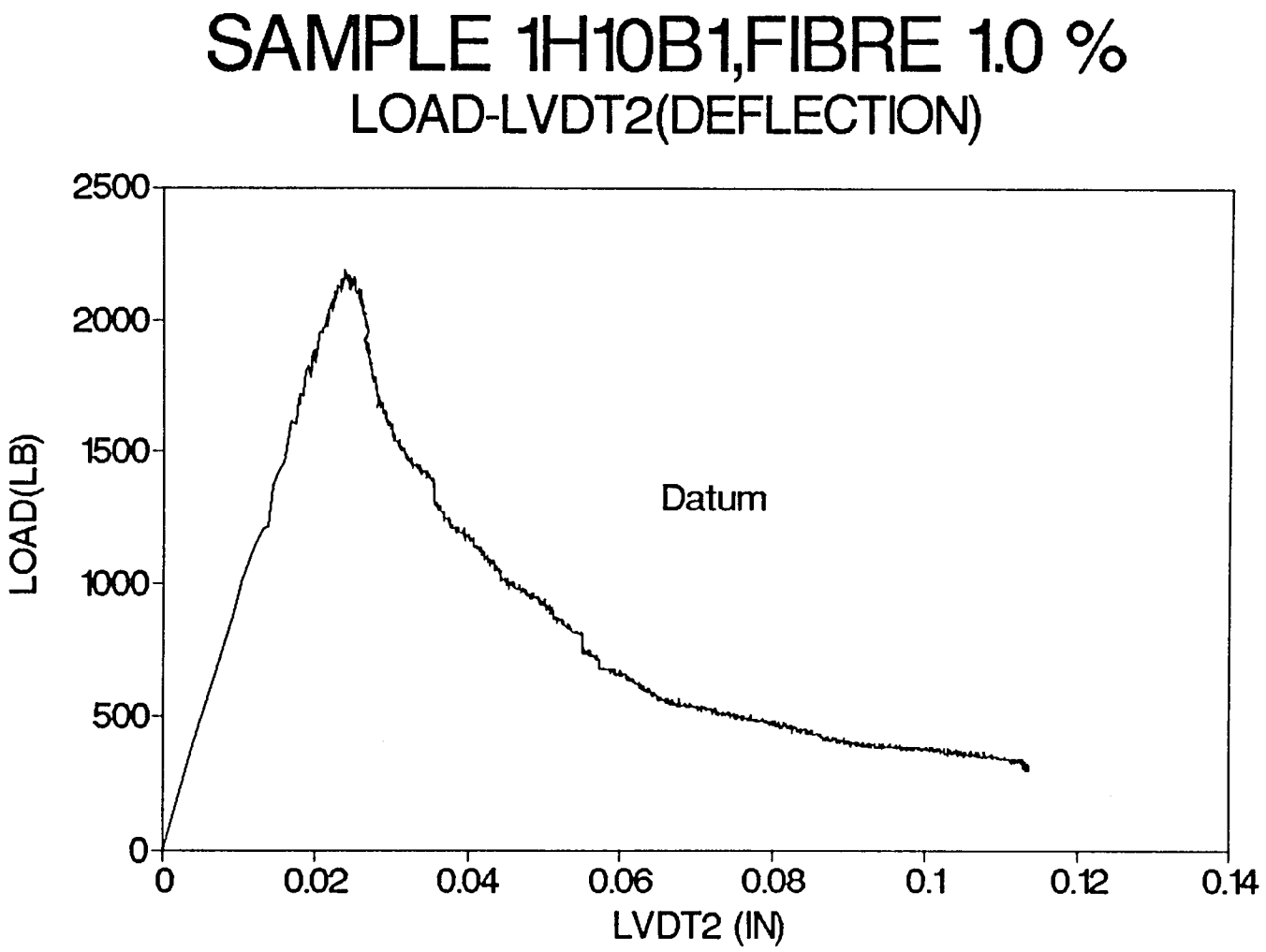

Figure A 1.1c Load-Deflection (Datum) Relationship

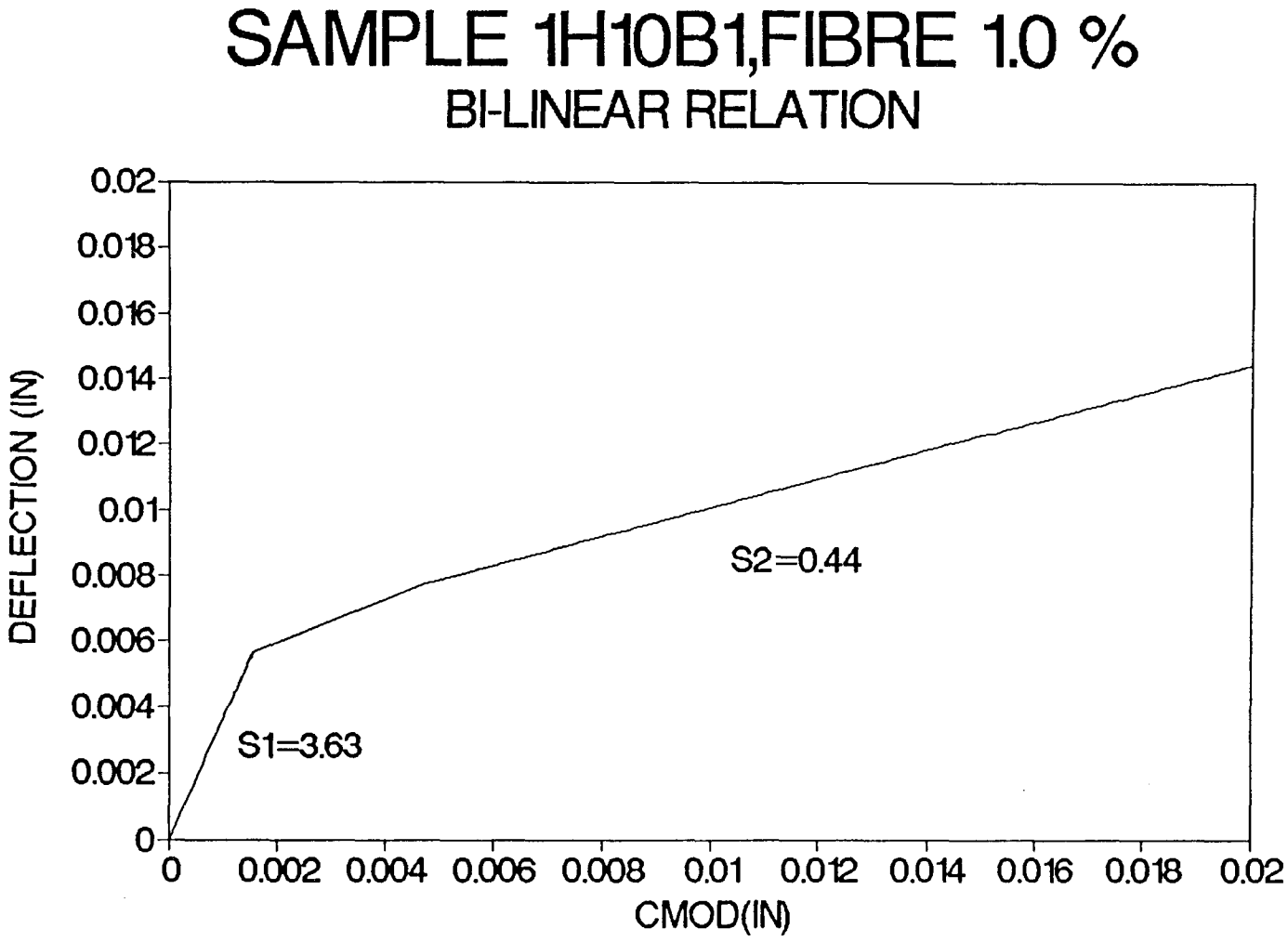

Figure A 1.1d Bilinear CMOD-Deflection Relationship

BEAM CODE	3H15B1	
CAST DATE		
TEST DATE	1-6-92	
LENGTH	27.0	inch
DEPTH	6.1	inch
WIDTH	3.0	inch
KNOTCH DEPTH	1.1	inch
SPAN LENGTH	24	inch
LEG SPAN	24.0	inch
FIBRE TYPE	HAREX	
length	1.0	inch
%	1.5	%
wt. (fibre)	10.3	lbs
MIX P CEMENT TYPEI	34.6	lbs
SAND PASSED #4 SIE	80.2	lbs
#3/8 inch AGGREGAT	80.2	lbs
WATER	15.9	lbs
MAXIMUM LOAD	3681.64	lbs
A	0.181169	
V1(A)	1.446189	
V2(A)	0.149259	
S/D	3.958442	
E	3202588	psi
S1	3.572175	
S2	0.955862	

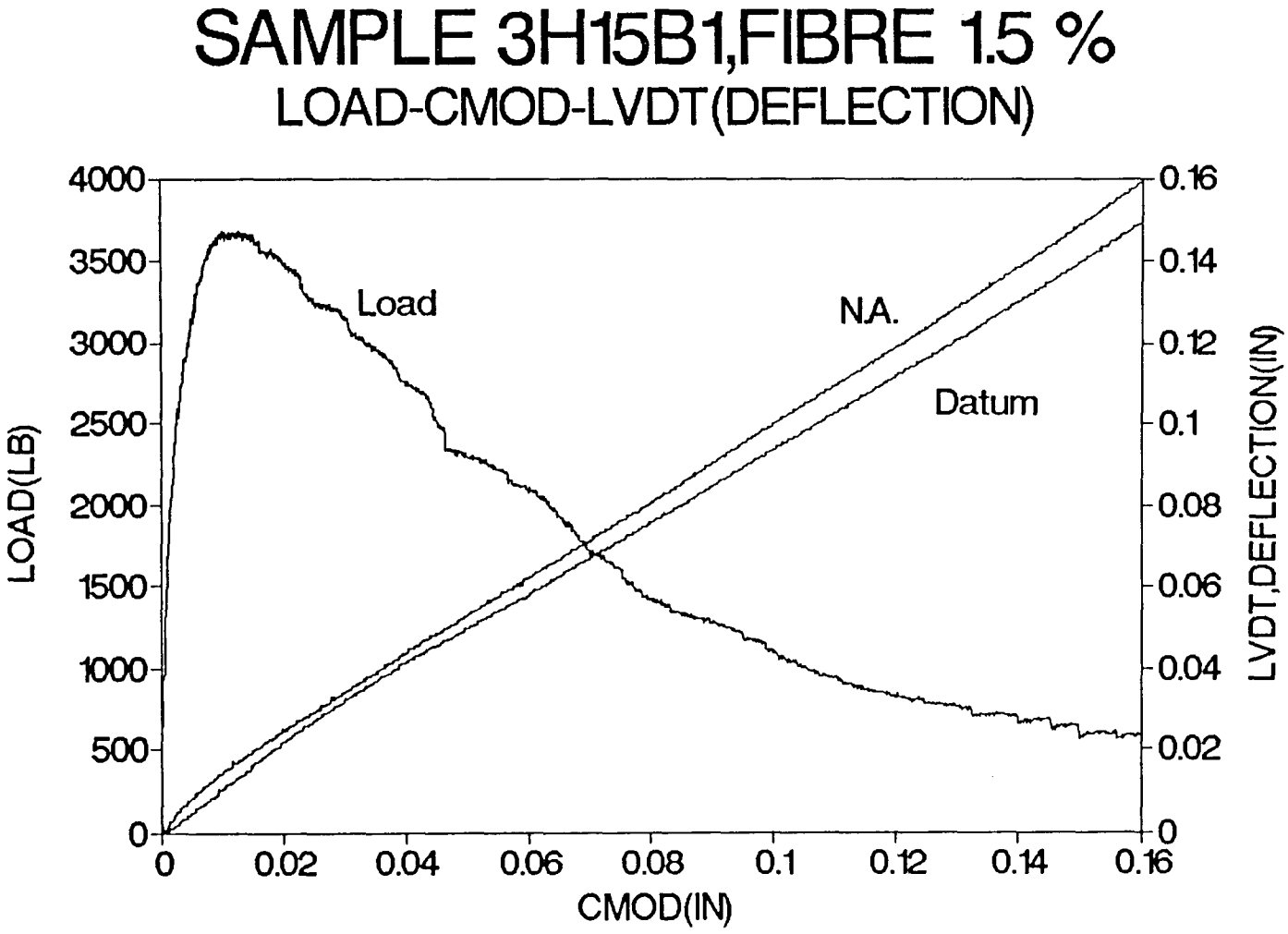

Figure A 1.2a Load-CMOD-Deflection Relationship

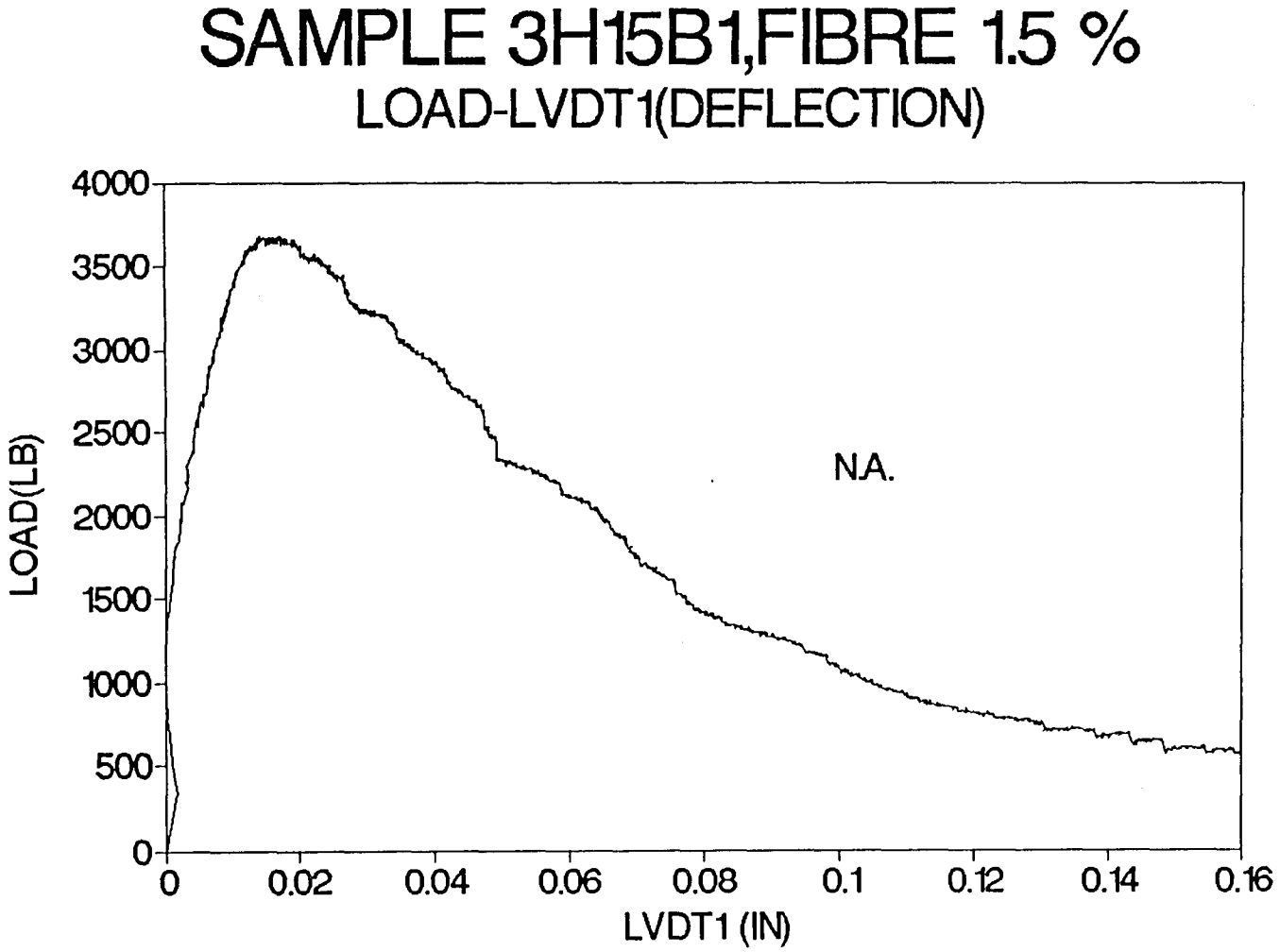

Figure A 1.2b Load-Deflection (N.A.) Relationship

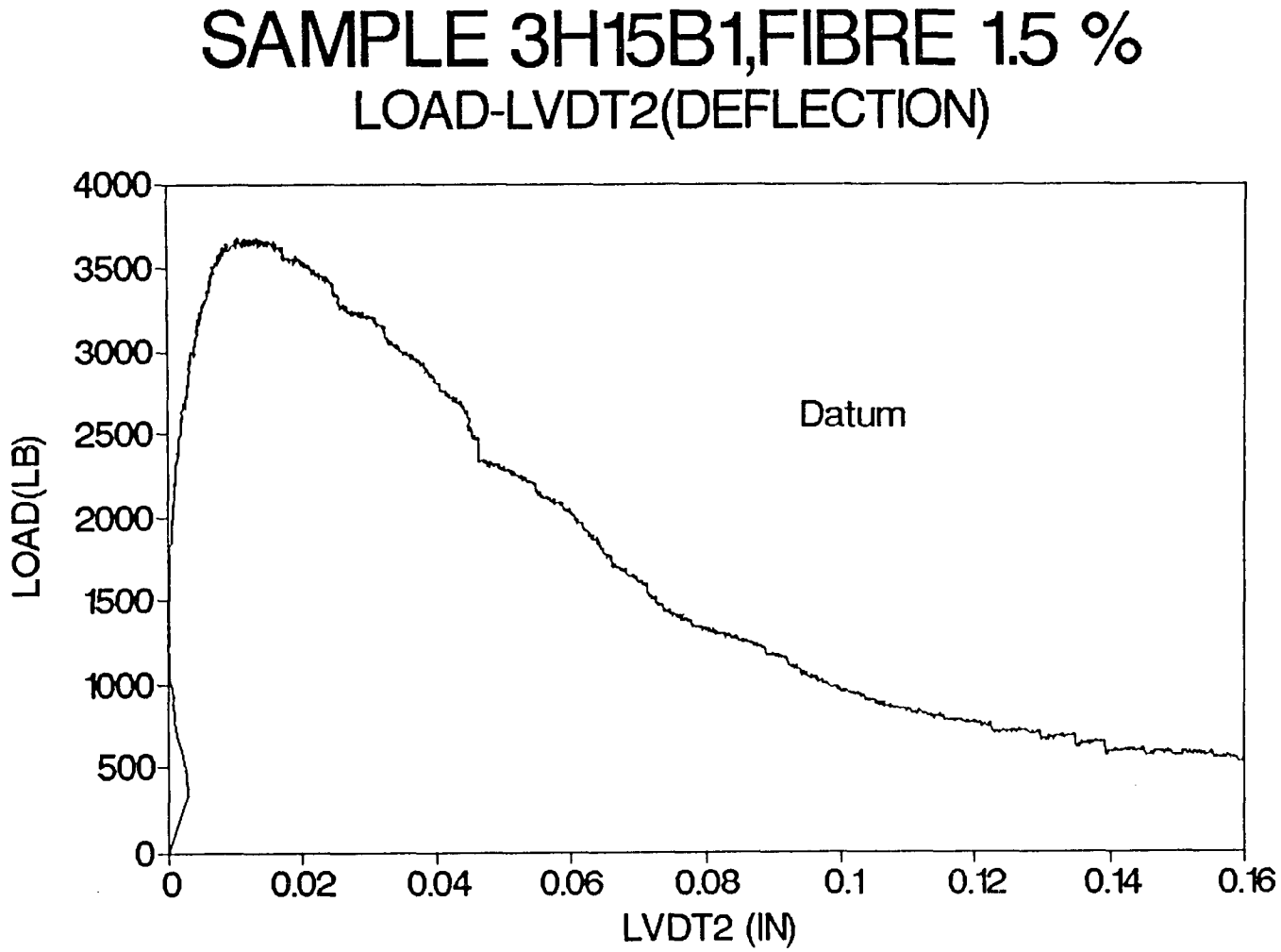

Figure A 1.2c Load-Deflection (Datum) Relationship

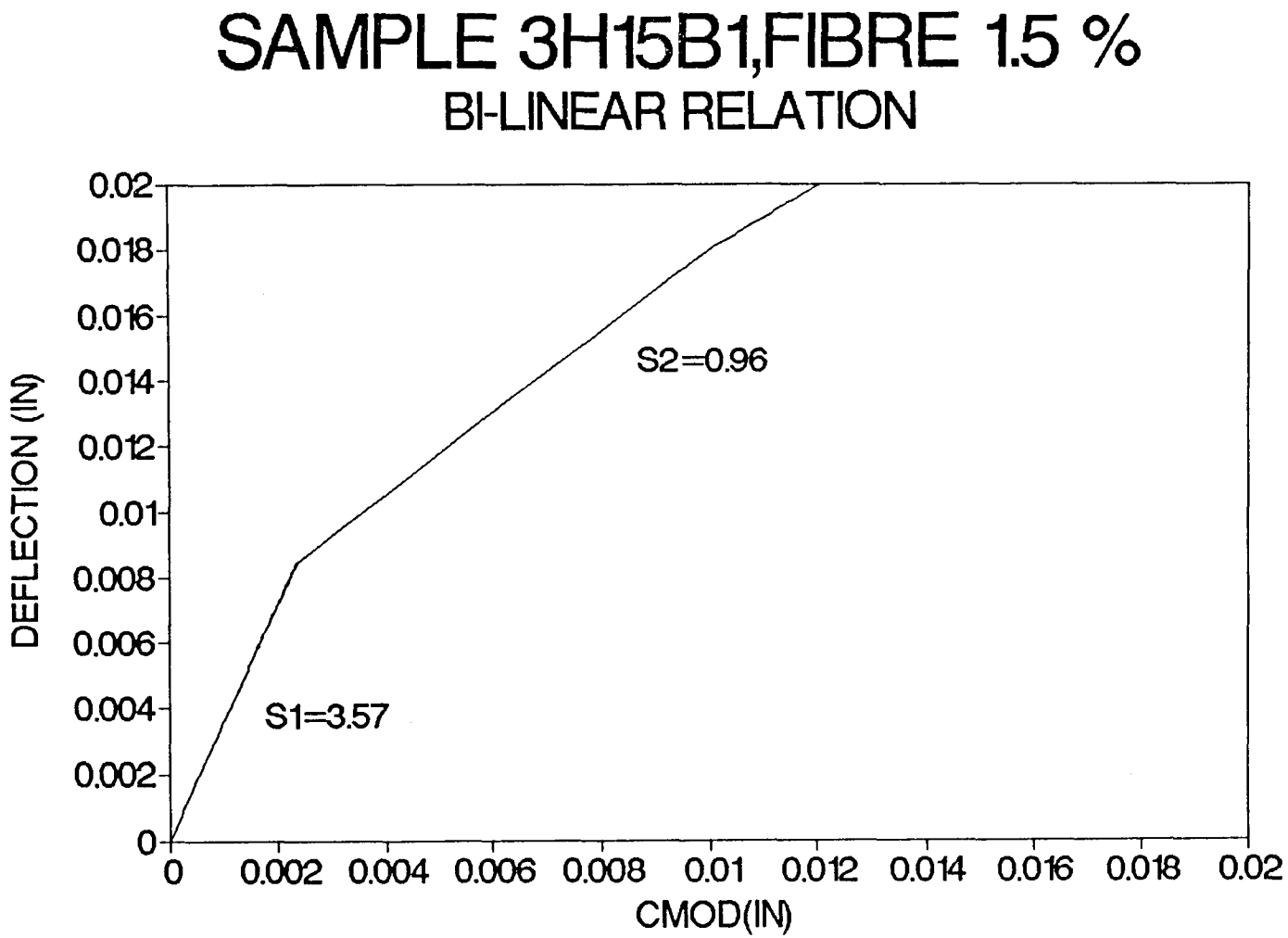

Figure A 1.2d Bilinear CMOD-Deflection Relationship

BEAM CODE		1C05B1
CAST DATE		8-28-91
TEST DATE		12-19-91
LENGTH		27.1 inch
DEPTH		6.1 inch
WIDTH		3.0 inch
KNOTCH DEPTH		1.1 inch
SPAN LENGTH		24 inch
LEG SPAN		24.0 inch
FIBRE TYPE		CRIMPED
length		1.0 inch
%		0.5 %
wt. (fibre)		3.4 lbs
MIX P	CEMENT TYPEI	35.0 lbs
	SAND PASSED #4 SIE	81.0 lbs
	#3/8 inch AGGREGAT	81.0 lbs
	WATER	16.1 lbs
MAXIMUM LOAD		1640.63 lbs
A		0.175974
V1(A)		1.439495
V2(A)		0.141296
S/D		3.958442
E		3079912 psi
S1		3.663293
S2		1.052603

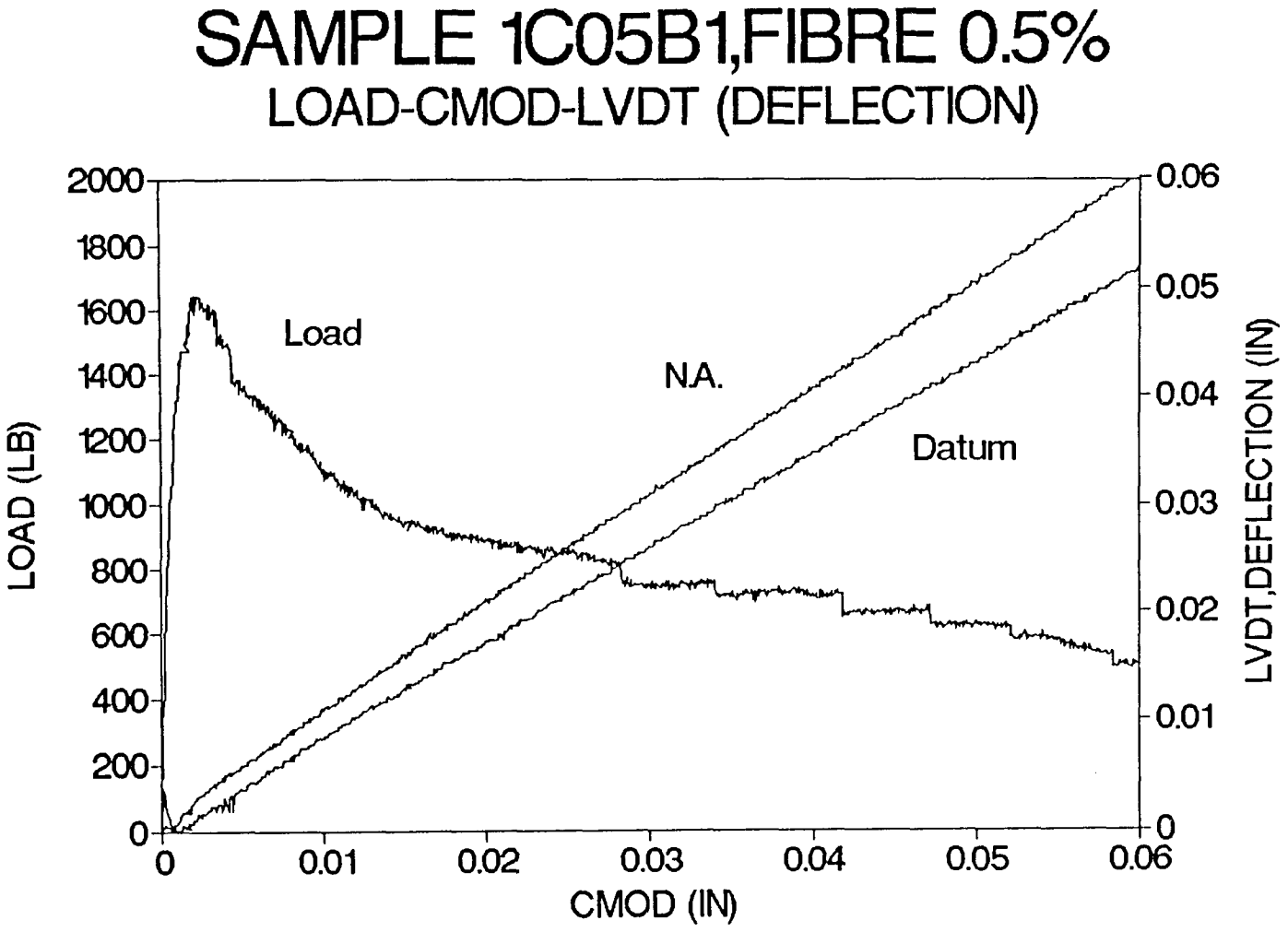

Figure A 1.3a Load-CMOD-Deflection Relationship

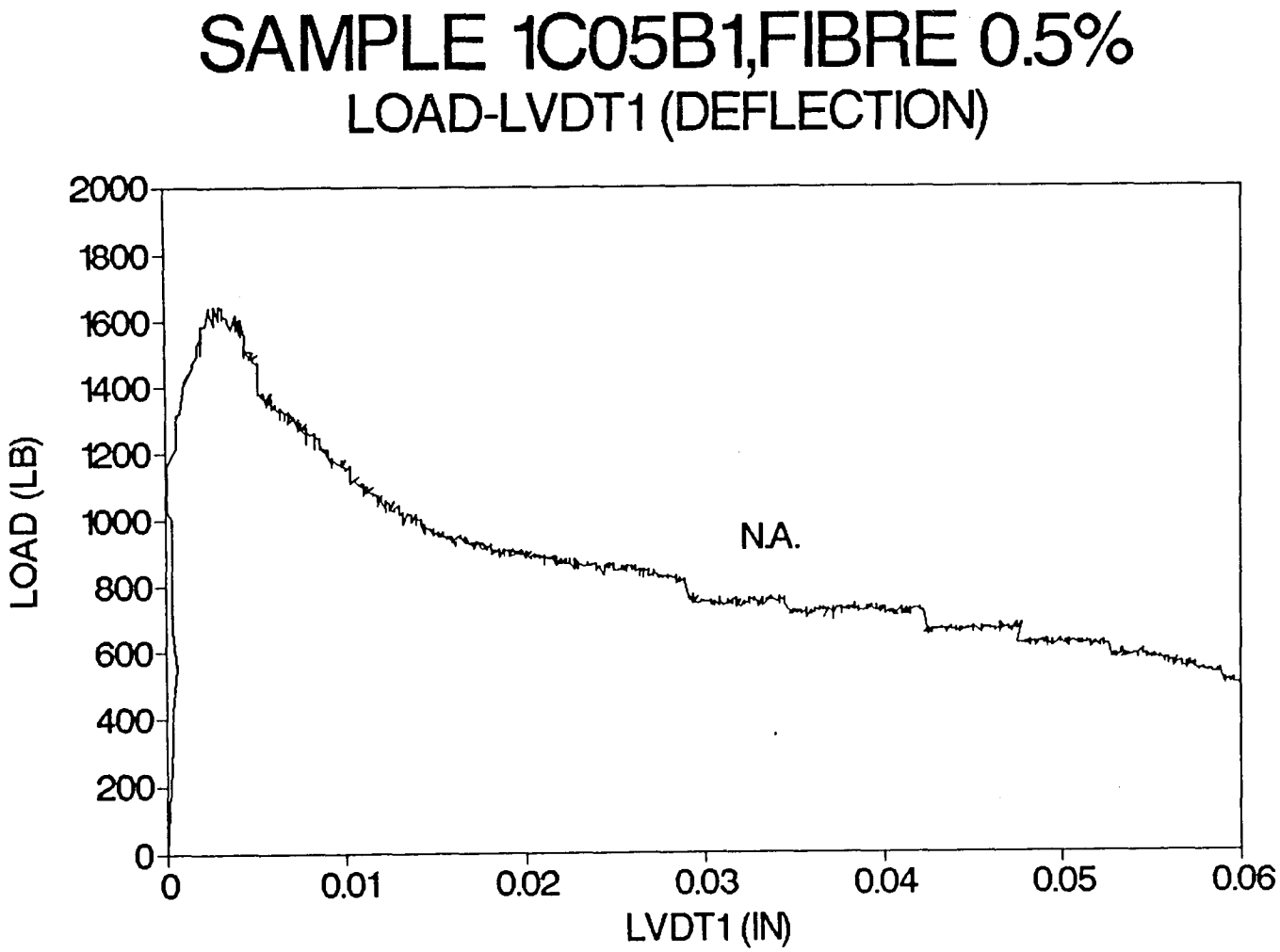

Figure A 1.3b Load-Deflection (N.A.) Relationship

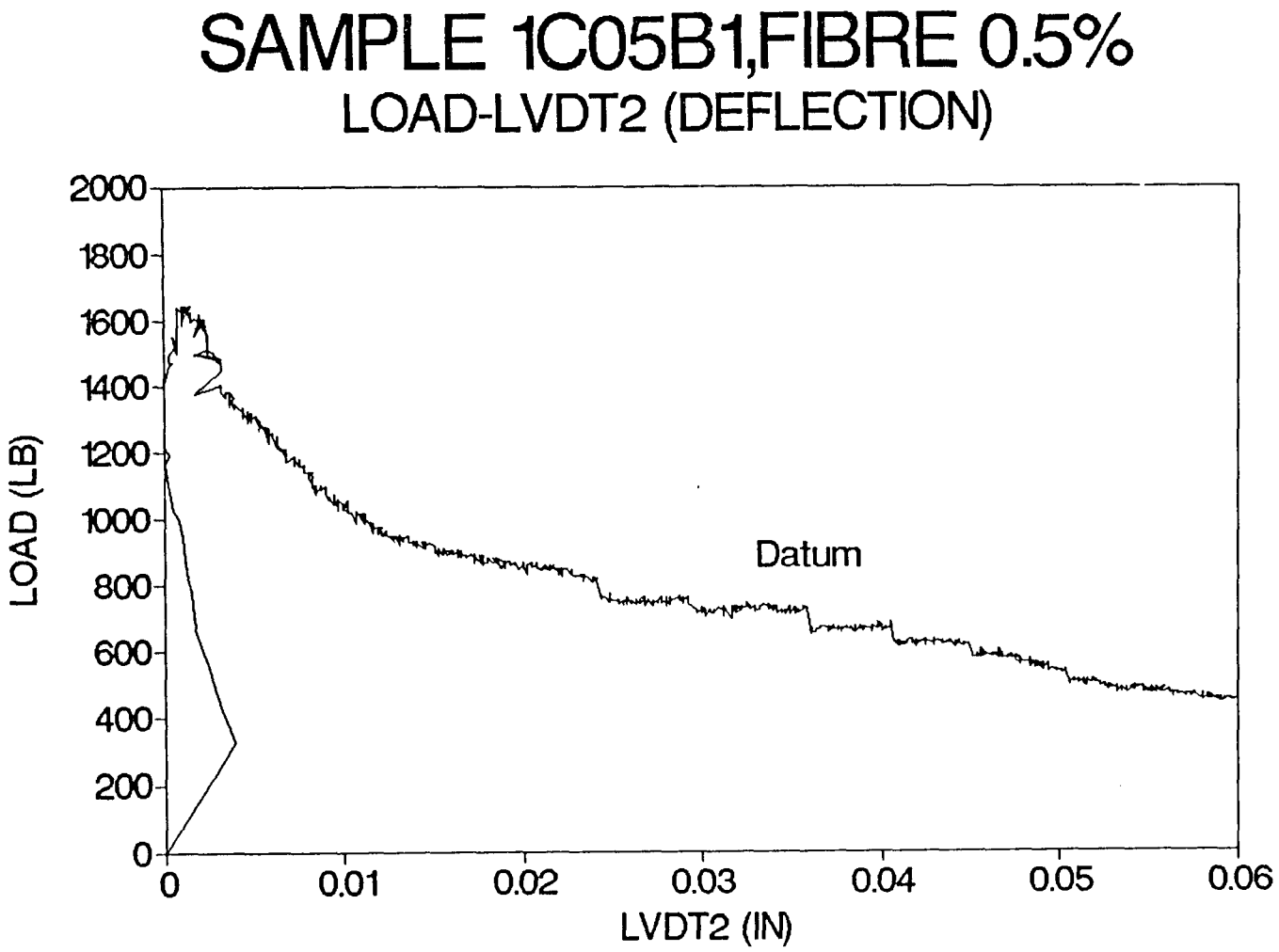

Figure A 1.3c Load-Deflection (Datum) Relationship

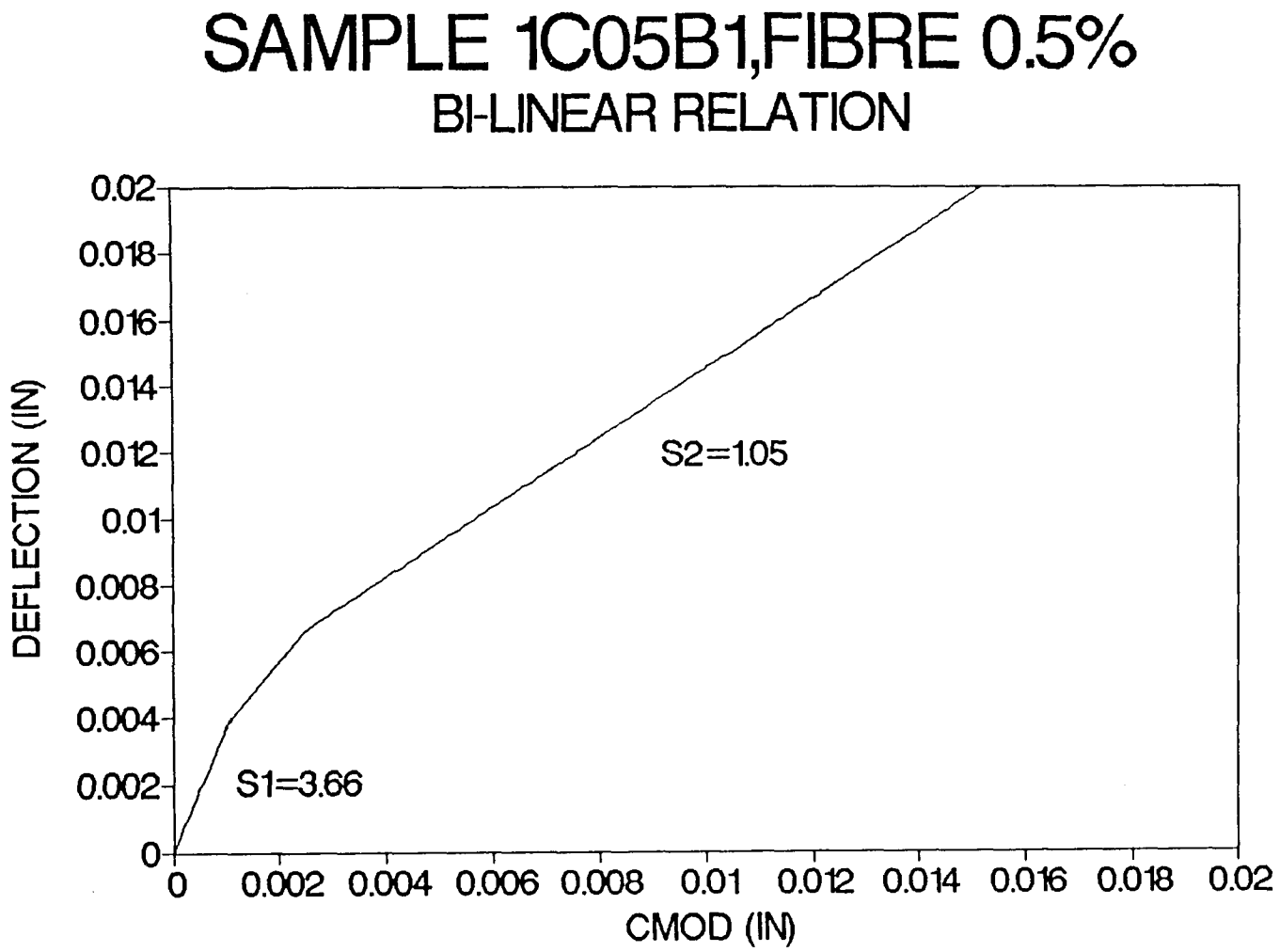

Figure A 1.3d Bilinear CMOD-Deflection Relationship

BEAM CODE		1C10B1
CAST DATE		9-3-91
TEST DATE		12-19-91
LENGTH		27.1 inch
DEPTH		6.3 inch
WIDTH		3.0 inch
KNOTCH DEPTH		1.2 inch
SPAN LENGTH		24 inch
LEG SPAN		24.0 inch
FIBRE TYPE		CRIMPED
length		1.0 inch
%		1.0 %
wt. (fibre)		6.9 lbs
MIX P	CEMENT TYPEI	34.7 lbs
	SAND PASSED #4 SIE	80.6 lbs
	#3/8 inch AGGREGAT	80.6 lbs
	WATER	16.0 lbs
MAXIMUM LOAD		2036.13 lbs
A		0.190566
V1(A)		1.459284
V2(A)		0.164221
S/D		3.833962
E		3241097 psi
S1		3.419354
S2		1.052603

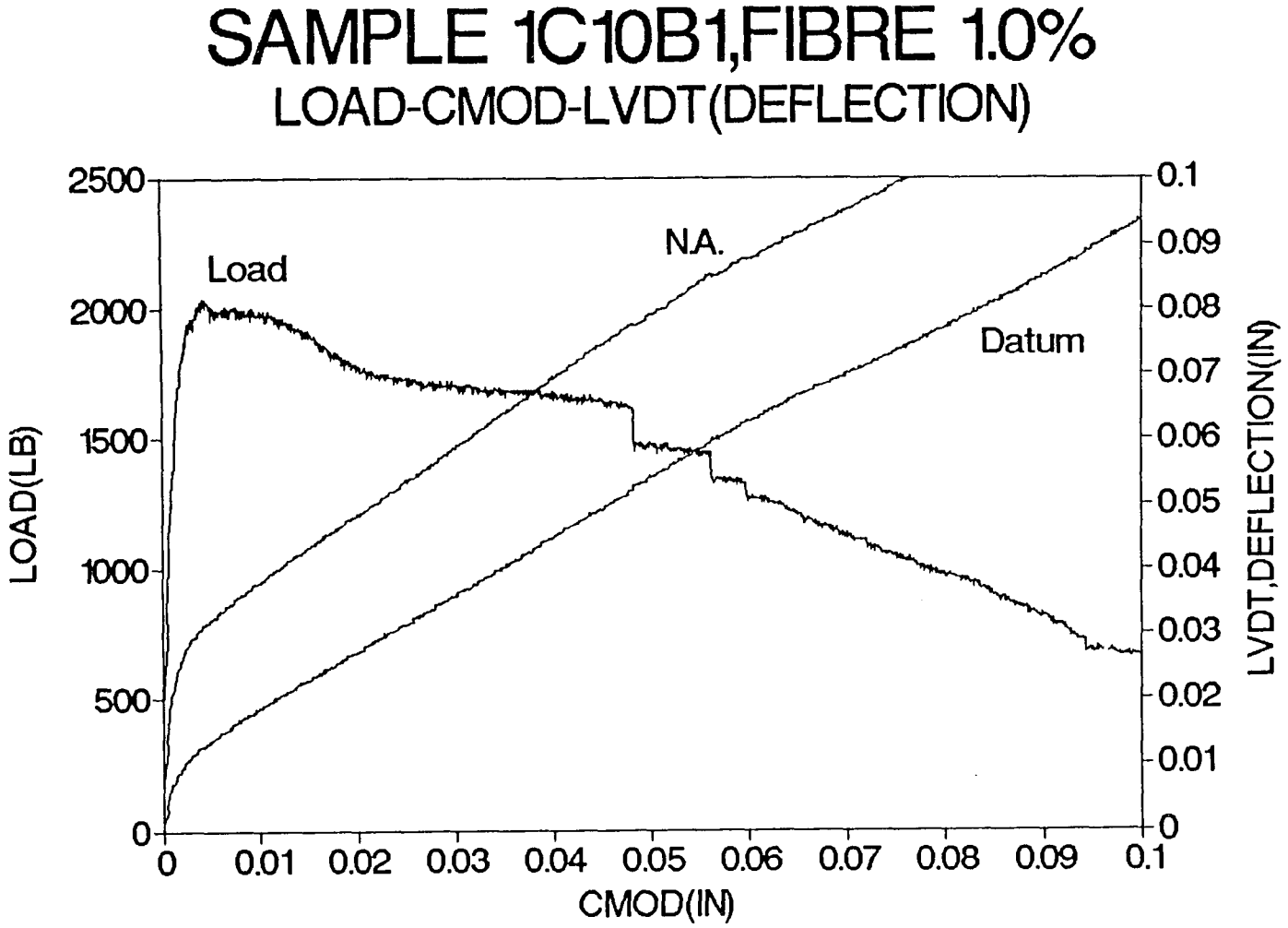

Figure A 1.4a Load-CMOD-Deflection Relationship

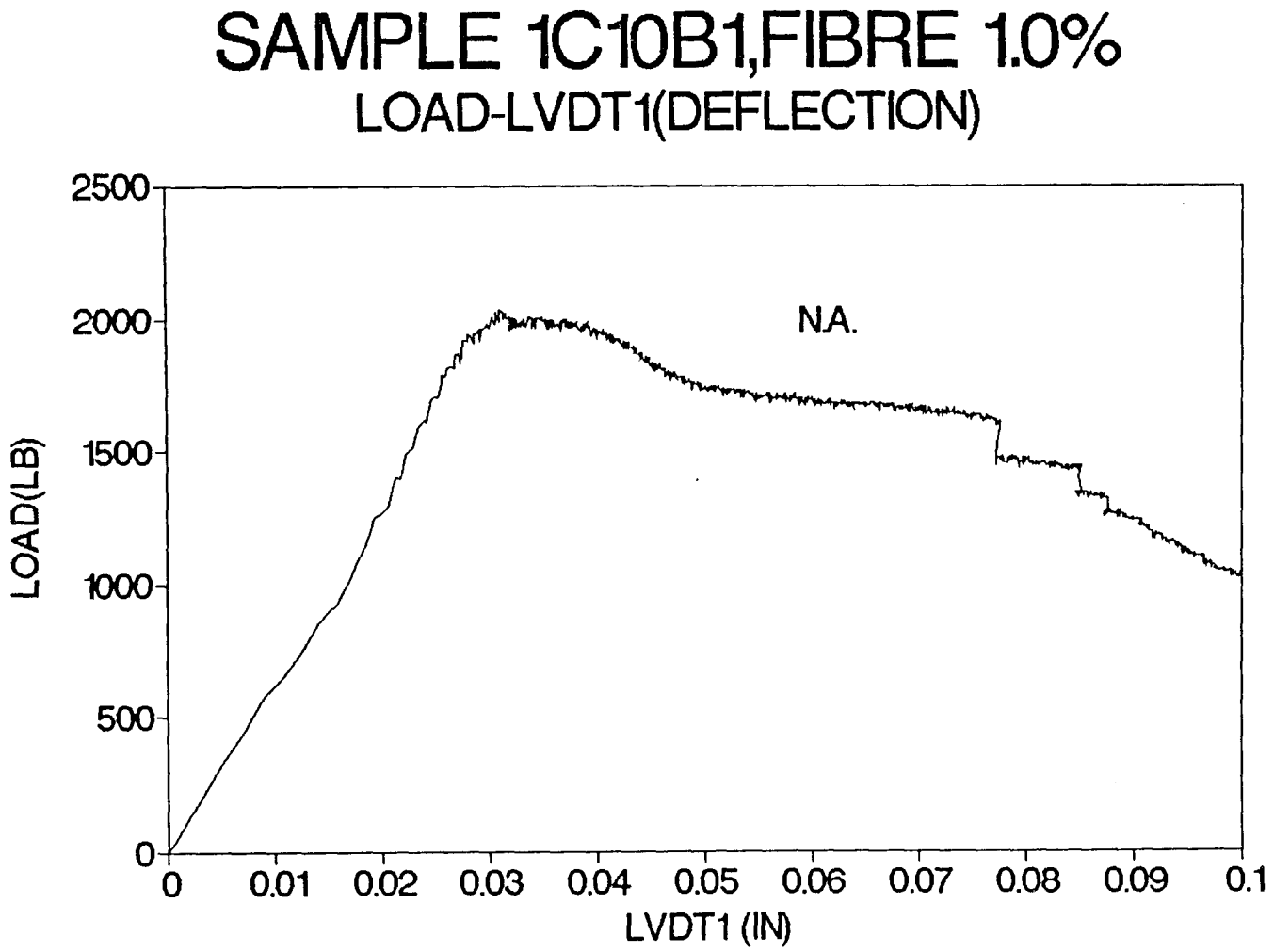

Figure A 1.4b Load-Deflection (N.A.) Relationship

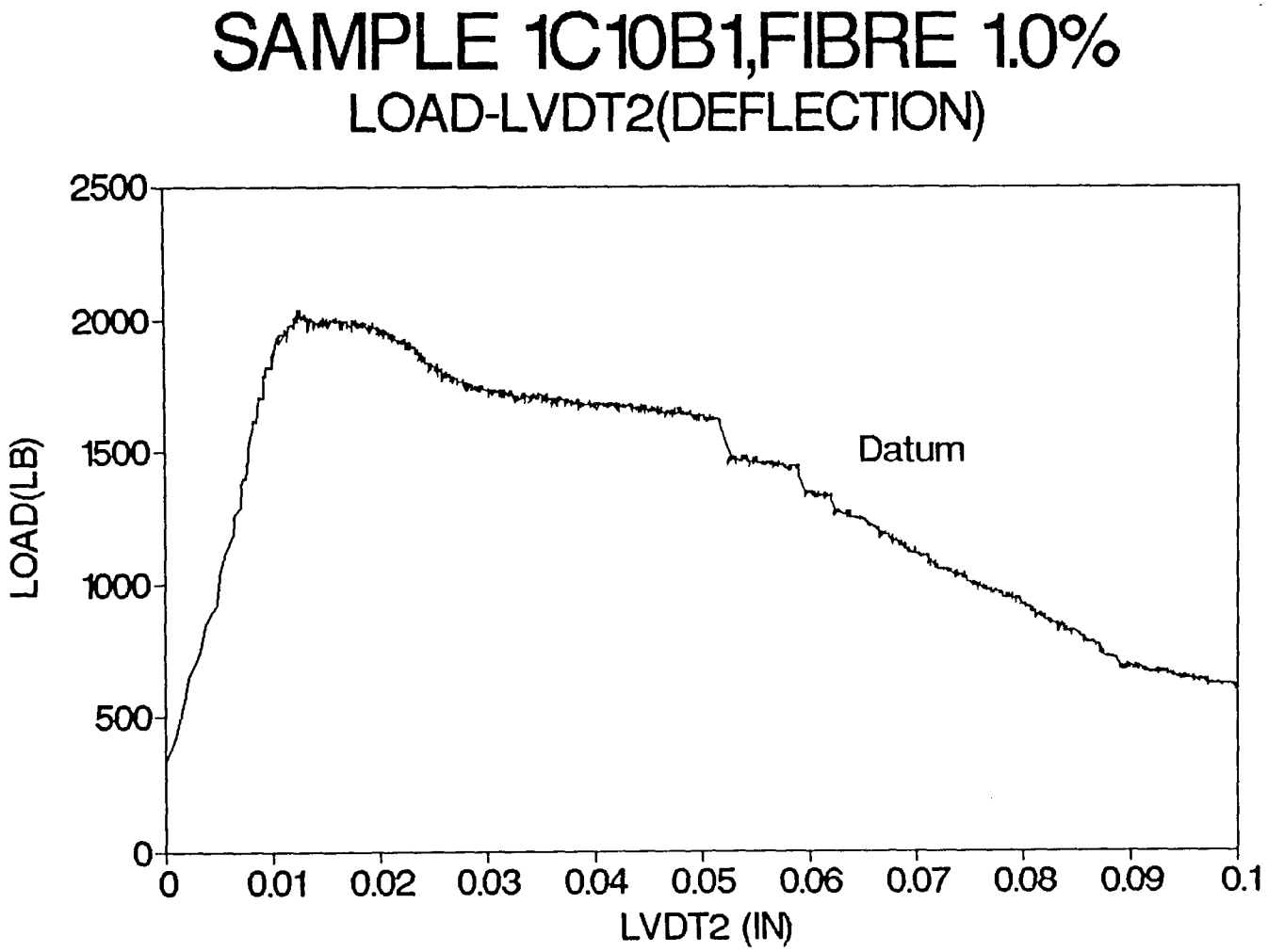

Figure A 1.4c Load-Deflection (Datum) Relationship

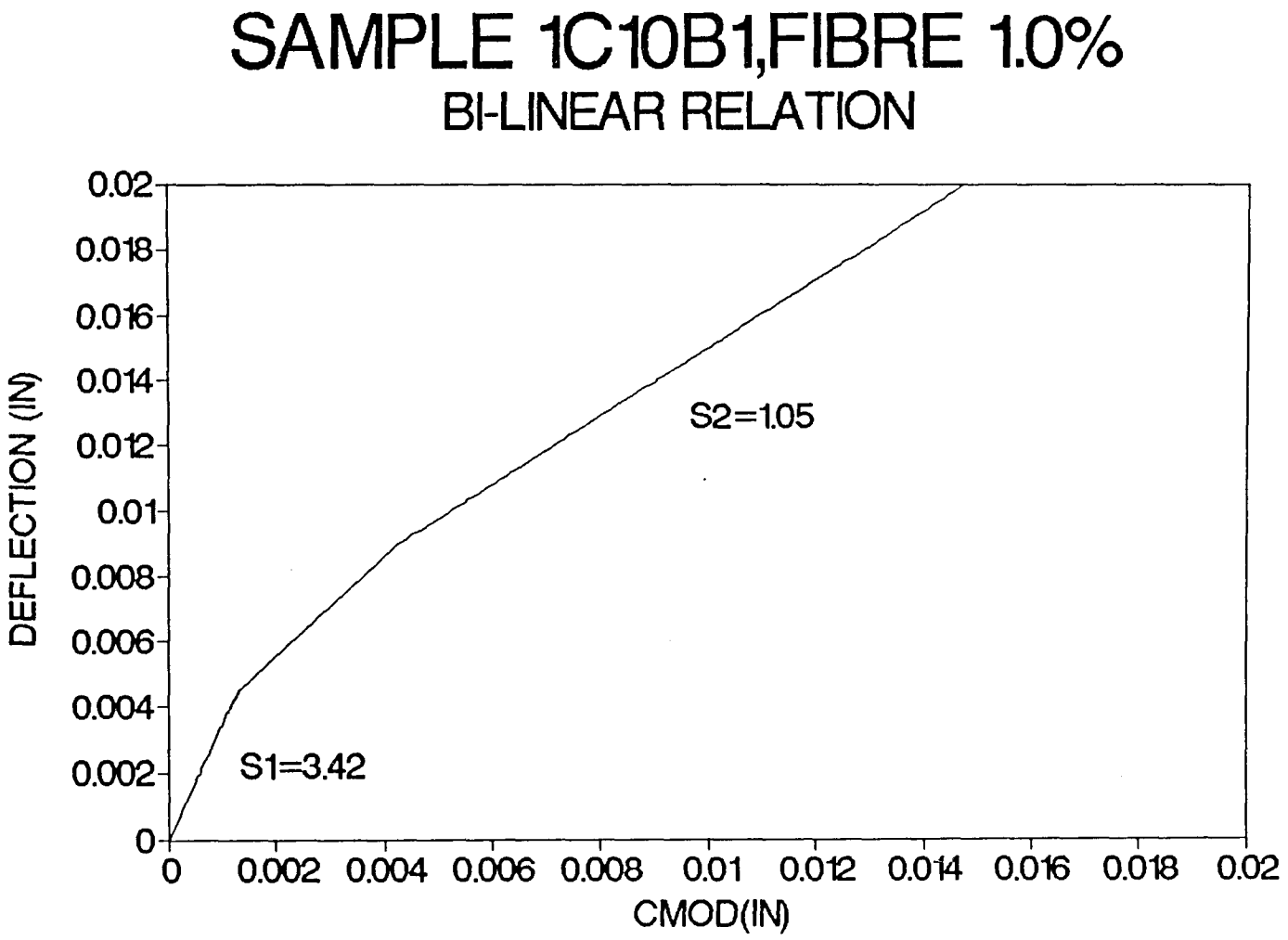

Figure A 1.4d Bilinear CMOD-Deflection Relationship

BEAM CODE	2C15B1	
CAST DATE	9-6-91	
TEST DATE	12-27-91	
LENGTH	27.0	inch
DEPTH	6.2	inch
WIDTH	3.0	inch
KNOTCH DEPTH	1.1	inch
SPAN LENGTH	24	inch
LEG SPAN	24.1	inch
FIBRE TYPE	CRIMPED	
length	1.0	inch
%	1.5	%
wt. (fibre)	10.3	lbs
MIX P CEMENT TYPEI	34.6	lbs
SAND PASSED #4 SIE	80.2	lbs
#3/8 inch AGGREGAT	80.2	lbs
WATER	15.9	lbs
MAXIMUM LOAD	2622.07	lbs
A	0.18038	
V1(A)	1.445147	
V2(A)	0.148035	
S/D	3.858228	
E	3210212	psi
S1	3.585694	
S2	0.955862	

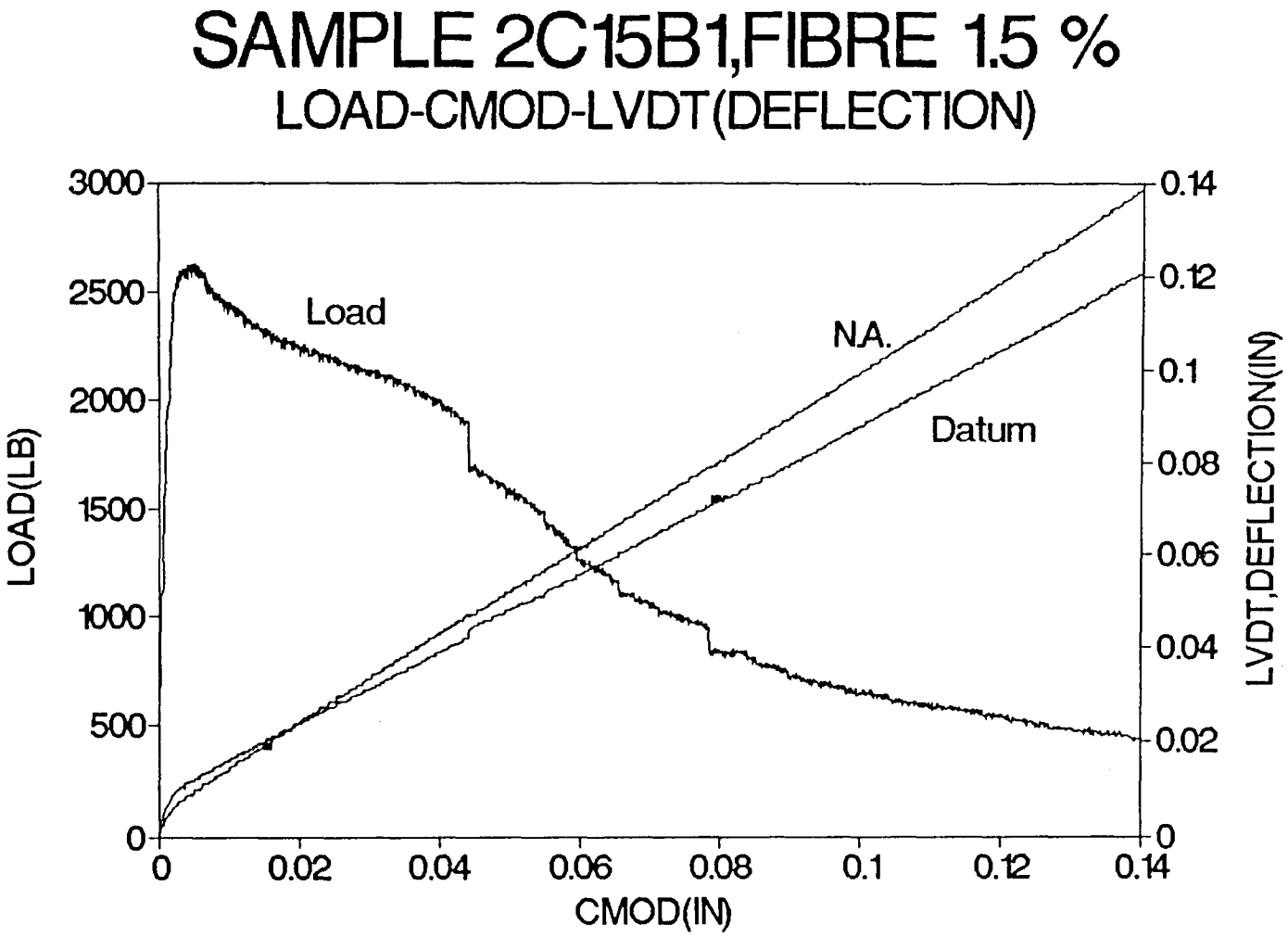

Figure A 1.5a Load-CMOD-Deflection Relationship

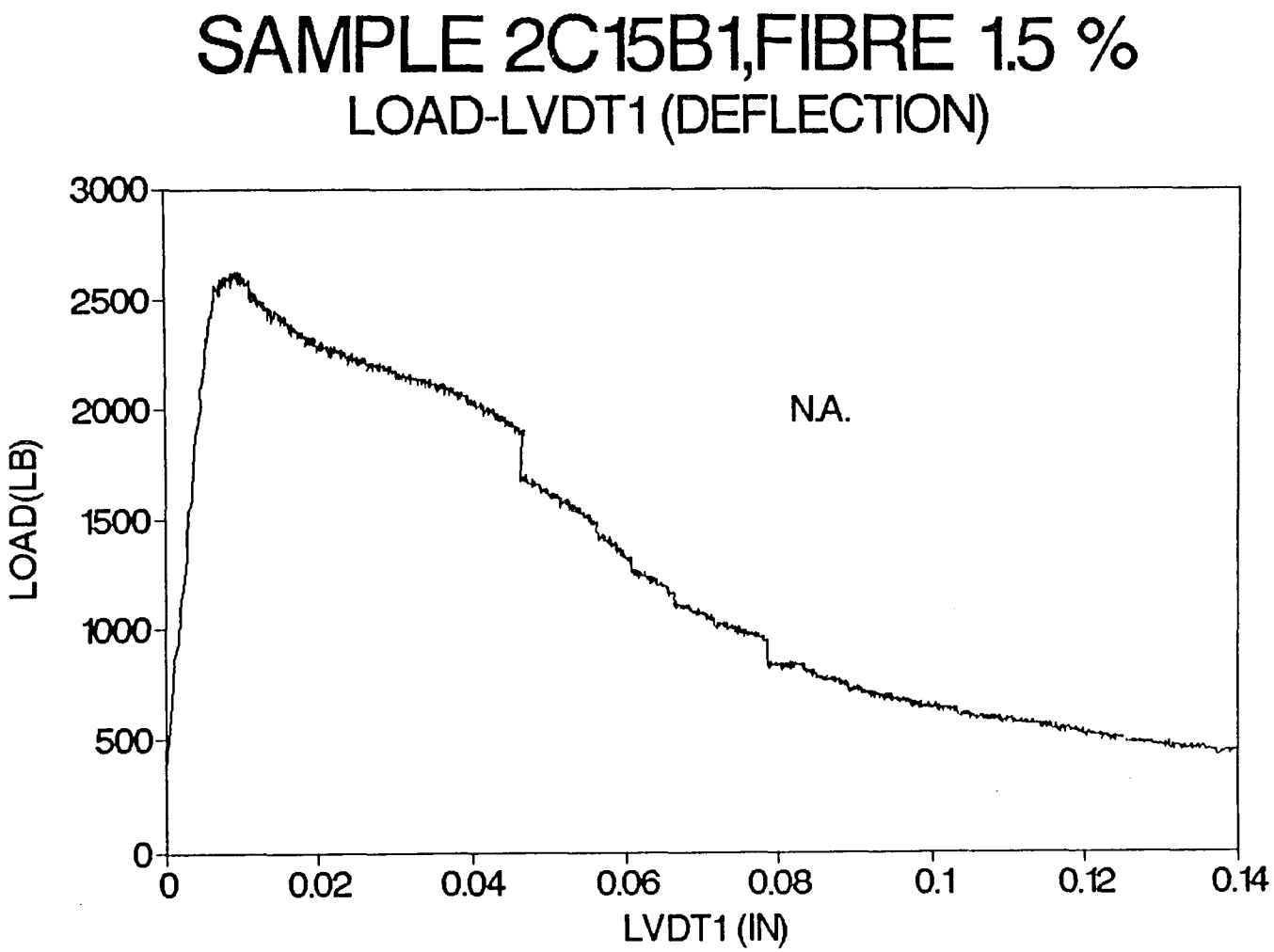

Figure A 1.5b Load-Deflection (N.A.) Relationship

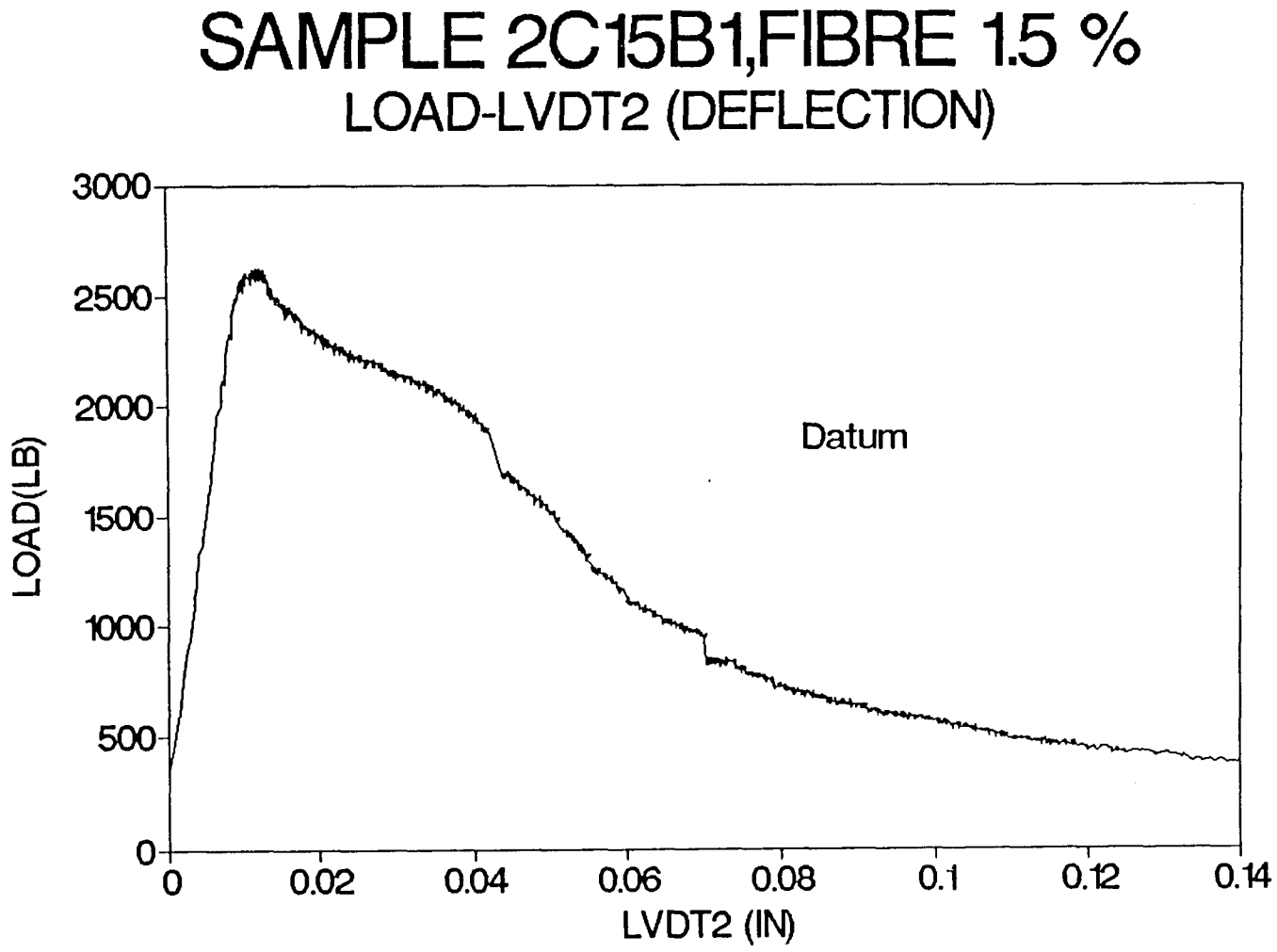

Figure A 1.5c Load-Deflection (Datum) Relationship

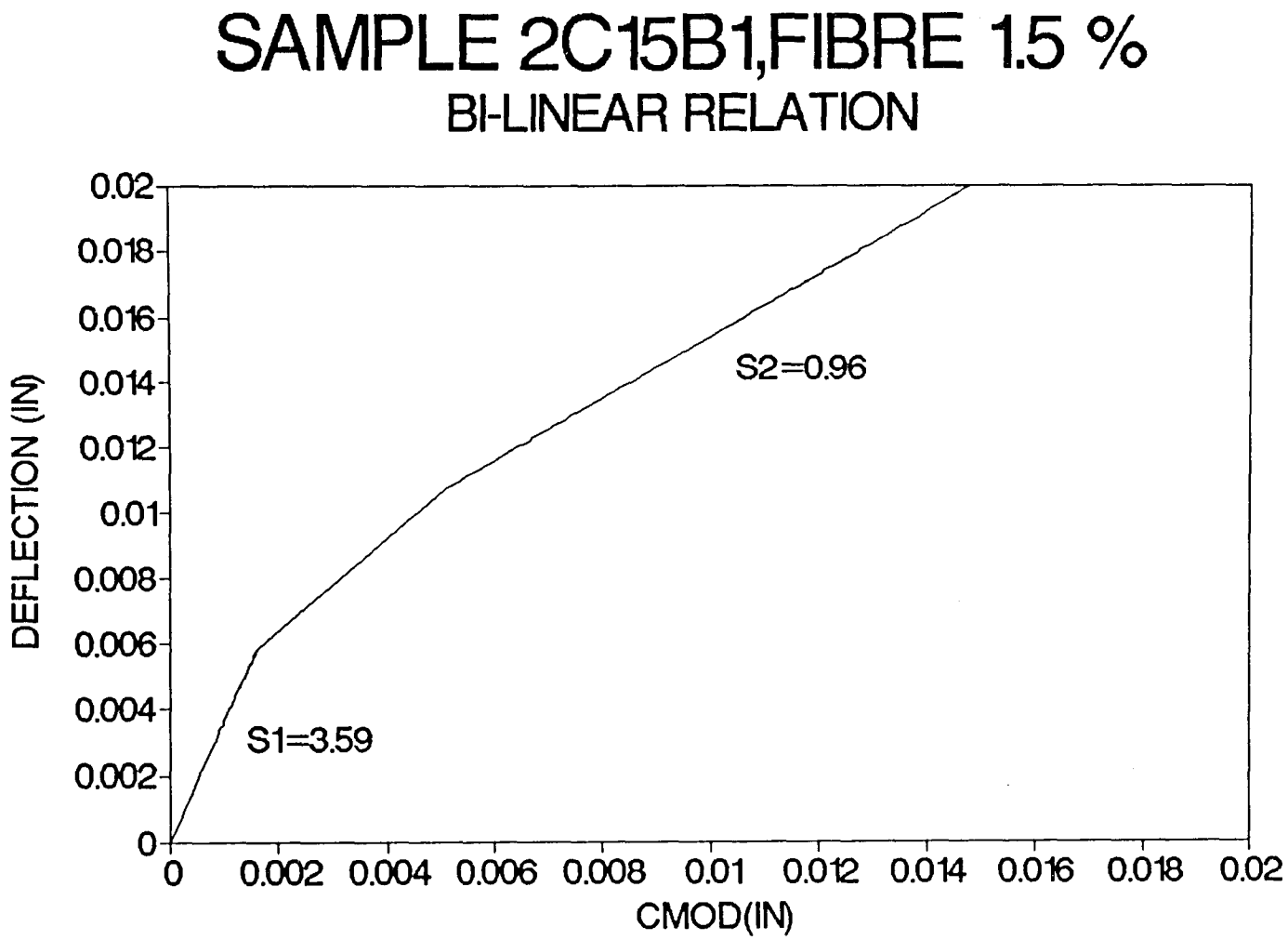

Figure A 1.5d Bilinear CMOD-Deflection Relationship

BEAM CODE	1D05B1	
CAST DATE	8-27-91	
TEST DATE	12-19-91	
LENGTH	27.0	inch
DEPTH	6.1	inch
WIDTH	3.1	inch
KNOTCH DEPTH	1.1	inch
SPAN LENGTH	24	inch
LEG SPAN	23.9	inch
FIBRE TYPE	DRAMIX	
length	1.0	inch
%	0.5	%
wt. (fibre)	3.4	lbs
MIX P CEMENT TYPEI	35.0	lbs
SAND PASSED #4 SIE	81.0	lbs
#3/8 inch AGGREGAT	81.0	lbs
WATER	16.1	lbs
MAXIMUM LOAD	1420.9	lbs
A	0.177419	
V1(A)	1.441319	
V2(A)	0.14349	
S/D	3.932903	
E	2963948	psi
S1	3.637431	
S2	0.972238	

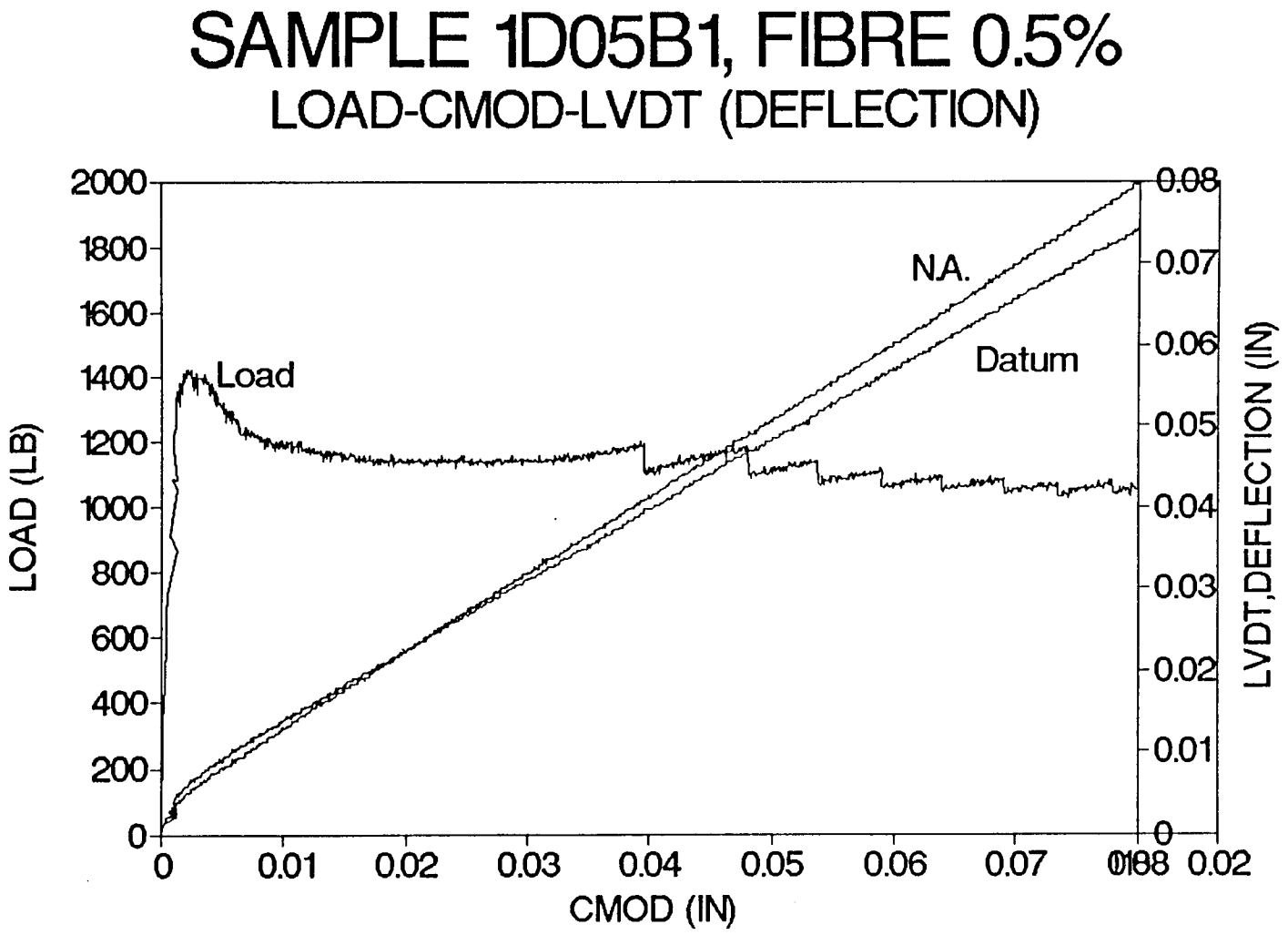

Figure A 1.6a Load-CMOD-Deflection Relationship

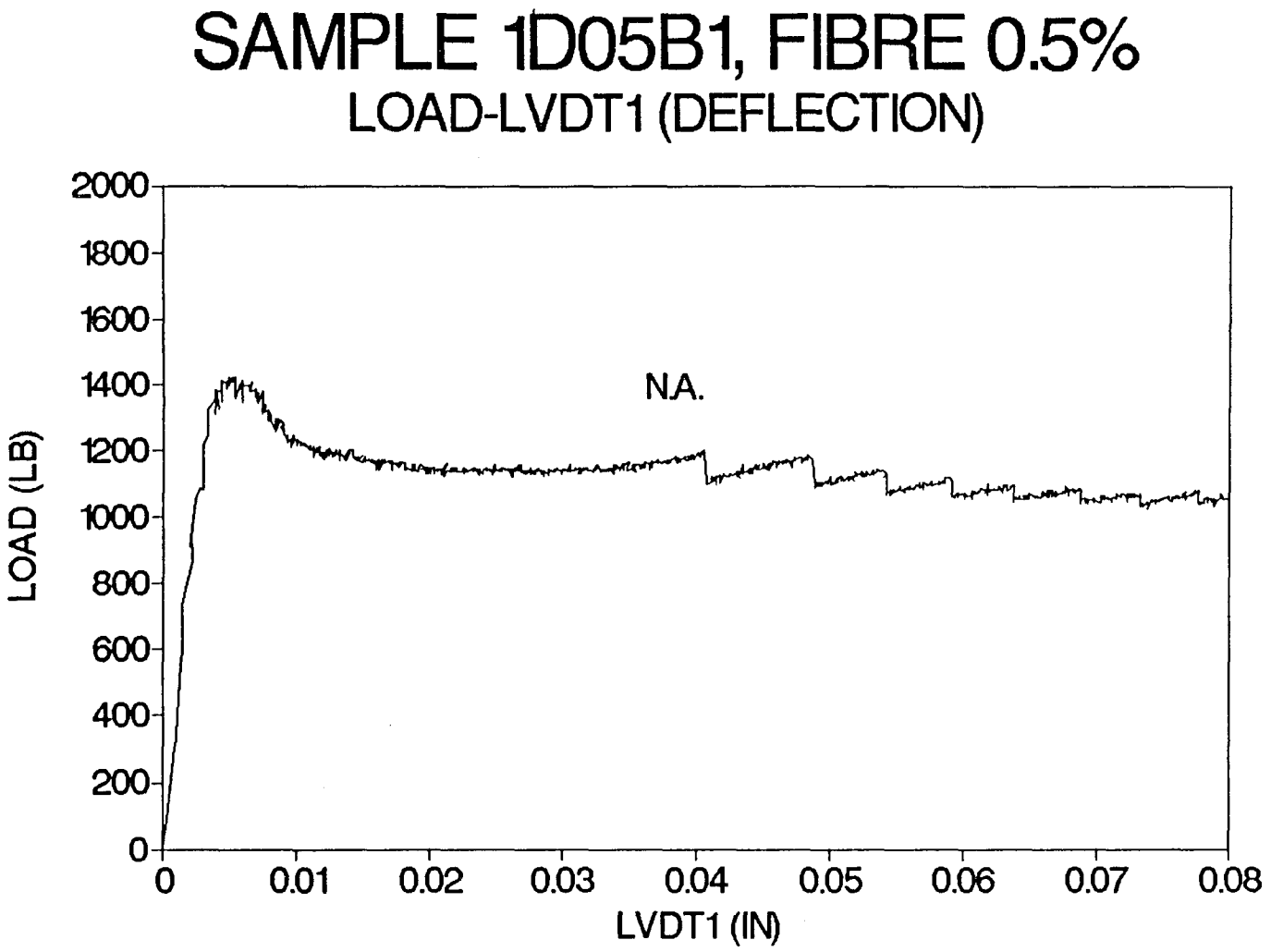

Figure A 1.6b Load-Deflection (N.A.) Relationship

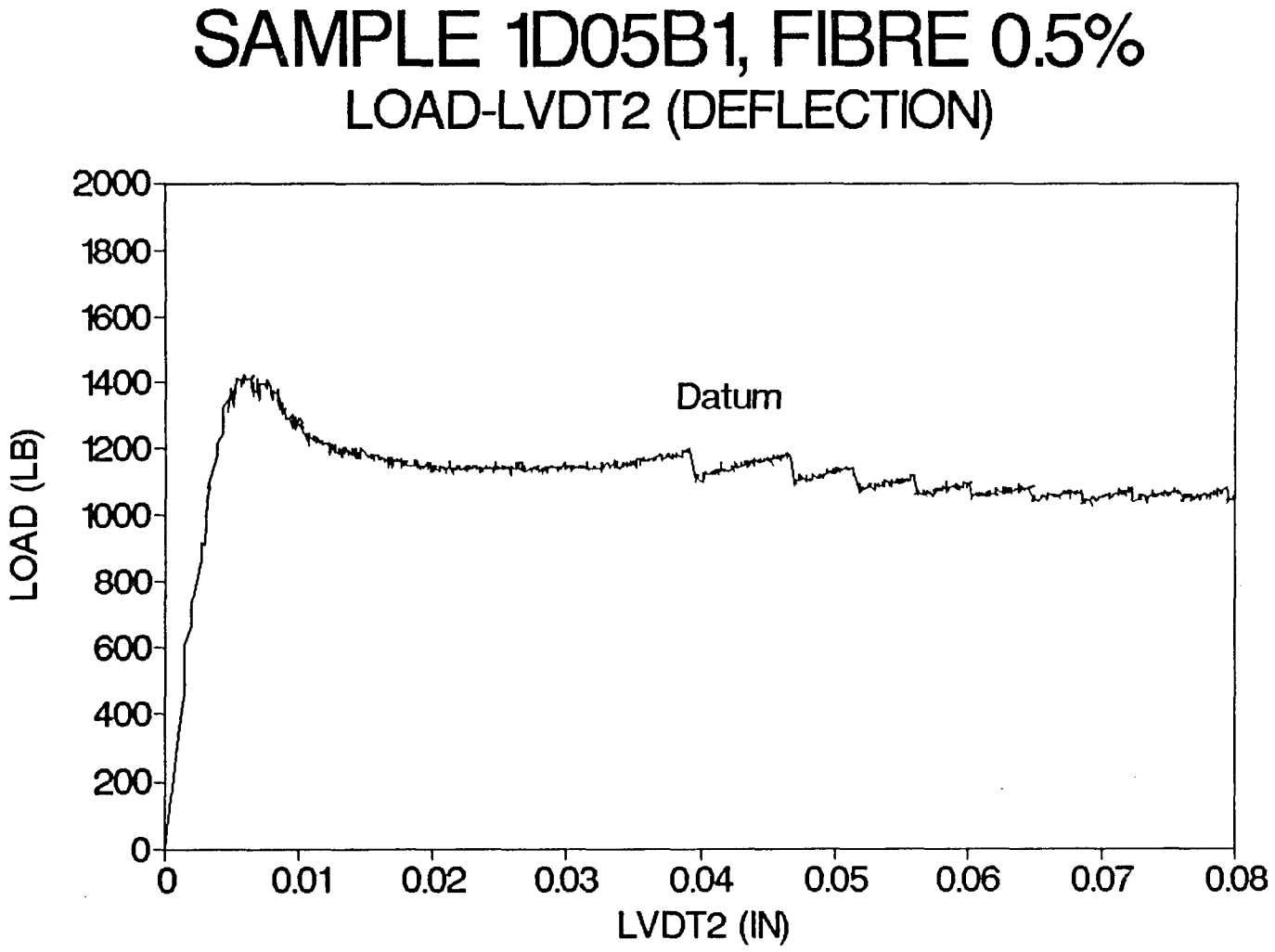

Figure A 1.6c Load-Deflection (Datum) Relationship

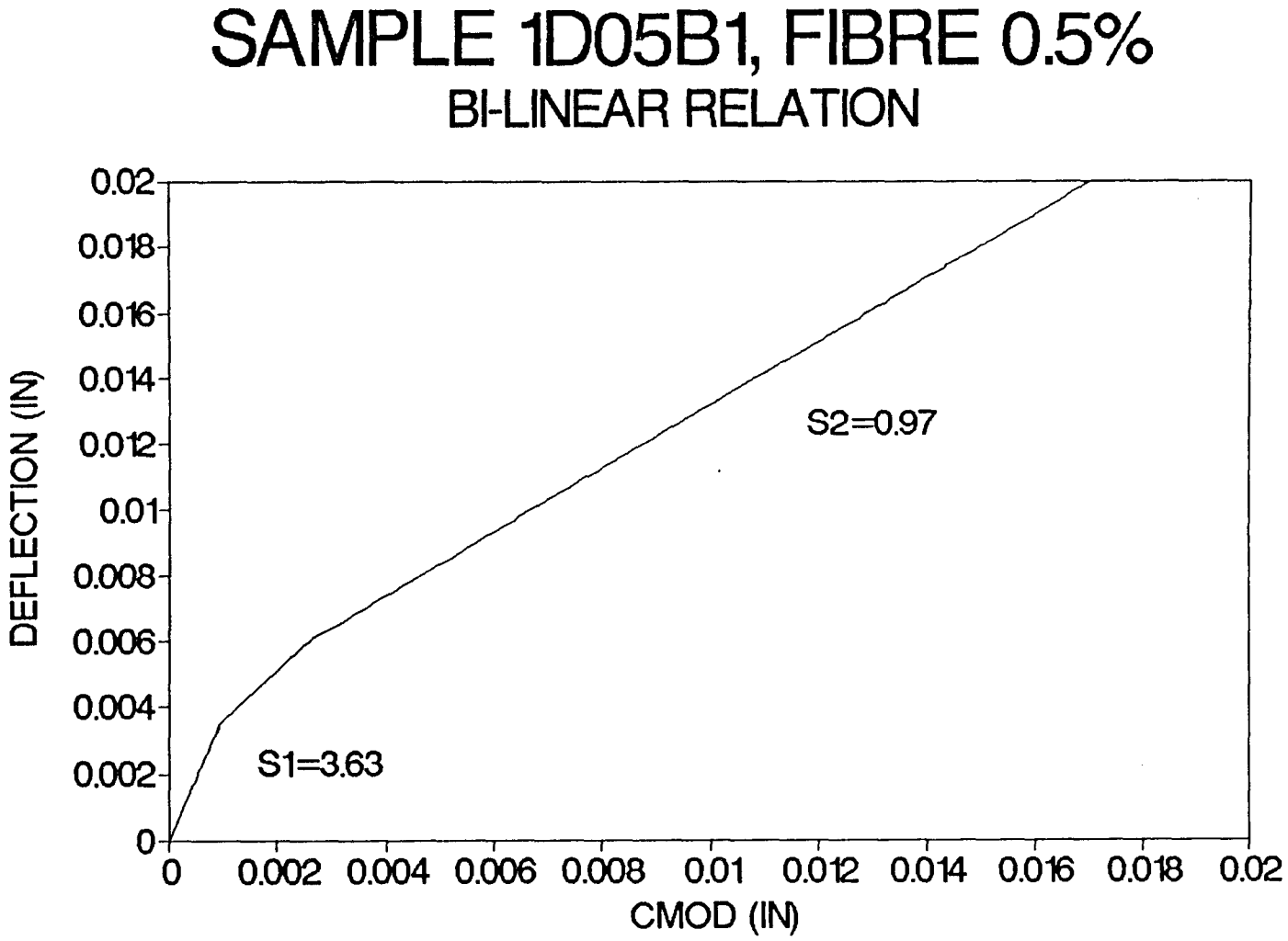

Figure A 1.6d Bilinear CMOD-Deflection Relationship

BEAM CODE	2D10B1	
CAST DATE		
TEST DATE	01-3-92	
LENGTH	27.1	inch
DEPTH	6.1	inch
WIDTH	3.0	inch
KNOTCH DEPTH	1.2	inch
SPAN LENGTH	24	inch
LEG SPAN	23.7	inch
FIBRE TYPE	DRAMIX	
length	1.0	inch
%	1.0	%
wt. (fibre)	6.9	lbs
MIX P CEMENT TYPEI	34.7	lbs
SAND PASSED #4 SIE	80.6	lbs
#3/8 inch AGGREGAT	80.6	lbs
WATER	16.0	lbs
MAXIMUM LOAD	285156	lbs
A	0.190323	
V1(A)	1.458928	
V2(A)	0.163825	
S/D	3.932903	
E	3044797	psi
S1	3.423133	
S2	0.942017	

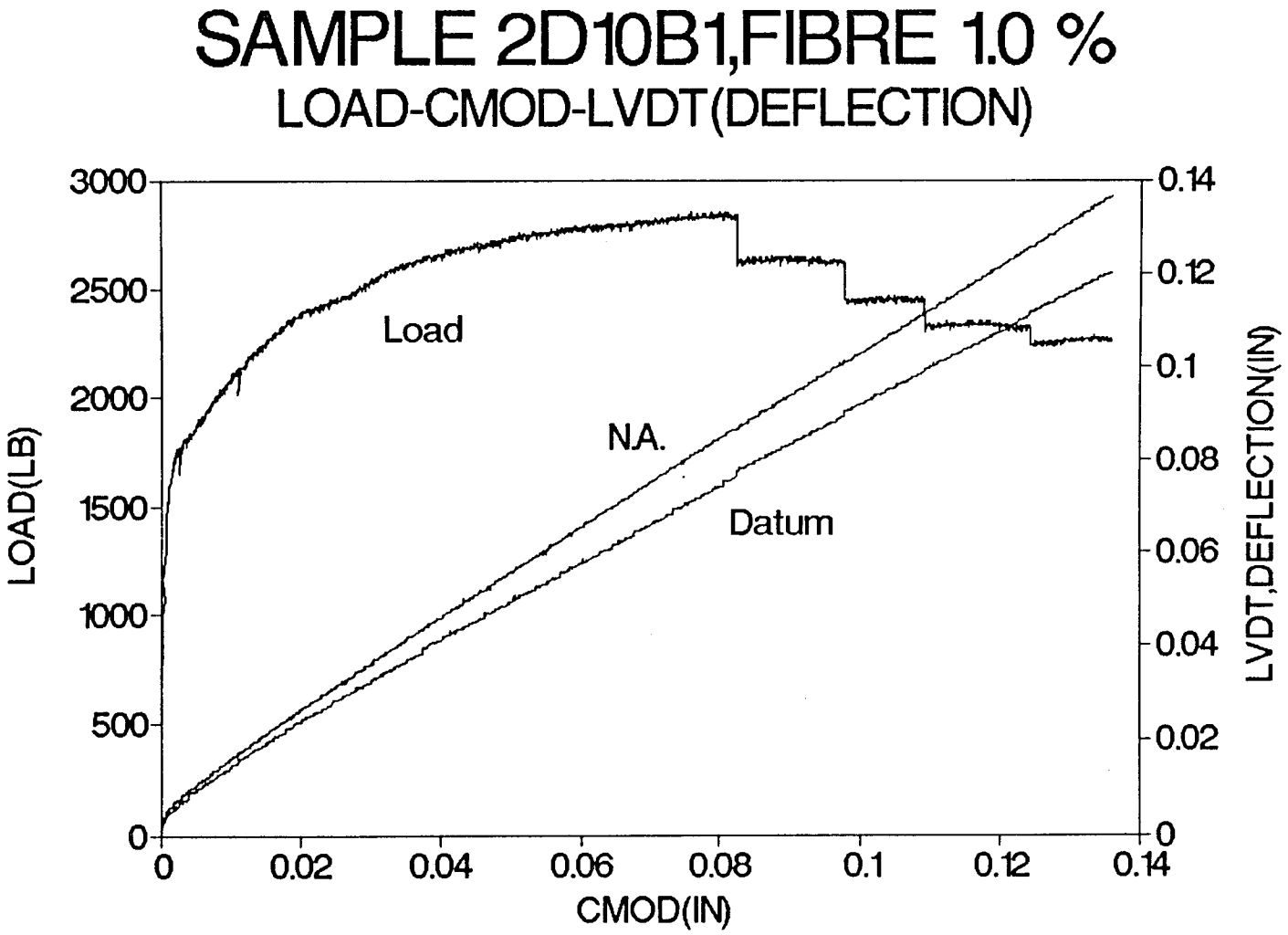

Figure A 1.7a Load-CMOD-Deflection Relationship

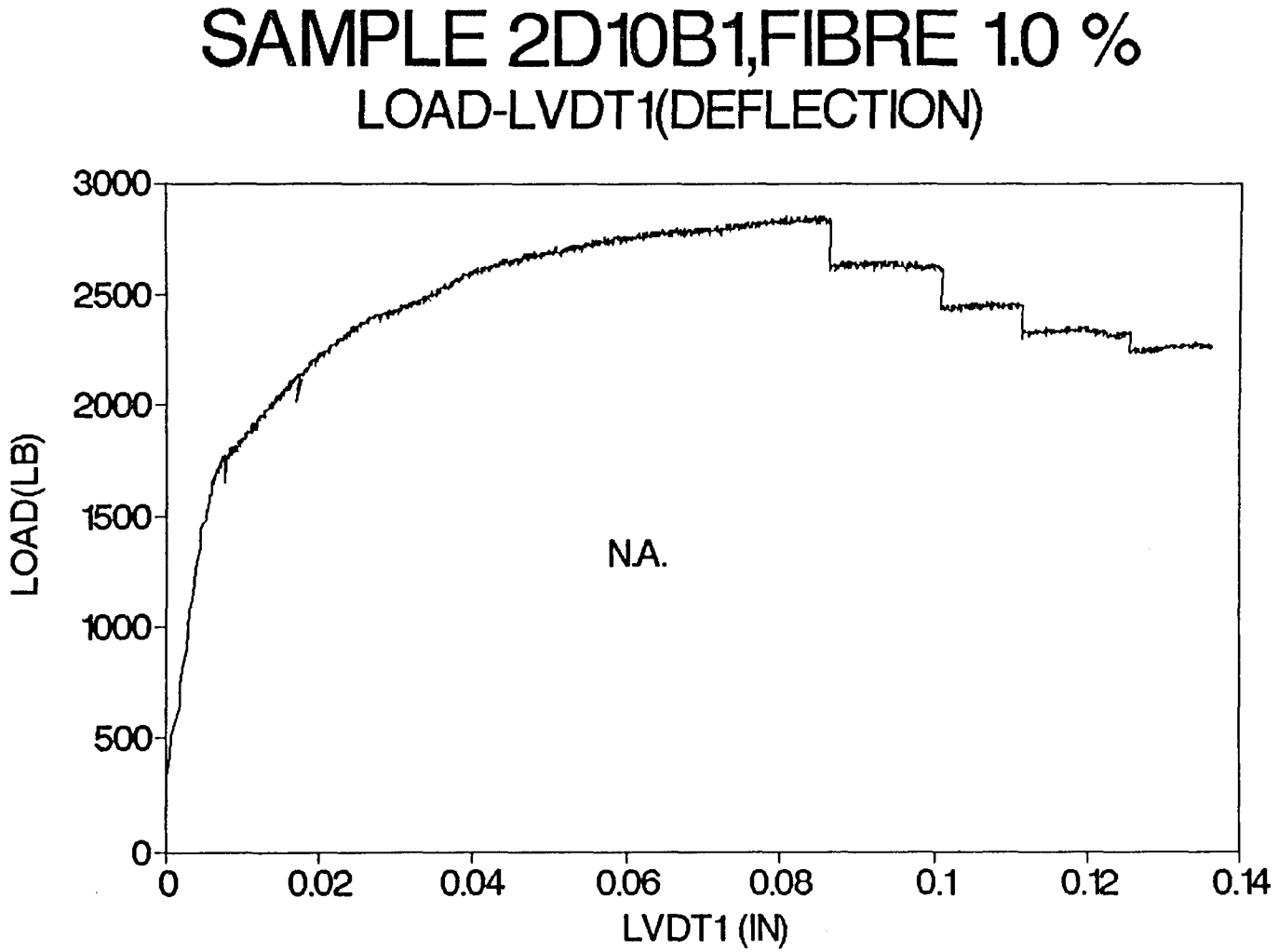

Figure A 1.7b Load-Deflection (N.A.) Relationship

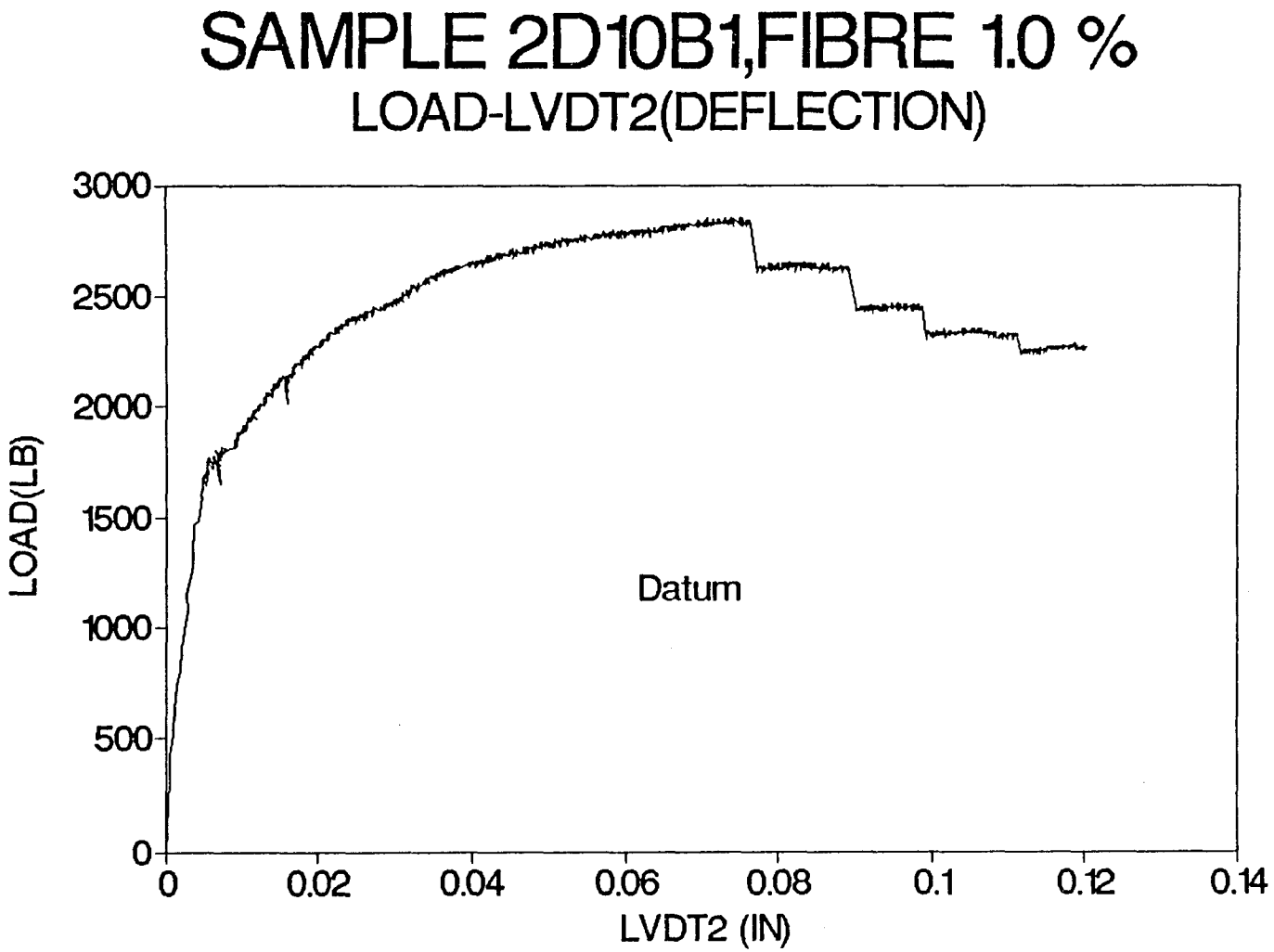

Figure A 1.7c Load-Deflection (Datum) Relationship

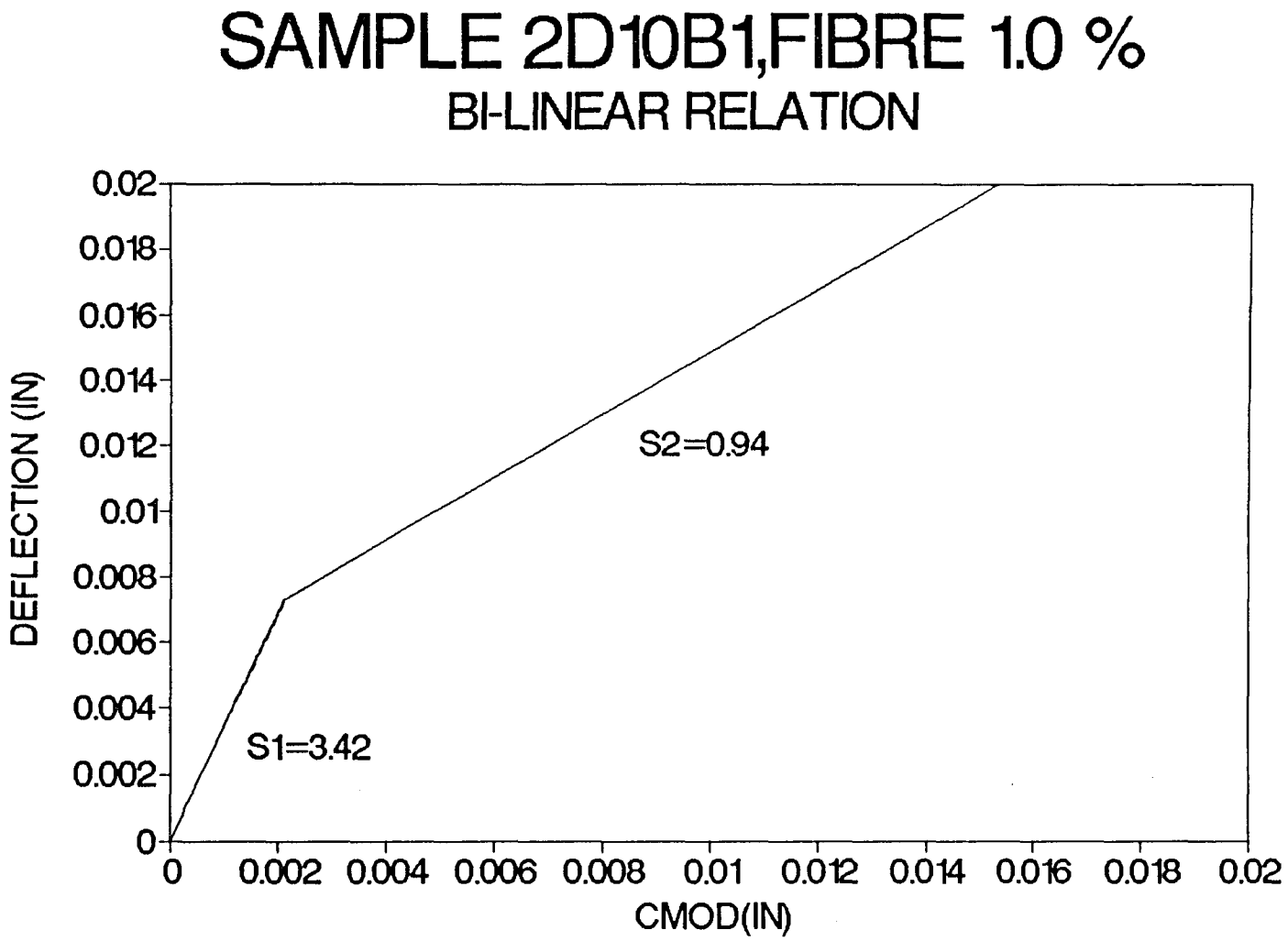

Figure A 1.7d Bilinear CMOD-Deflection Relationship

BEAM CODE	3D15B1	
CAST DATE		
TEST DATE	1-6-92	
LENGTH	27.0	inch
DEPTH	6.0	inch
WIDTH	3.0	inch
KNOTCH DEPTH	1.1	inch
SPAN LENGTH	24	inch
LEG SPAN	23.9	inch
FIBRE TYPE	DRAMIX	
length	1.0	inch
%	1.5	%
wt. (fibre)	10.3	lbs
MIX P CEMENT TYPEI	34.6	lbs
SAND PASSED #4 SIE	80.2	lbs
#3/8 inch AGGREGAT	80.2	lbs
WATER	15.9	lbs
MAXIMUM LOAD	3002.93	lbs
A	0.178431	
V1(A)	1.442614	
V2(A)	0.145036	
S/D	3.984314	
E	3210212	psi
S1	3.619561	
S2	1.025027	

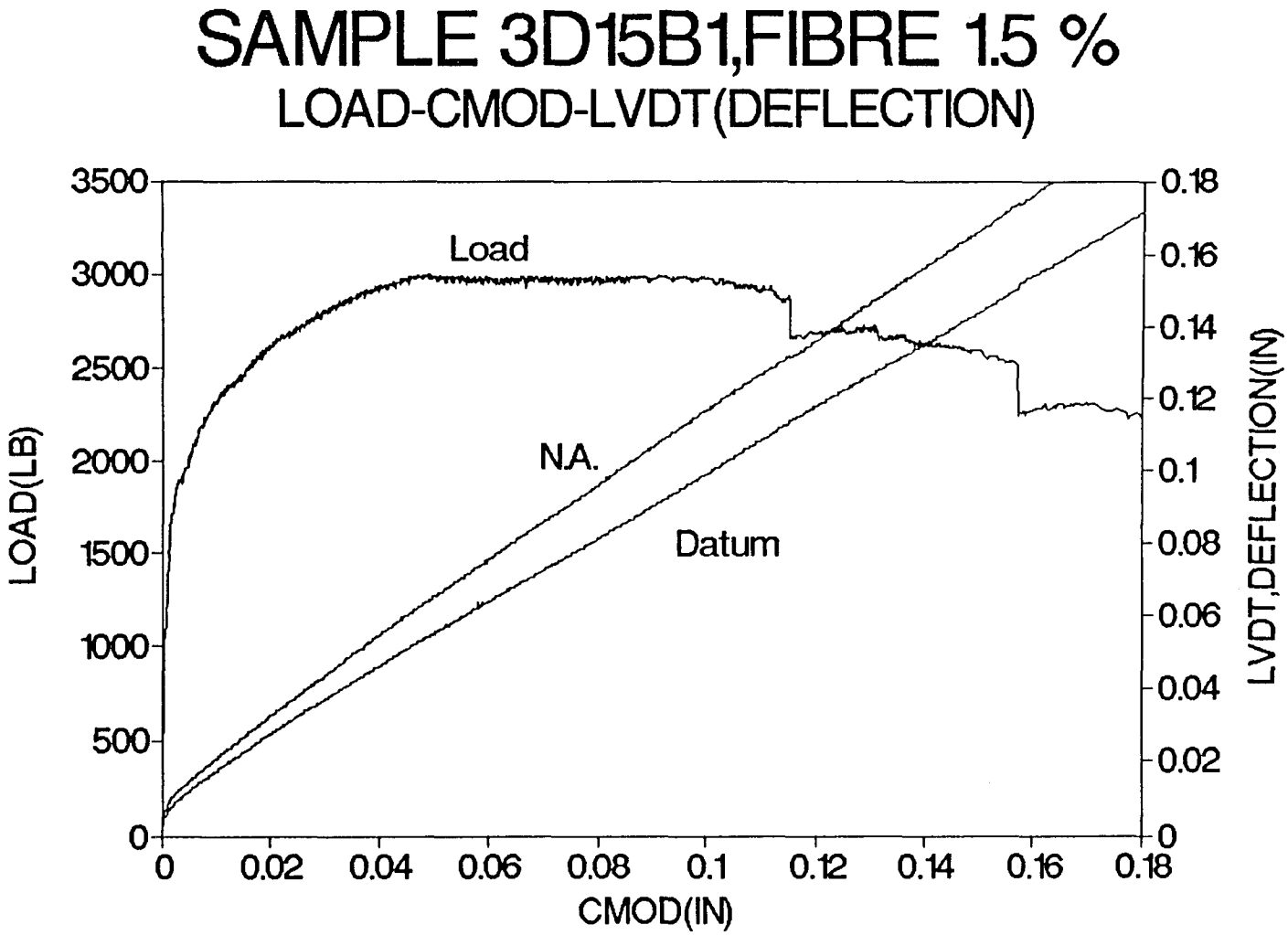

Figure A 1.8a Load-CMOD-Deflection Relationship

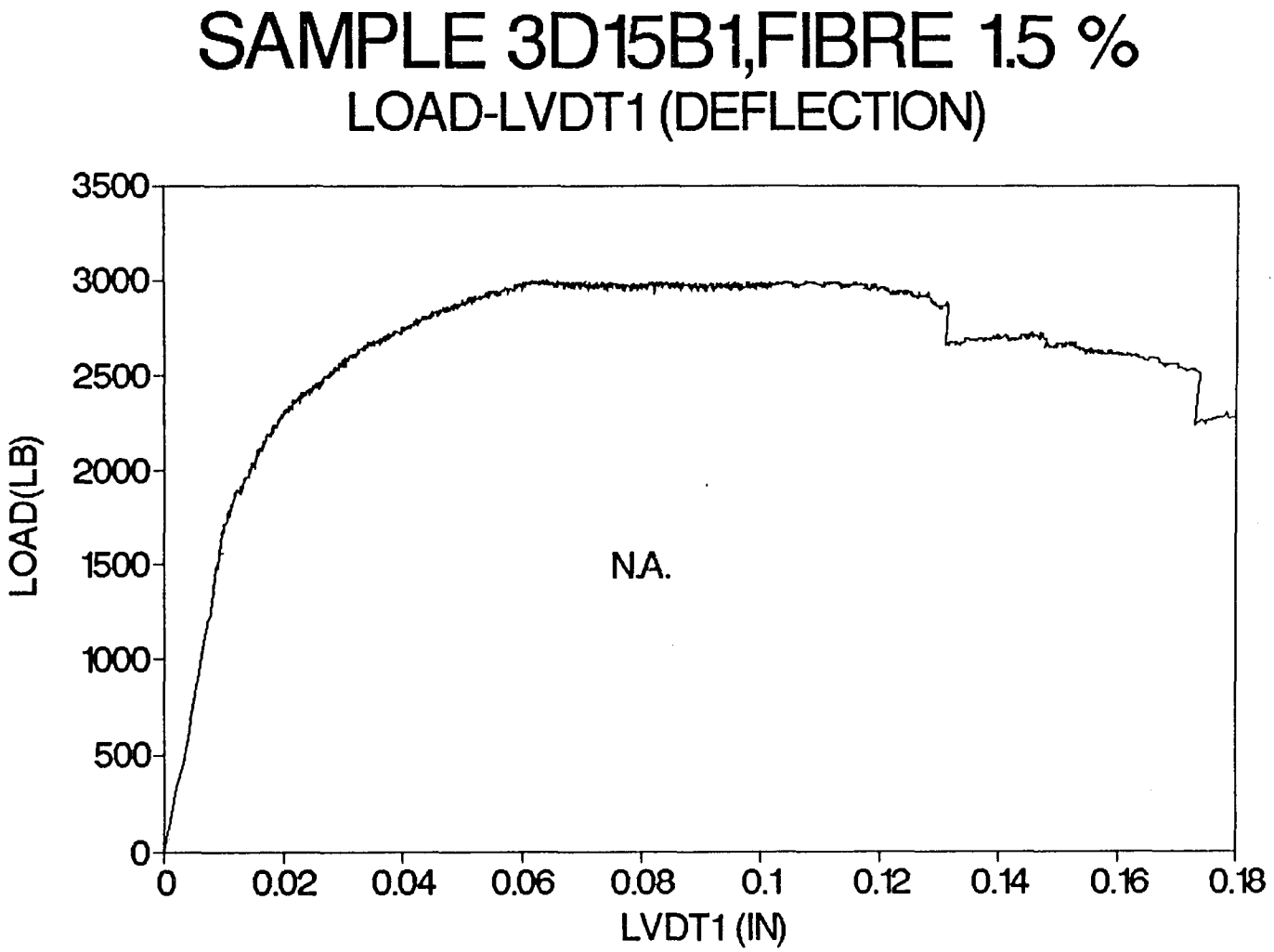

Figure A 1.8b Load-Deflection (N.A.) Relationship

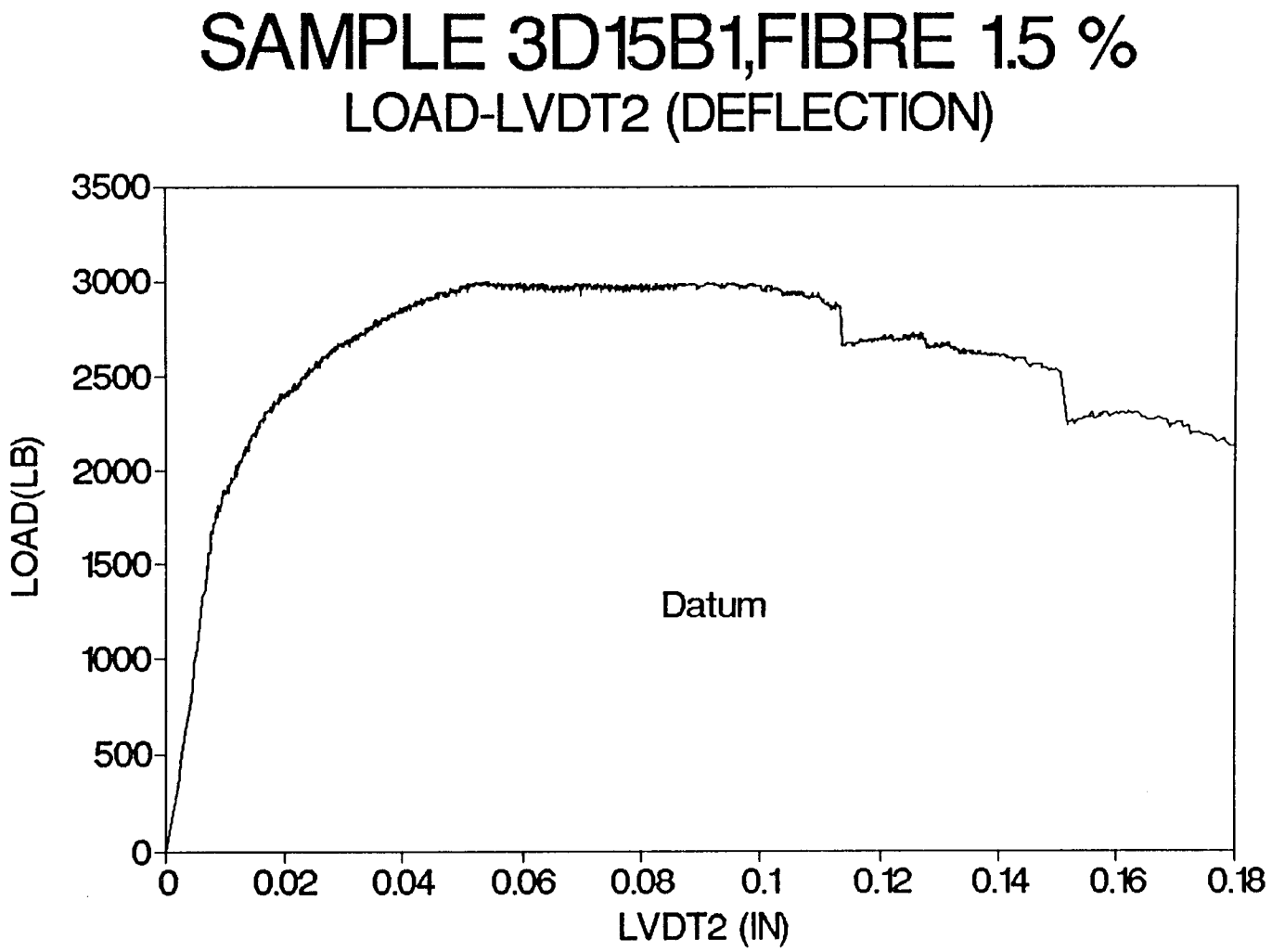

Figure A 1.8c Load-Deflection (Datum) Relationship

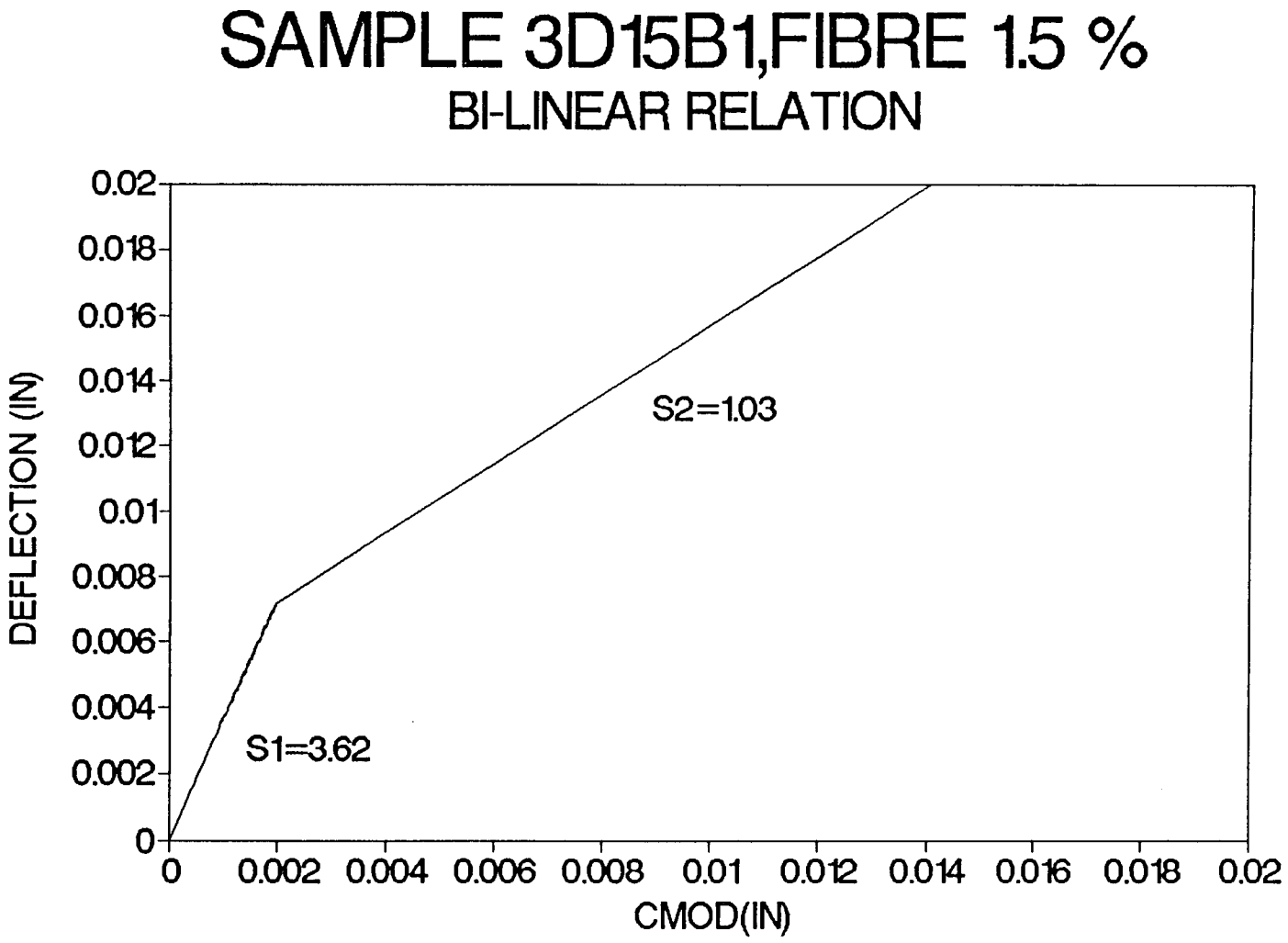

Figure A 1.8d Bilinear CMOD-Deflection Relationship

BEAM CODE		1D10B2
CAST DATE		8-31-91
TEST DATE		12-18-91
LENGTH		27.0 inch
DEPTH		6.1 inch
WIDTH		3.1 inch
KNOTCH DEPTH		1.1 inch
SPAN LENGTH		24 inch
LEG SPAN		24.0 inch
FIBRE TYPE		DRAMIX
length		2.0 inch
%		1.0 %
wt. (fibre)		6.9 lbs
MIX P	CEMENT TYPEI	34.7 lbs
	SAND PASSED #4 SIE	80.6 lbs
	#3/8 inch AGGREGAT	80.6 lbs
	WATER	16.0 lbs
MAXIMUM LOAD		4165.04 lbs
A		0.181169
V1(A)		1.446189
V2(A)		0.149259
S/D		3.958442
E		3031313 psi
S1		3.572175
S2		0.992651

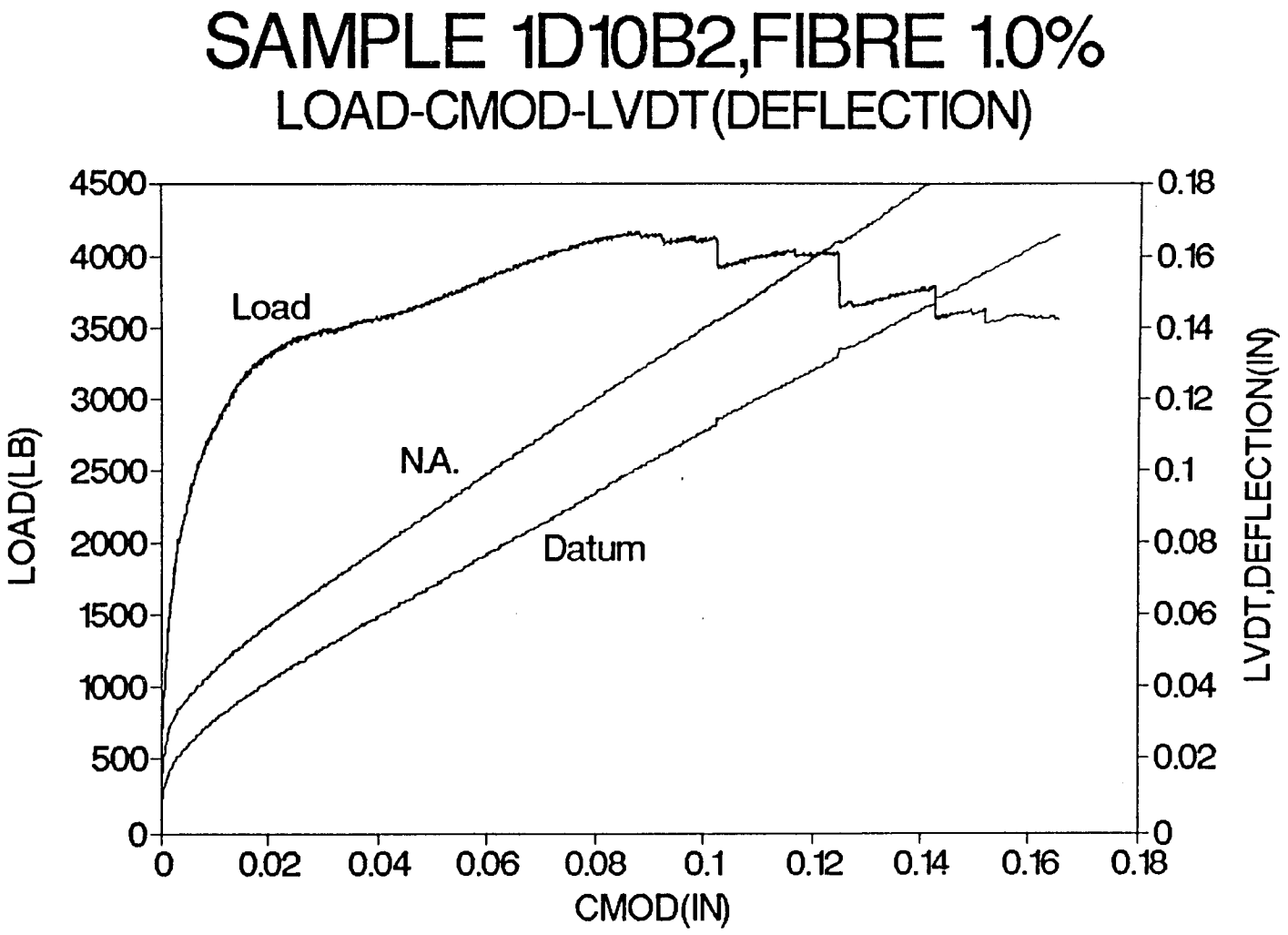

Figure A 1.9a Load-CMOD-Deflection Relationship

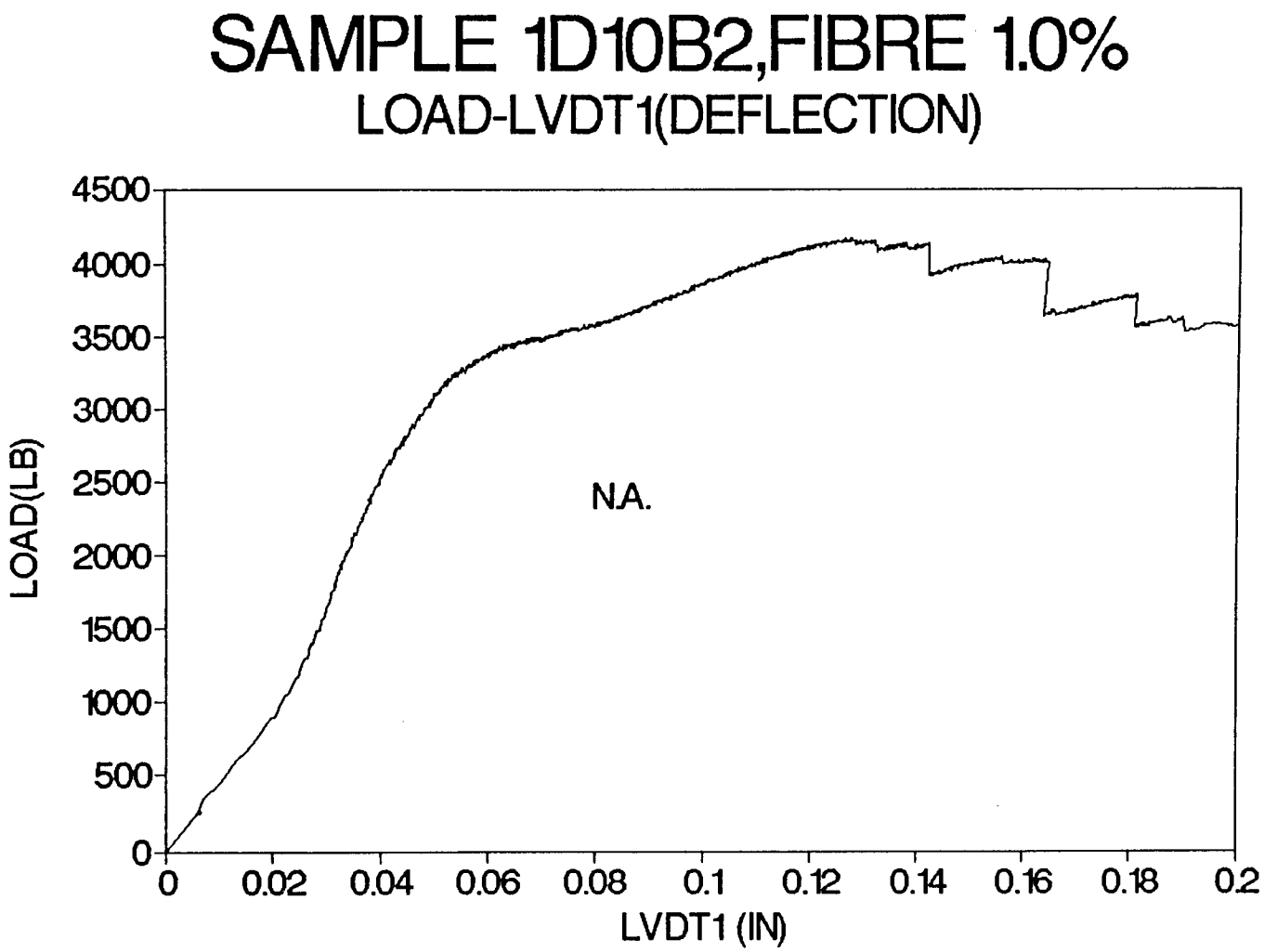

Figure A 1.9b Load-Deflection (N.A.) Relationship

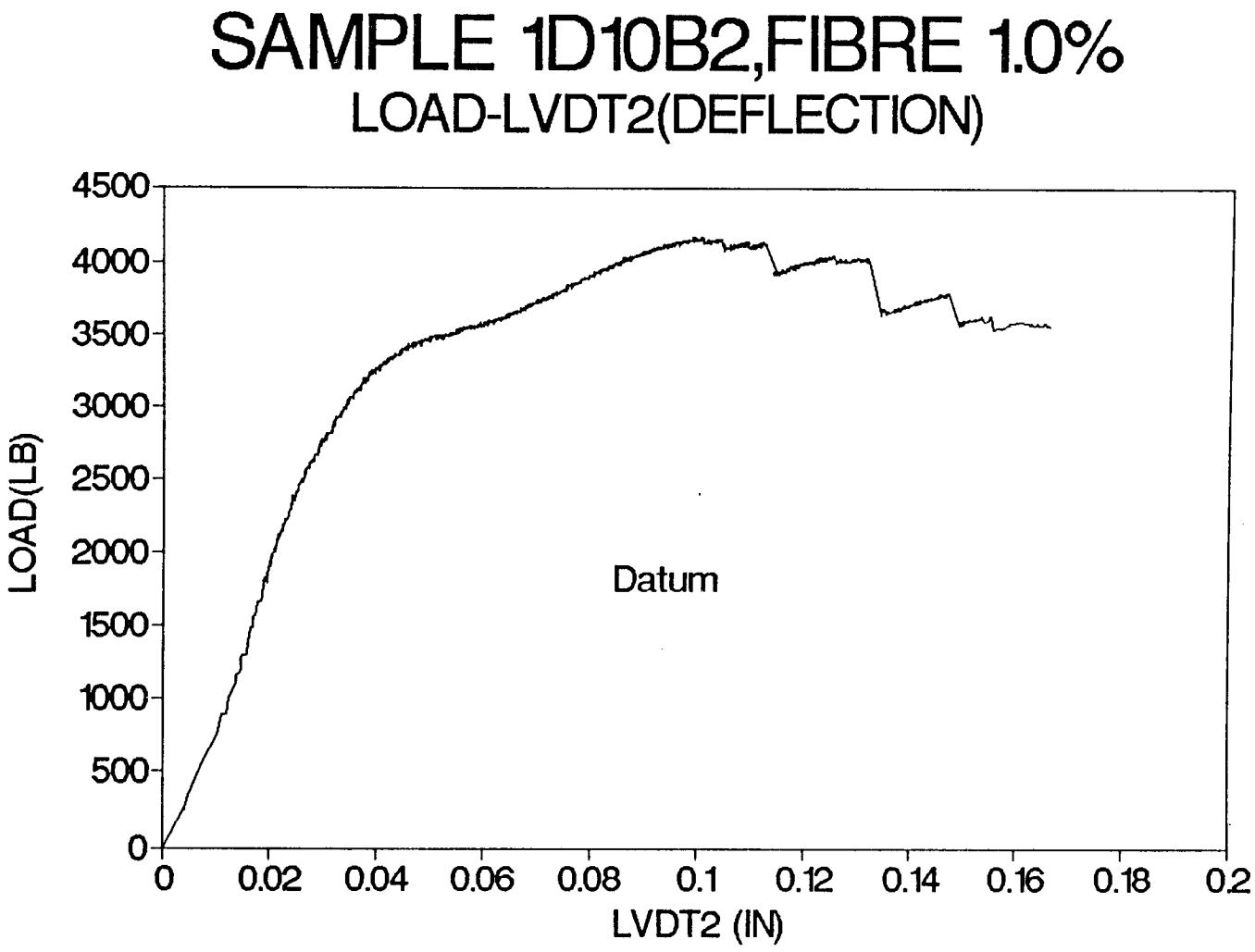

Figure A 1.9c Load-Deflection (Datum) Relationship

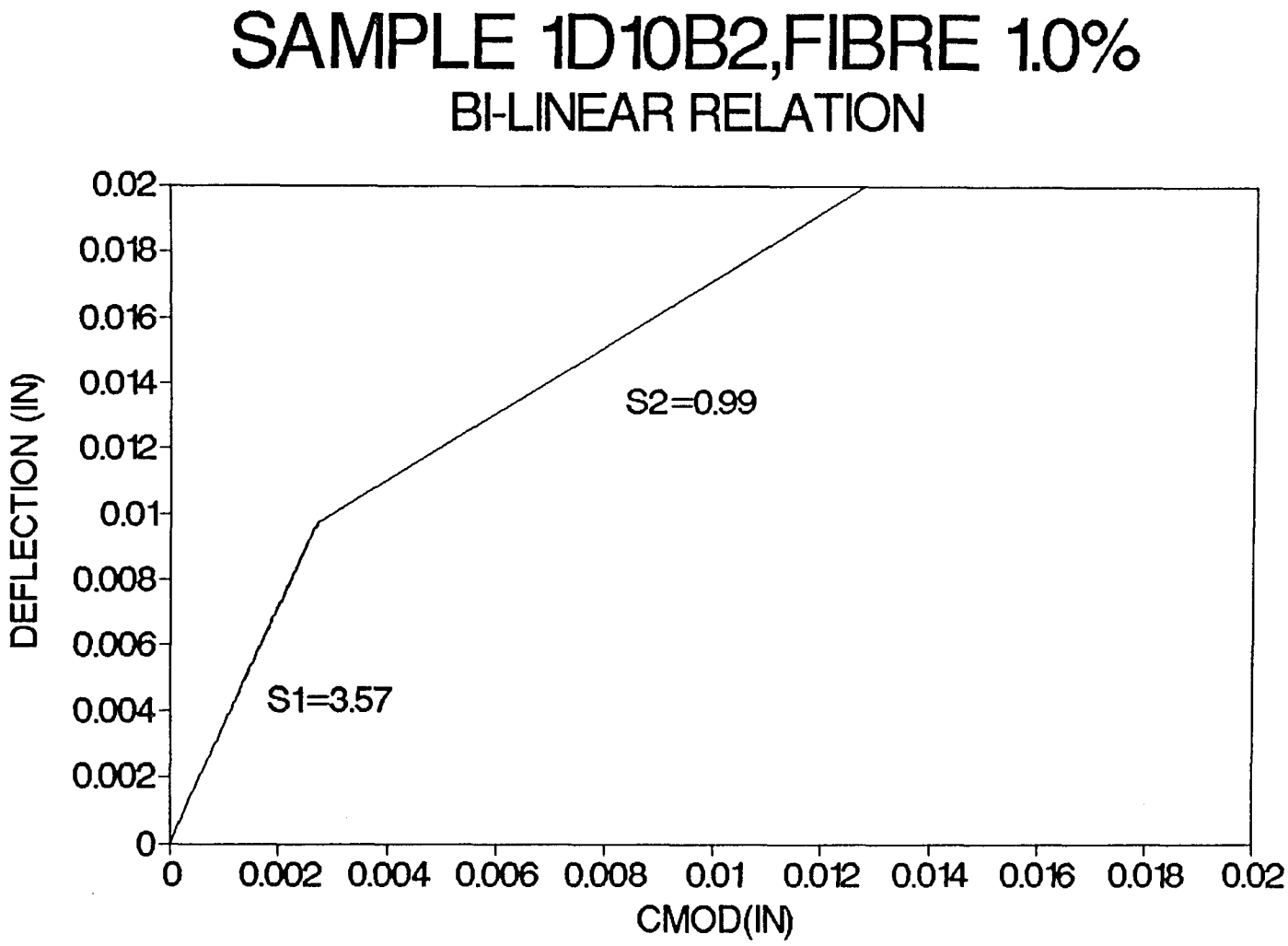

Figure A 1.9d Bilinear CMOD-Deflection Relationship

APPENDIX B

RESULTS FROM EXPERIMENTAL PROGRAM II

Figure A 2.1a to A 2.8d are results from Experimental Program II. Eight samples are shown here. Each sample has four figures and has a cover page which shows the dimensions and other informations of the sample.

BEAM CODE	4H15B1	
CAST DATE	9-7-91	
TEST DATE	1-15-92	
LENGTH	27.0	inch
DEPTH	6.0	inch
WIDTH	3.0	inch
KNOTCH DEPTH	1.1	inch
SPAN LENGTH	24	inch
LEG SPAN	24.0	inch
FIBRE TYPE	HAREX	
length	1.0	inch
%	1.5	%
wt. (fibre)	10.3	lbs
MIX P CEMENT TYPEI	34.6	lbs
SAND PASSED #4 SIE	80.2	lbs
#3/8 inch AGGREGAT	80.2	lbs
WATER	15.9	lbs
MAXIMUM LOAD	3125	lbs
A	0.178431	
V1(A)	1.442614	
V2(A)	0.145036	
S/D	3.984314	
E	3202588	psi
S1	3.619561	
S2	0.529	

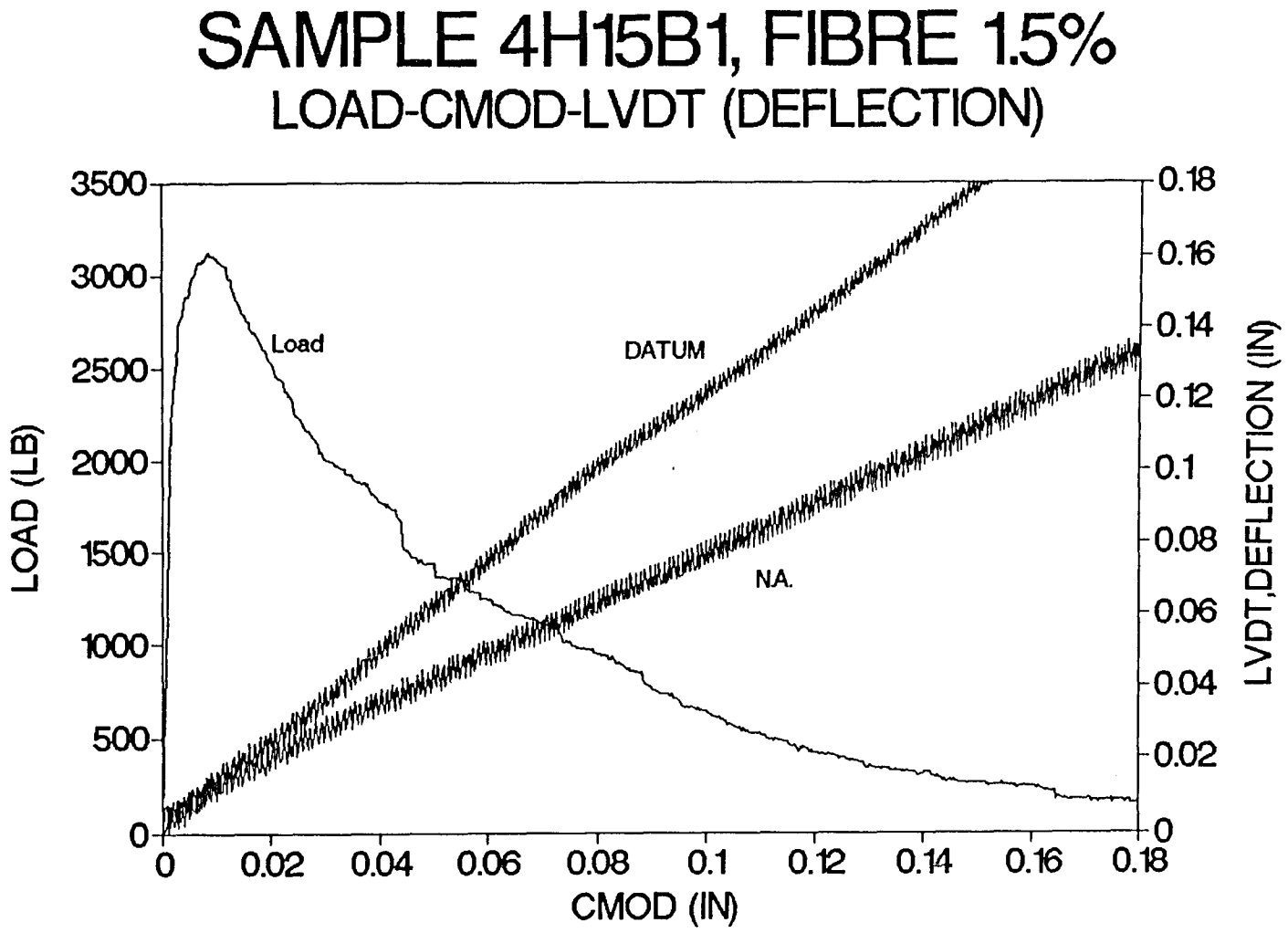

Figure A 2.1a Load-CMOD-Deflection Relationship

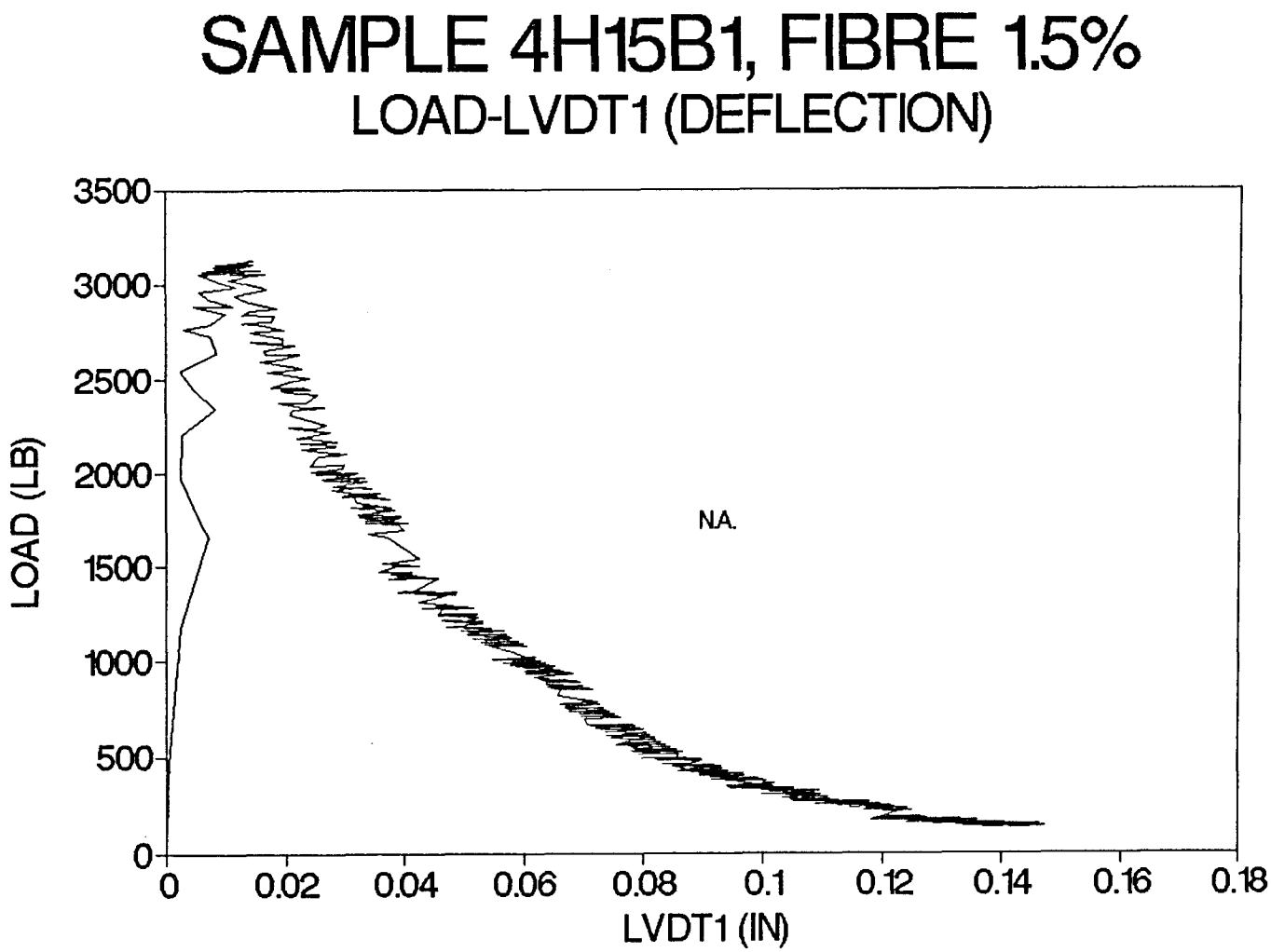

Figure A 2.1b Load-Deflection (N.A.) Relationship

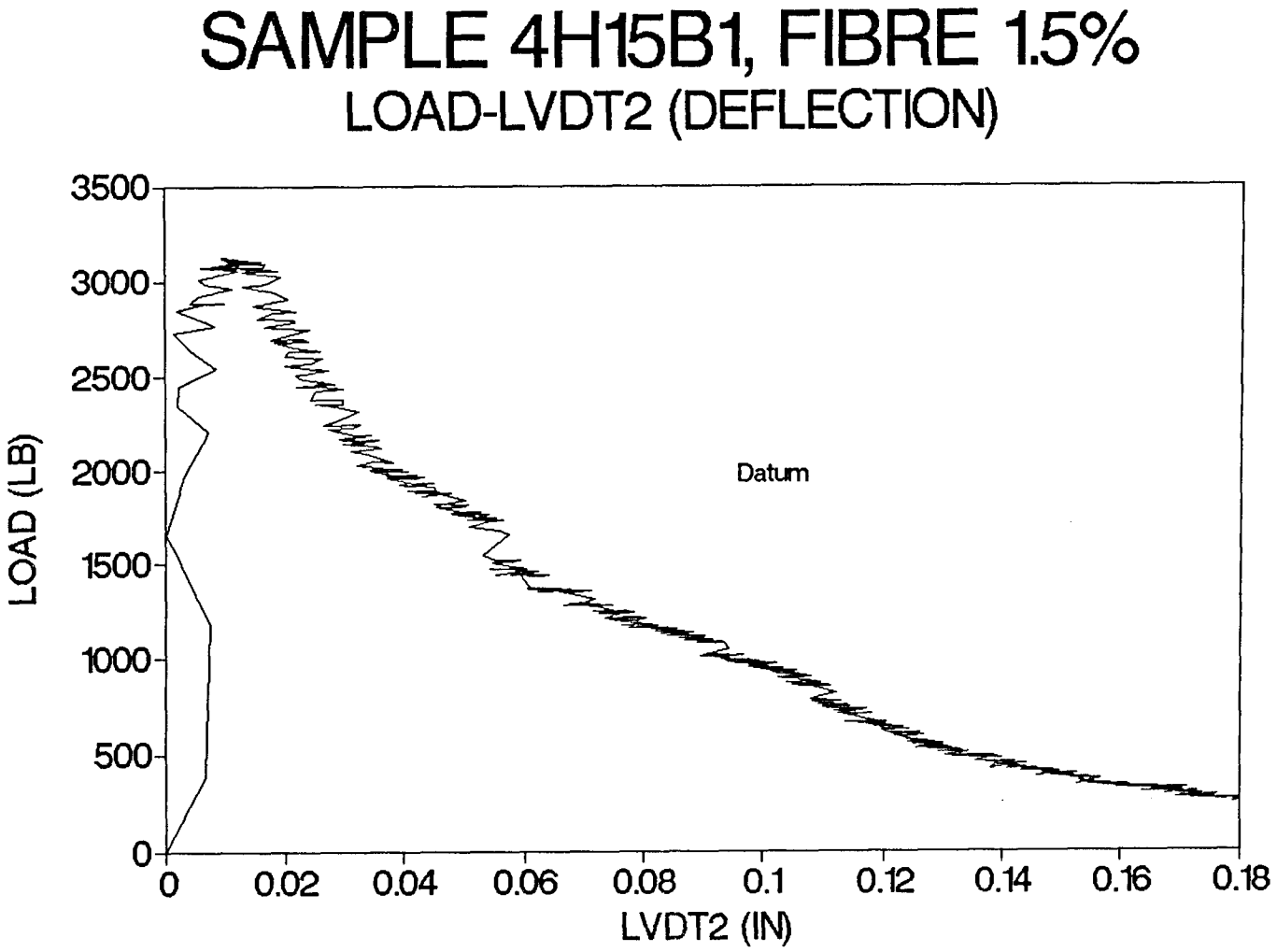

Figure A 2.1c Load-Deflection (Datum) Relationship

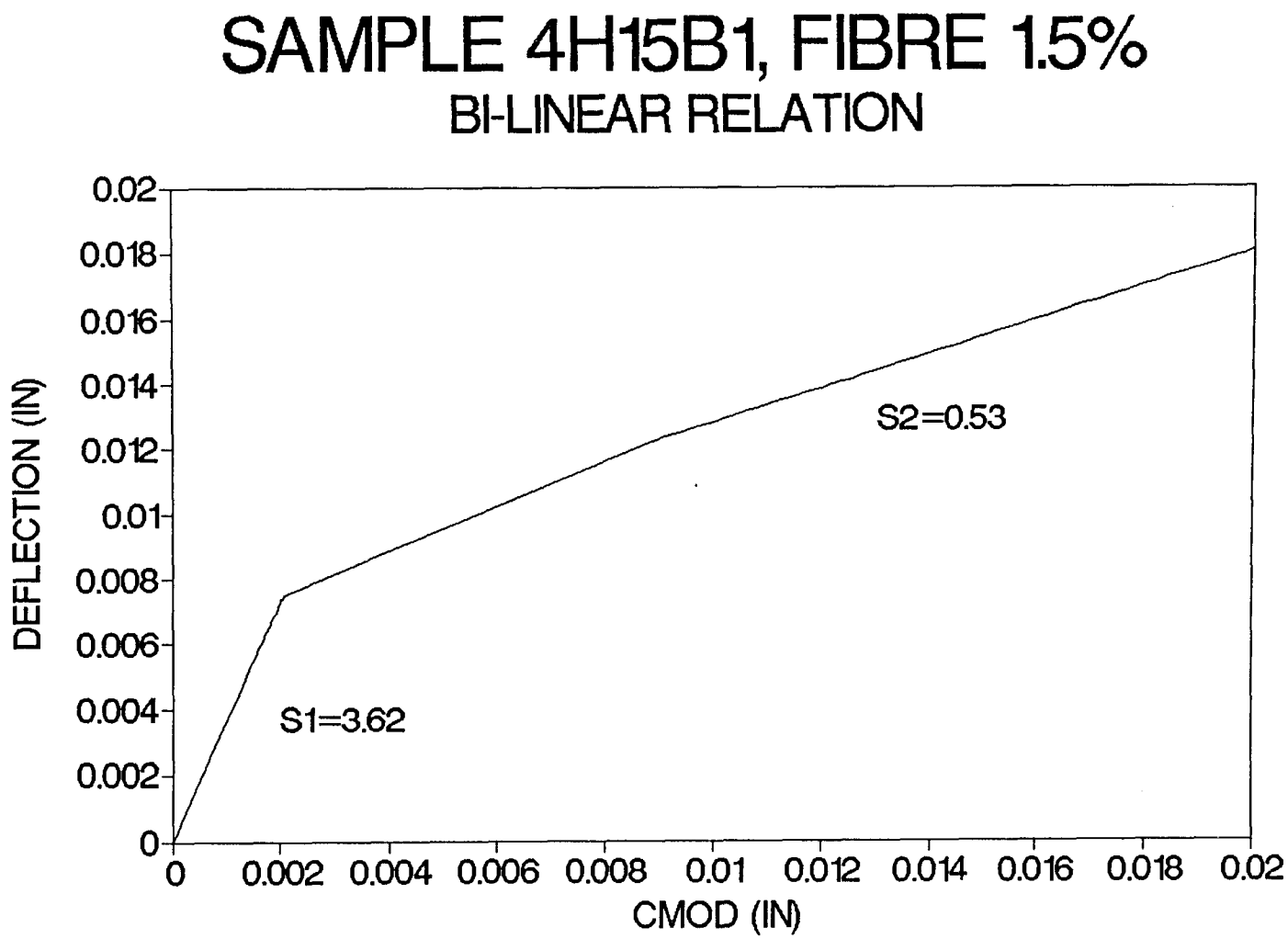

Figure A 2.1d Bilinear CMOD-Deflection Relationship

BEAM CODE		4C05B1
CAST DATE		8-28-91
TEST DATE		1-15-92
LENGTH		27.3 inch
DEPTH		6.0 inch
WIDTH		3.0 inch
KNOTCH DEPTH		1.1 inch
SPAN LENGTH		24 inch
LEG SPAN		23.5 inch
FIBRE TYPE		CRIMPED
length		1.0 inch
%		0.5 %
wt. (fibre)		3.4 lbs
MIX P	CEMENT TYPEI	35.0 lbs
	SAND PASSED #4 SIE	81.0 lbs
	#3/8 inch AGGREGAT	81.0 lbs
	WATER	16.1 lbs
MAXIMUM LOAD		1909.18 lbs
A		0.185621
V1(A)		1.452234
V2(A)		0.156257
S/D		3.984314
E		3079912 psi
S1		3.497947
S2		1.13288

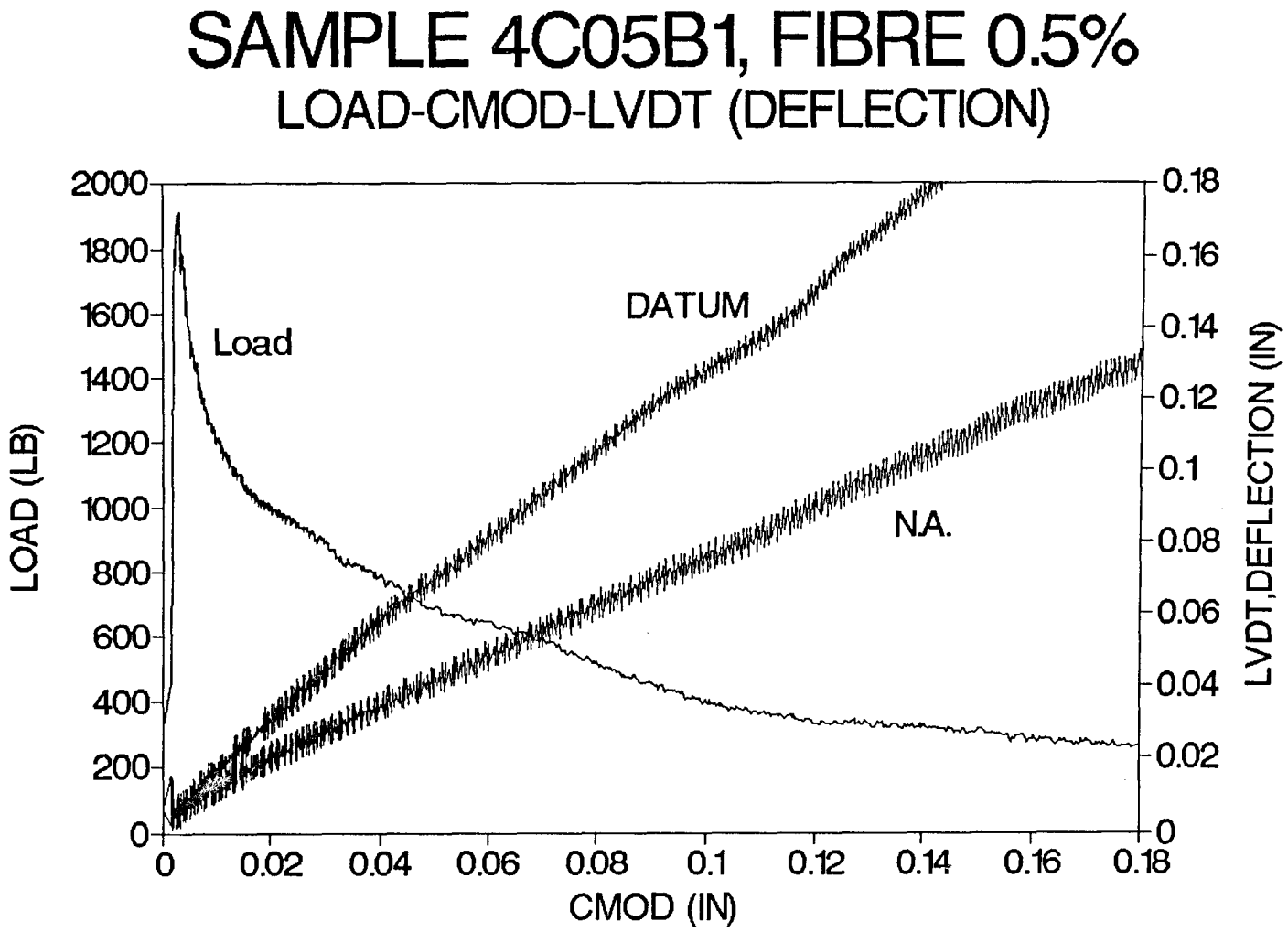

Figure A 2.2a Load-CMOD-Deflection Relationship

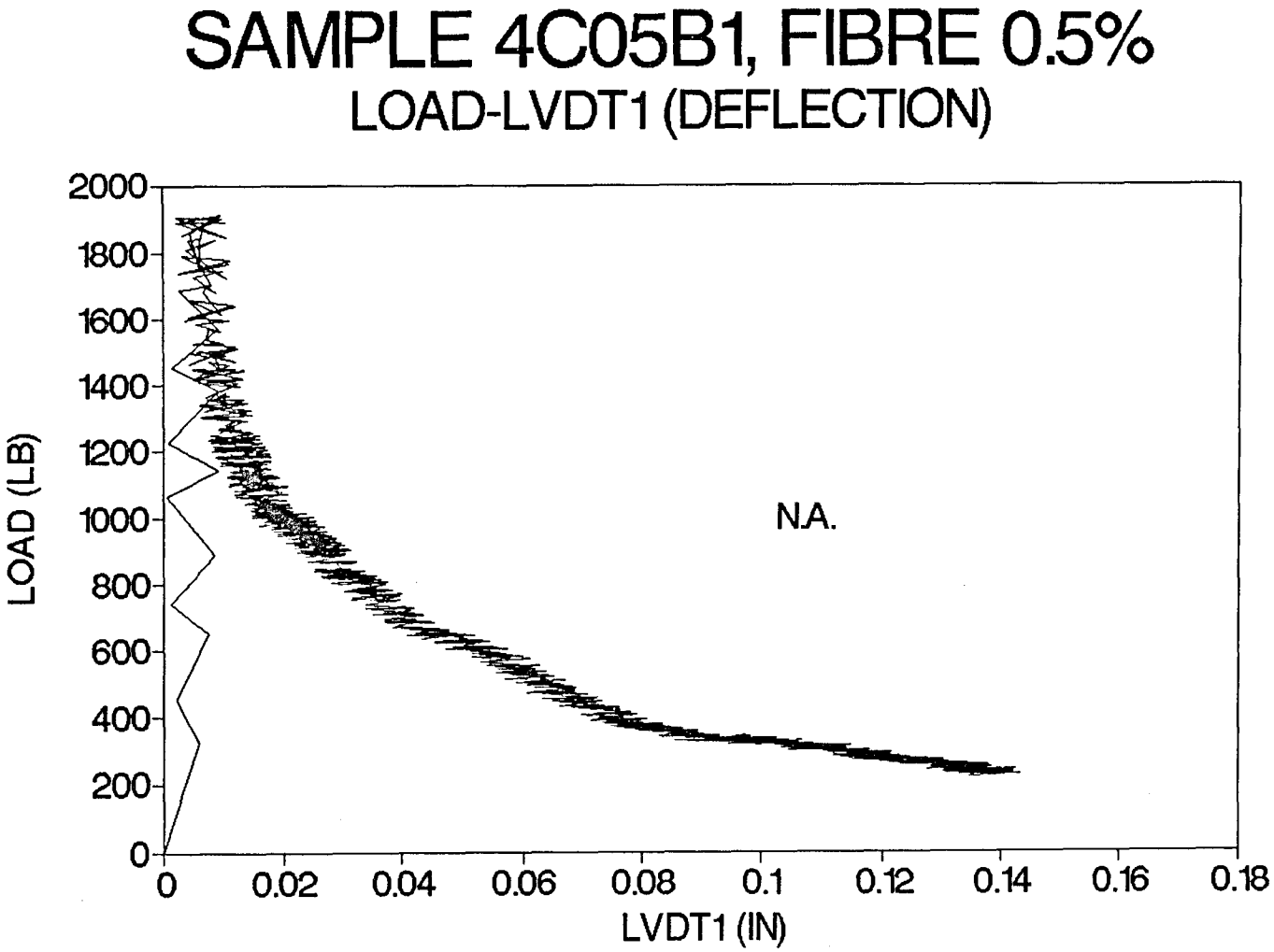

Figure A 2.2b Load-Deflection (N.A.) Relationship

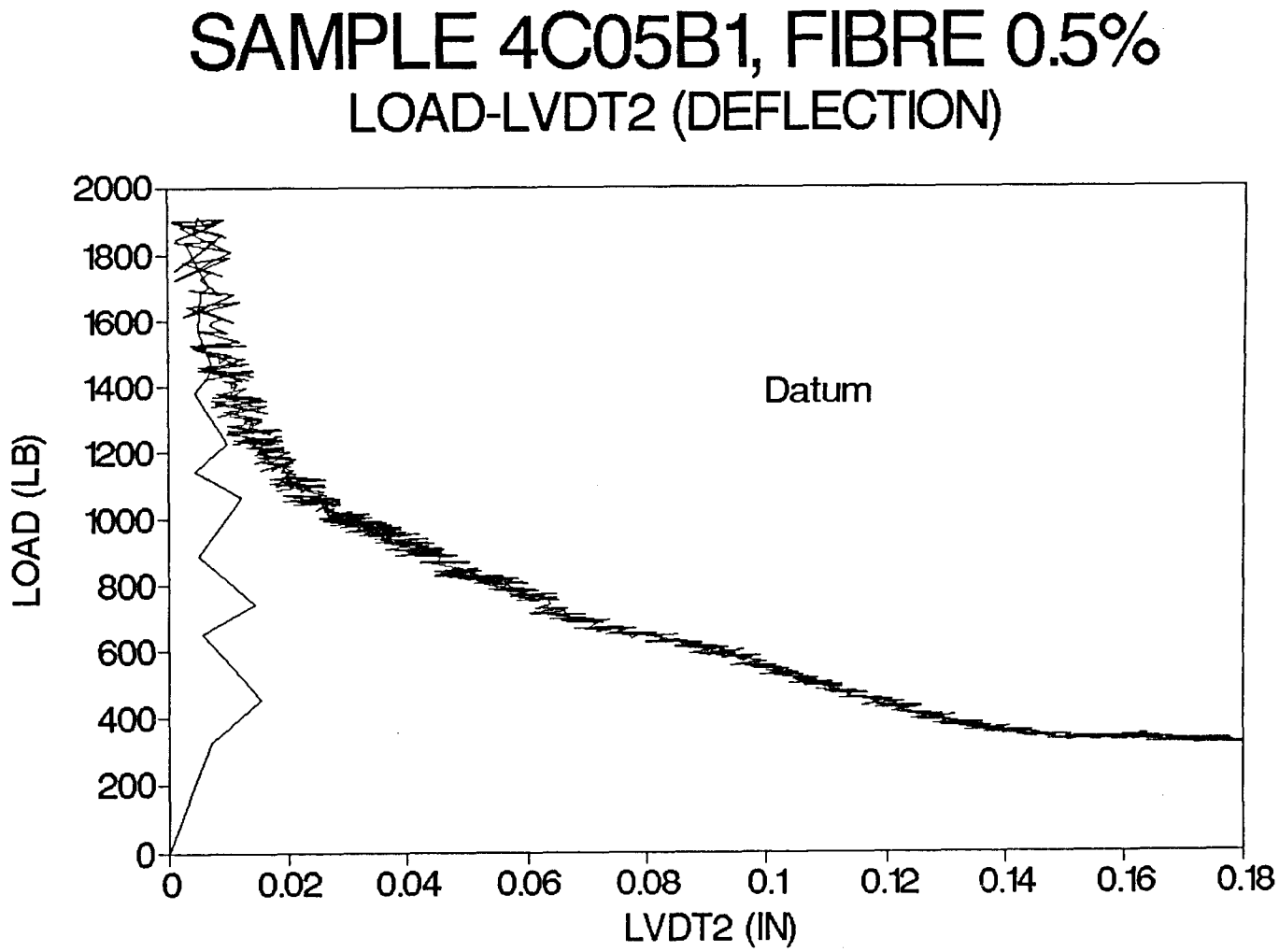

Figure A 2.2c Load-Deflection (Datum) Relationship

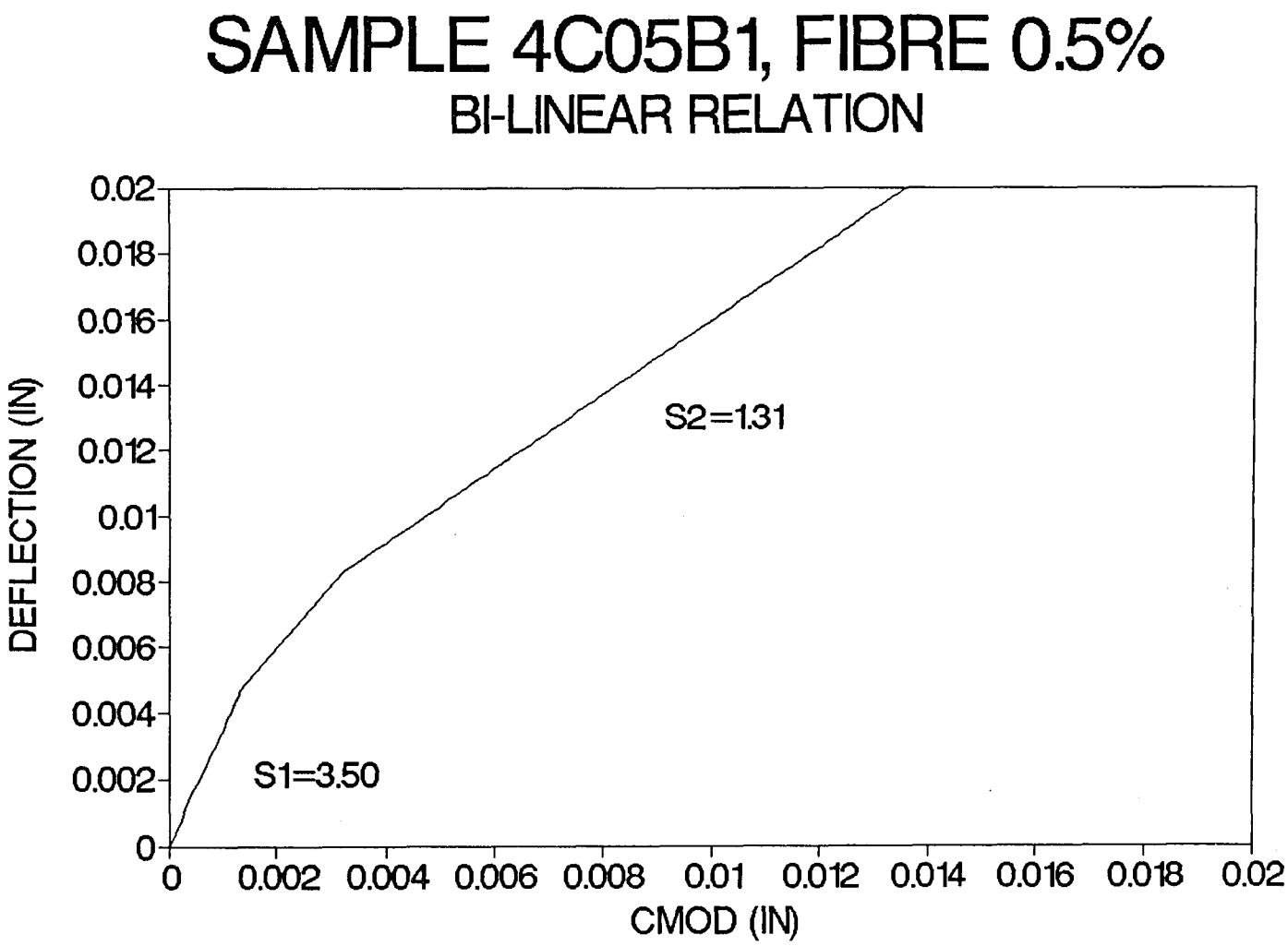

Figure A 2.2d Bilinear CMOD-Deflection Relationship

BEAM CODE		4C10B1
CAST DATE		9-3-91
TEST DATE		1-15-92
LENGTH		27.1 inch
DEPTH		6.1 inch
WIDTH		3.1 inch
KNOTCH DEPTH		1.1 inch
SPAN LENGTH		24 inch
LEG SPAN		23.9 inch
FIBRE TYPE		CRIMPED
length		1.0 inch
%		1.0 %
wt. (fibre)		6.9 lbs
MIX P	CEMENT TYPEI	34.7 lbs
	SAND PASSED #4 SIE	80.6 lbs
	#3/8 inch AGGREGAT	80.6 lbs
	WATER	16.0 lbs
MAXIMUM LOAD		2099.61 lbs
A		0.17987
V1(A)		1.444479
V2(A)		0.147248
S/D		3.958442
E		3241097 psi
S1		3.594484
S2		0.615351

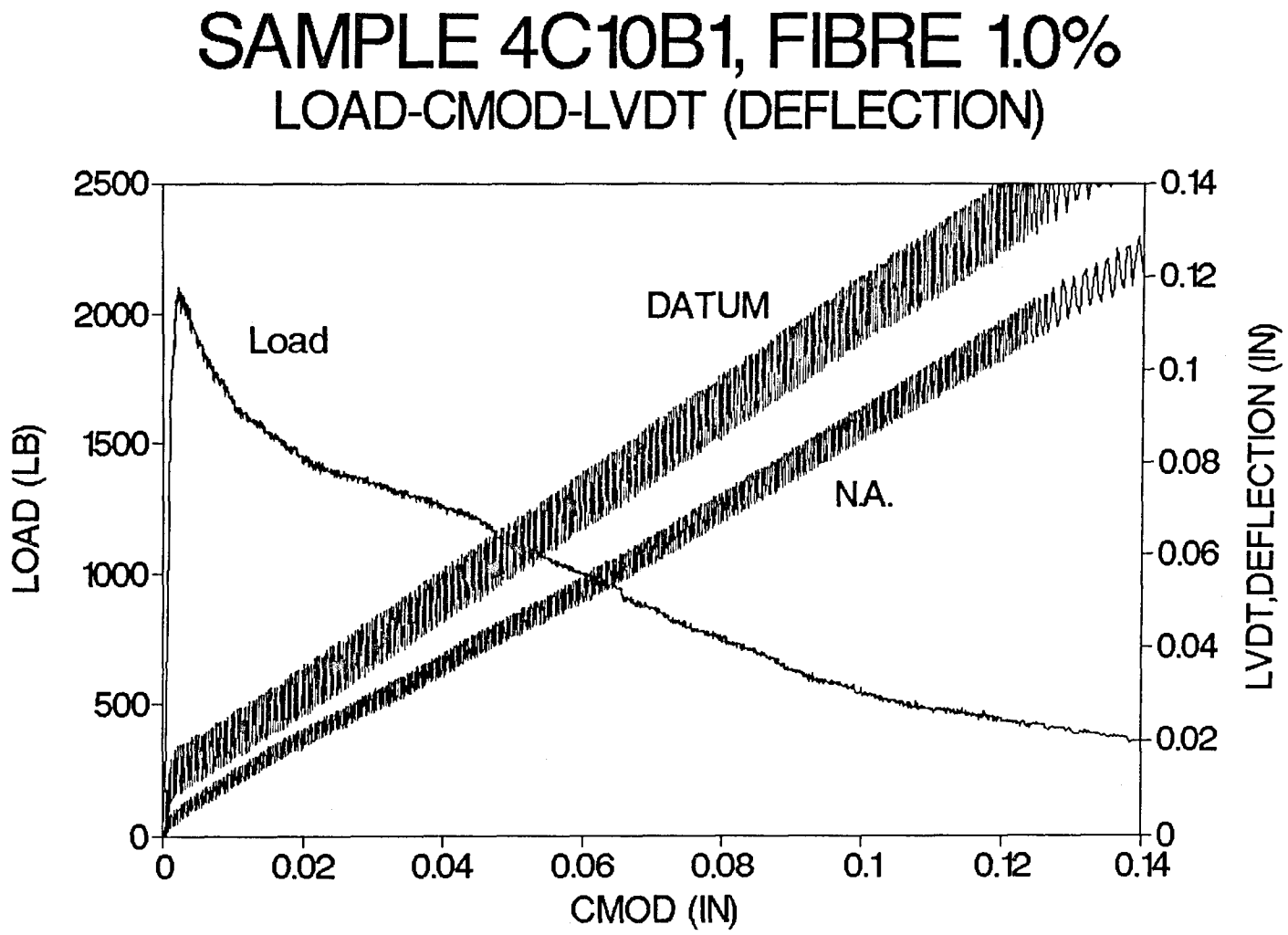

Figure A 2.3a Load-CMOD-Deflection Relationship

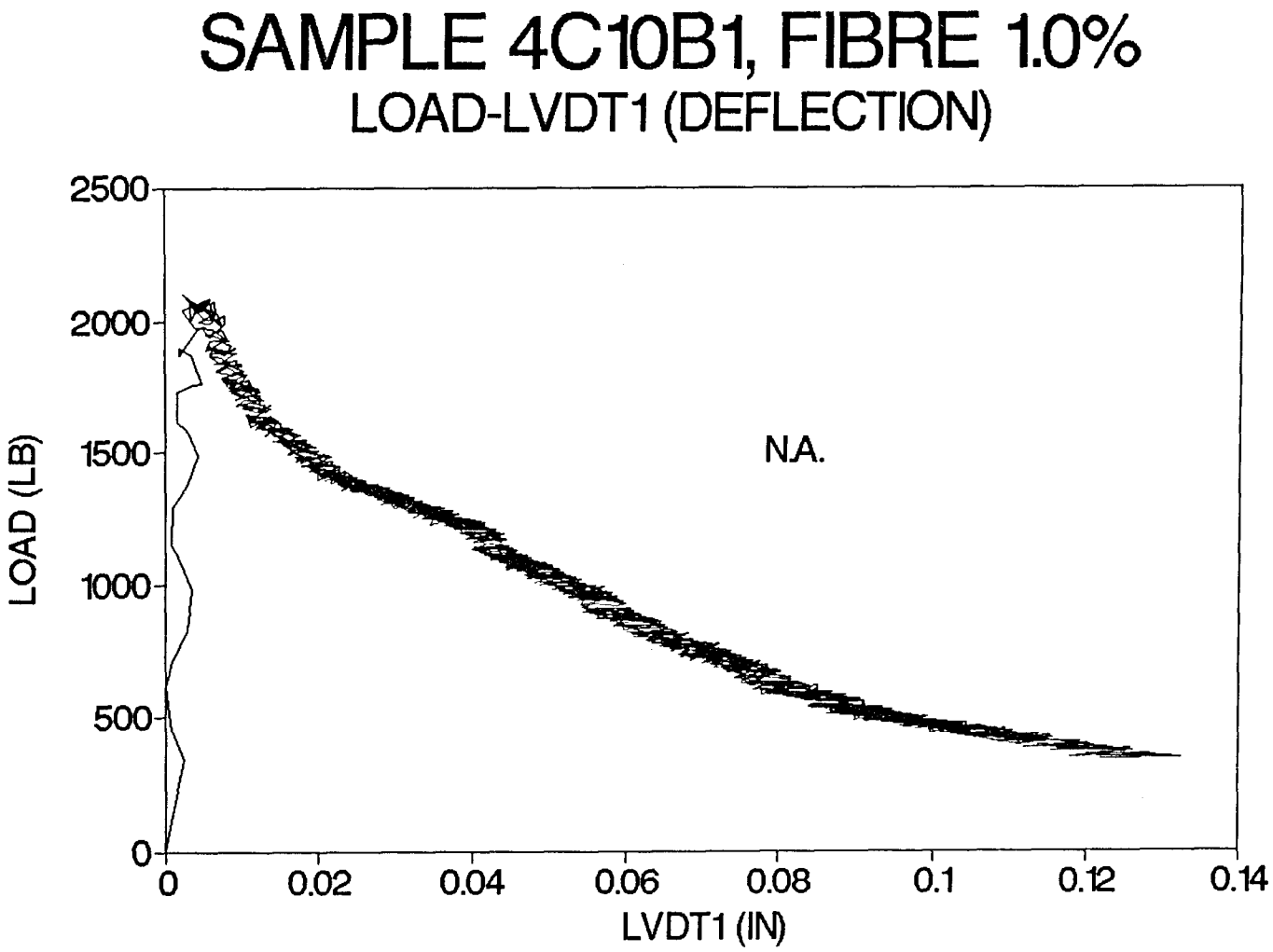

Figure A 2.3b Load-Deflection (N.A.) Relationship

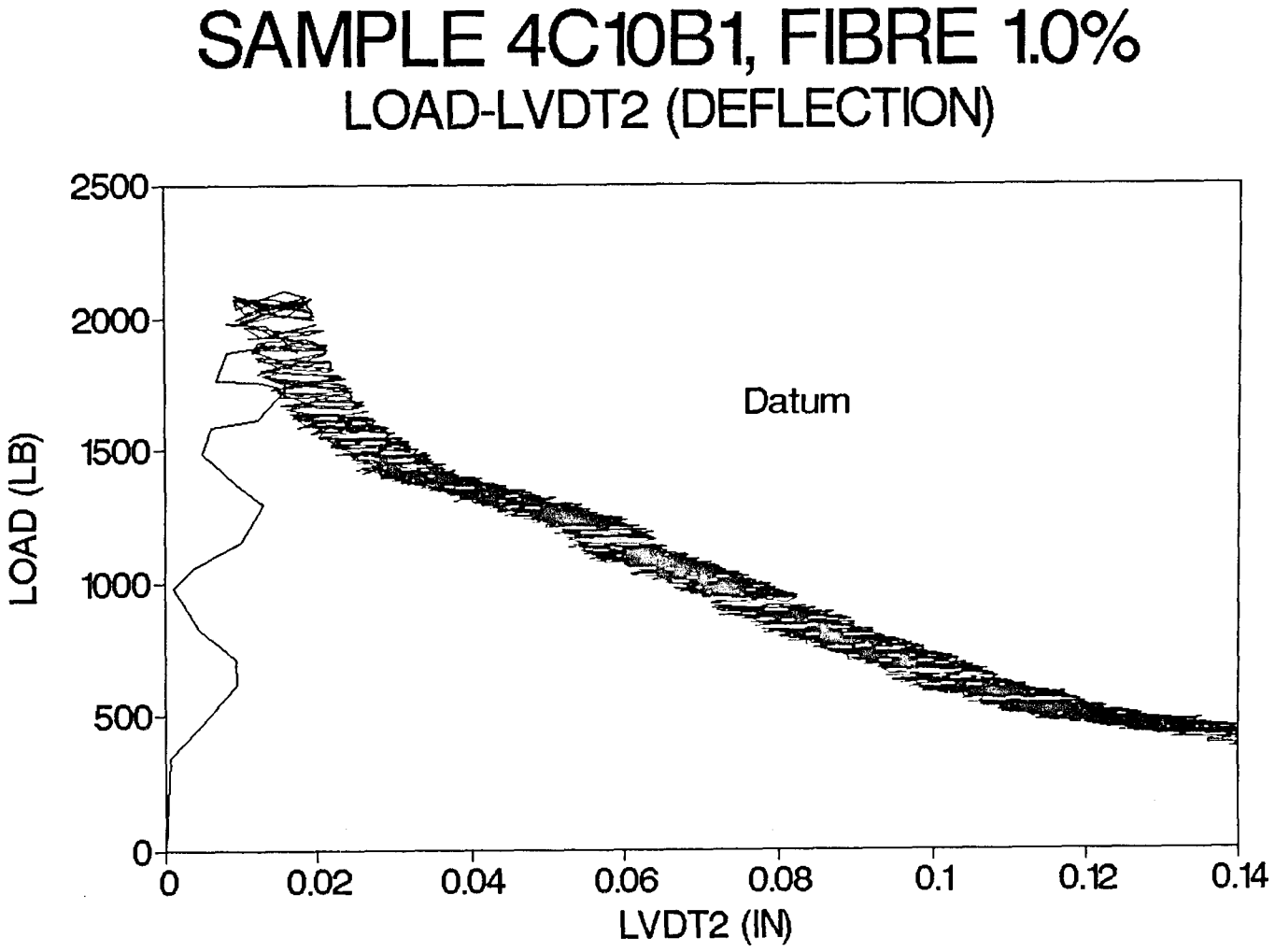

Figure A 2.3c Load-Deflection (Datum) Relationship

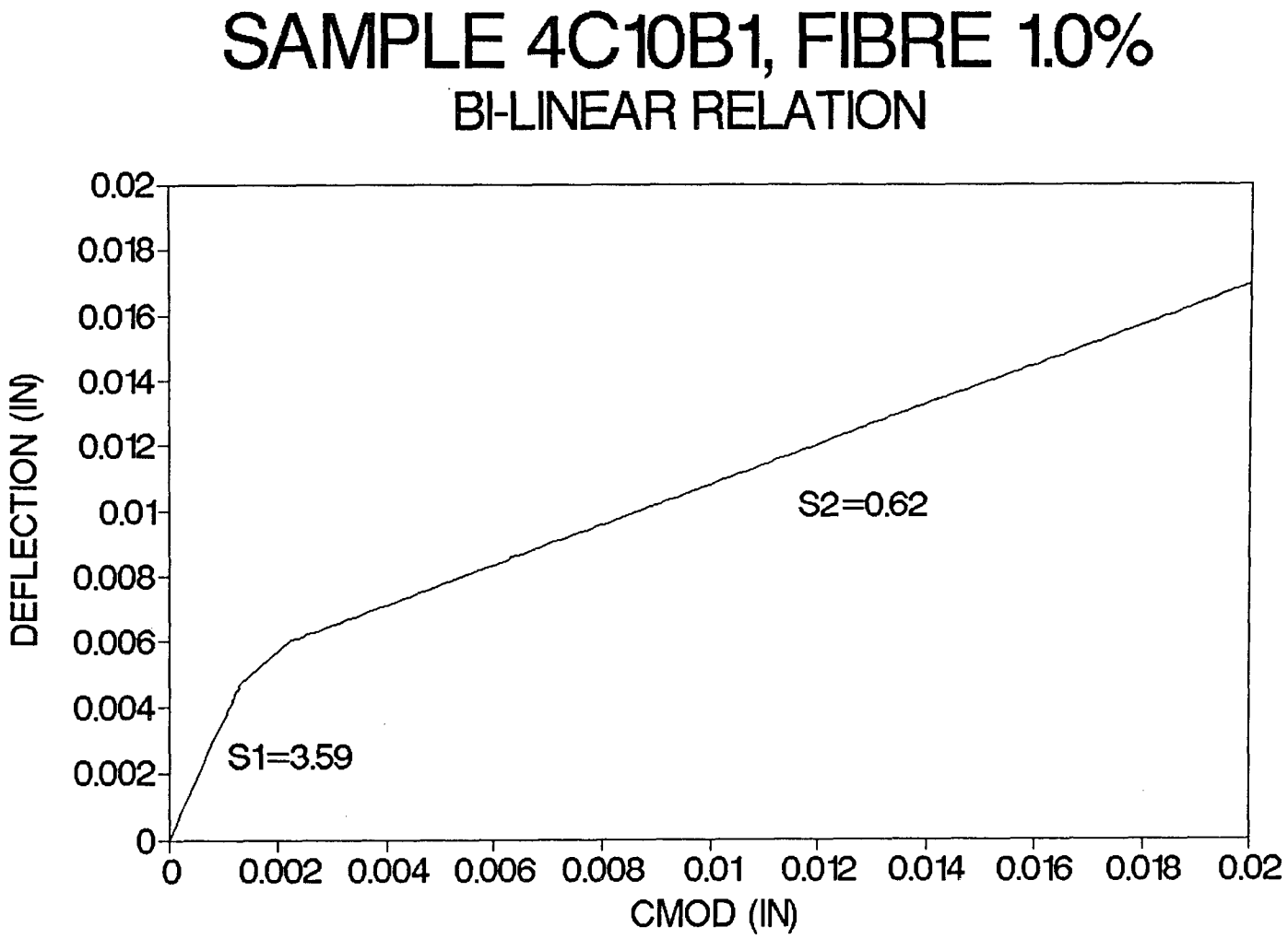

Figure A 2.3d Bilinear CMOD-Deflection Relationship

BEAM CODE		4C15B1
CAST DATE		9-6-91
TEST DATE		1-15-92
LENGTH		27.0 inch
DEPTH		6.1 inch
WIDTH		3.0 inch
KNOTCH DEPTH		1.0 inch
SPAN LENGTH		24 inch
LEG SPAN		23.9 inch
FIBRE TYPE		CRIMPED
length		1.0 inch
%		1.5 %
wt. (fibre)		10.3 lbs
MIX P	CEMENT TYPEI	34.6 lbs
	SAND PASSED #4 SIE	80.2 lbs
	#3/8 inch AGGREGAT	80.2 lbs
	WATER	15.9 lbs
MAXIMUM LOAD		3188.48 lbs
A		0.170779
V1(A)		1.433184
V2(A)		0.133549
S/D		3.958442
E		3210212 psi
S1		3.759697
S2		0.8984

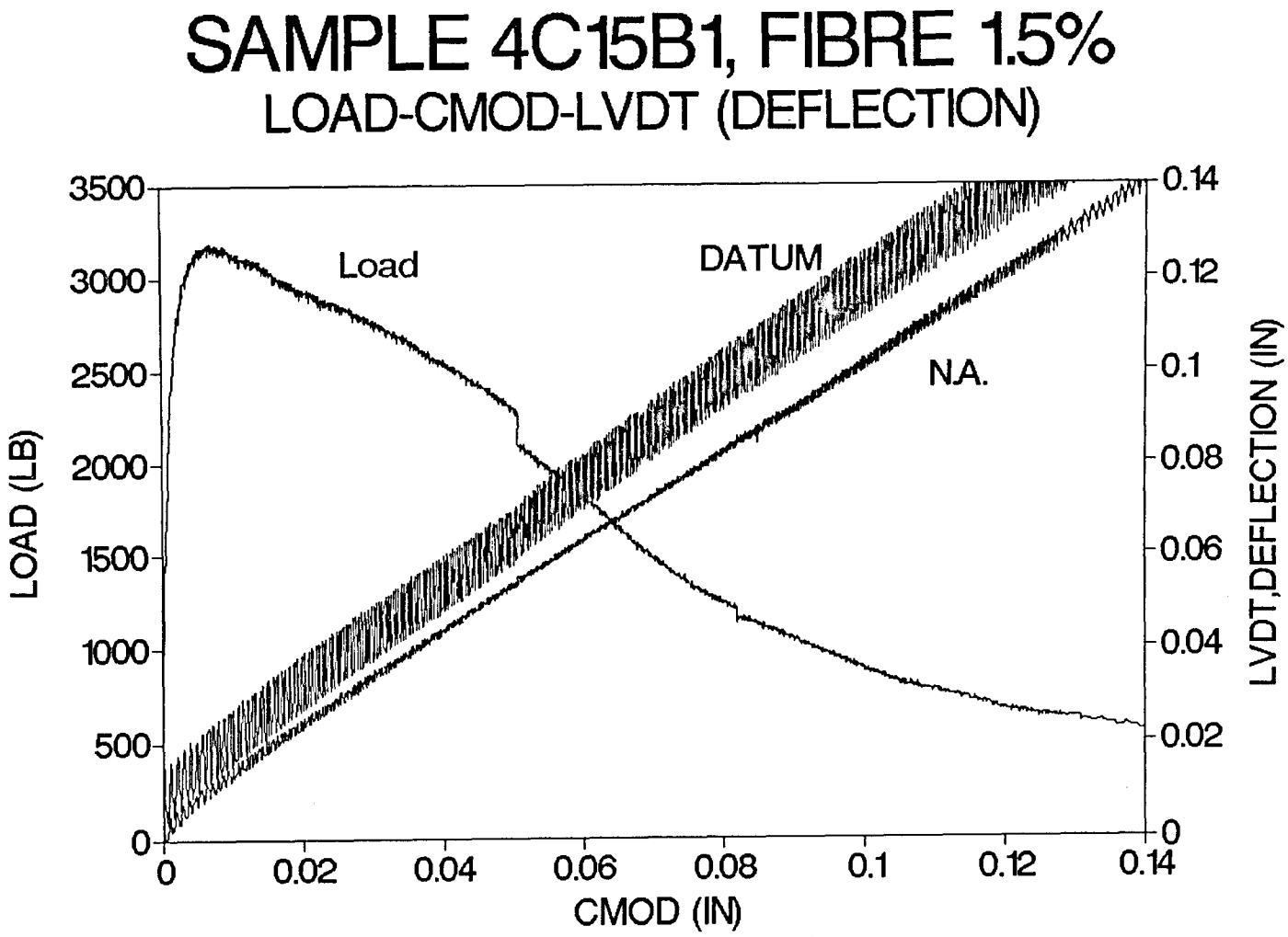

Figure A 2.4a Load-CMOD-Deflection Relationship

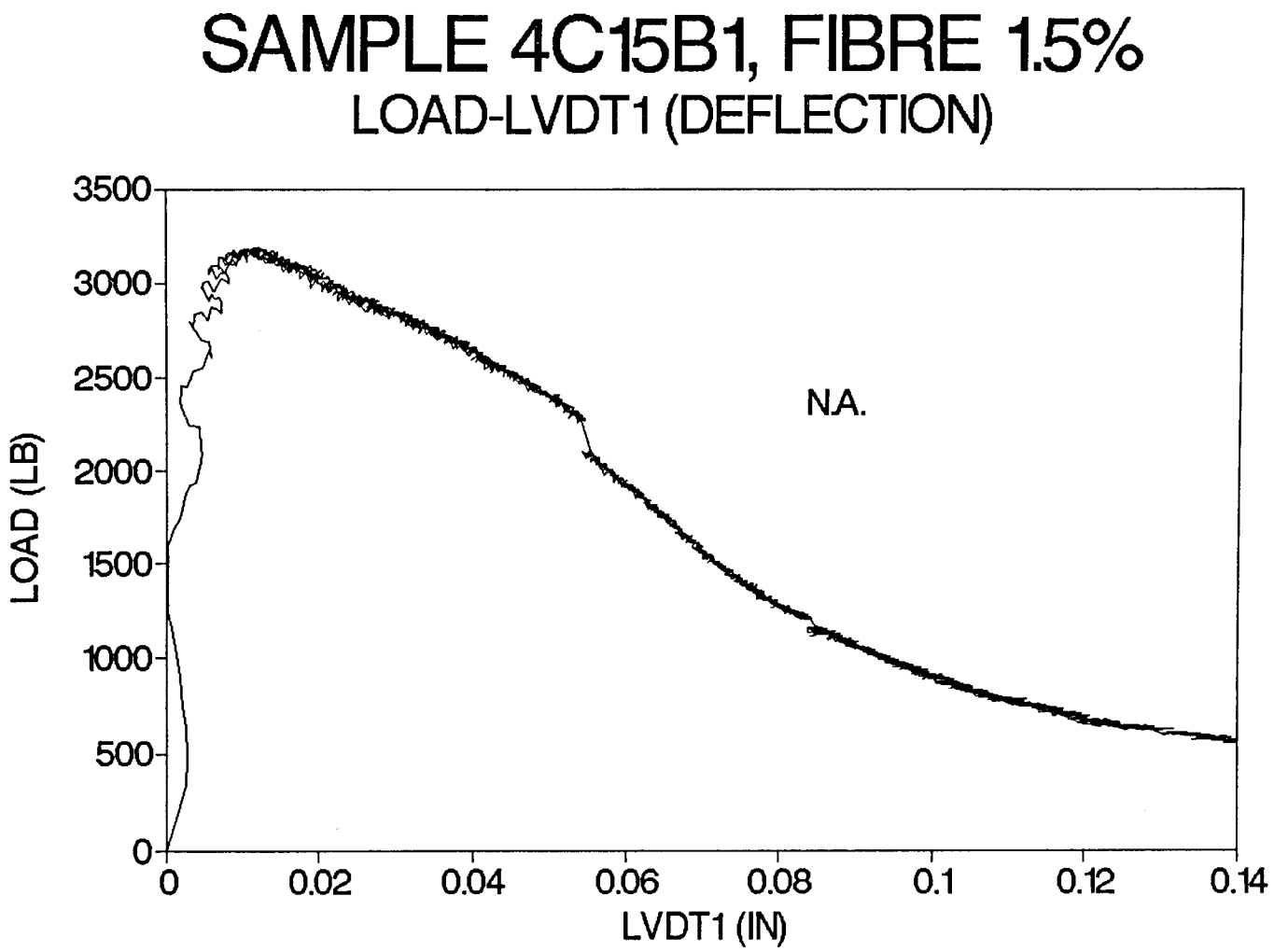

Figure A 2.4b Load-Deflection (N.A.) Relationship

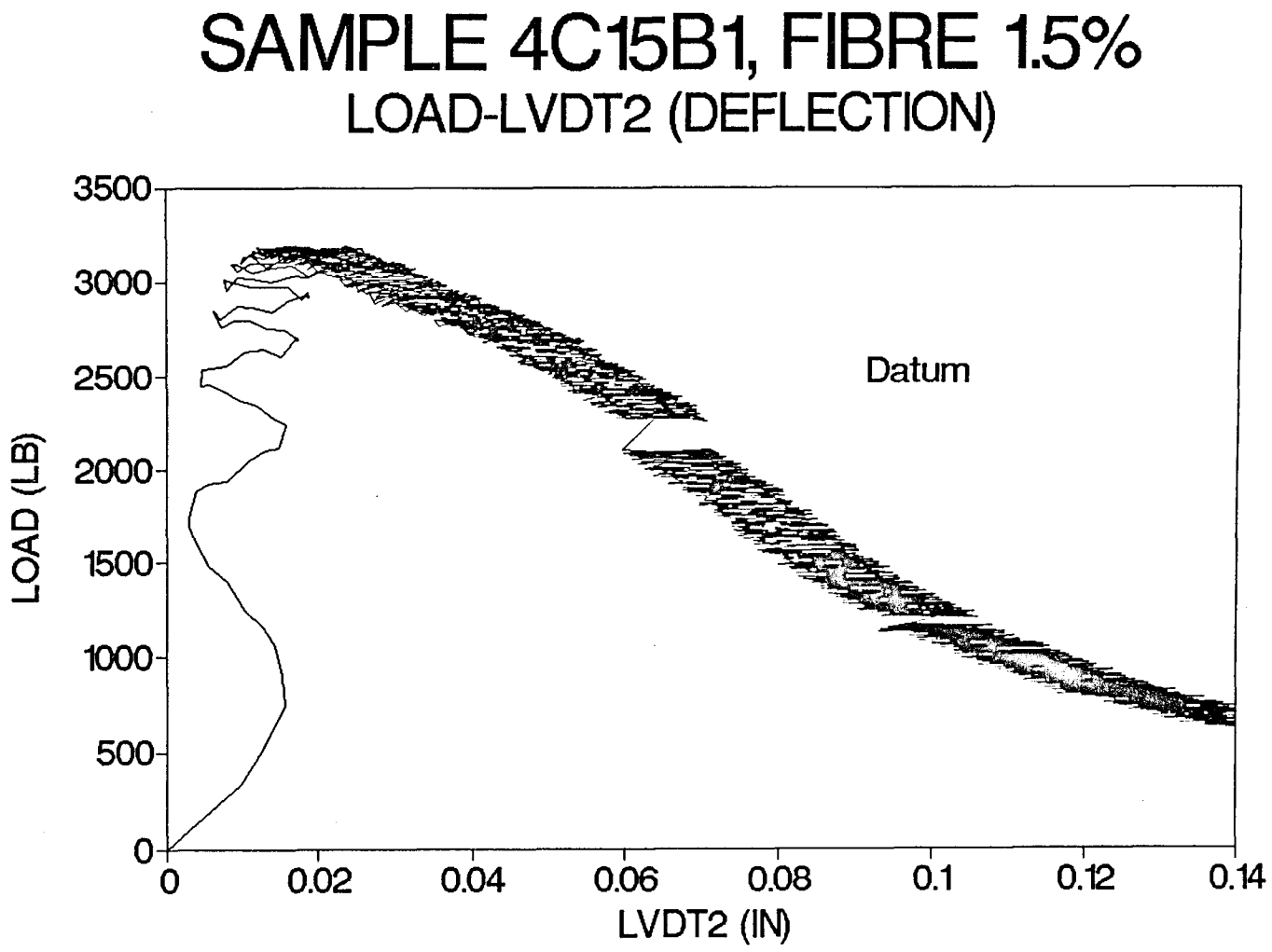

Figure A 2.4c Load-Deflection (Datum) Relationship

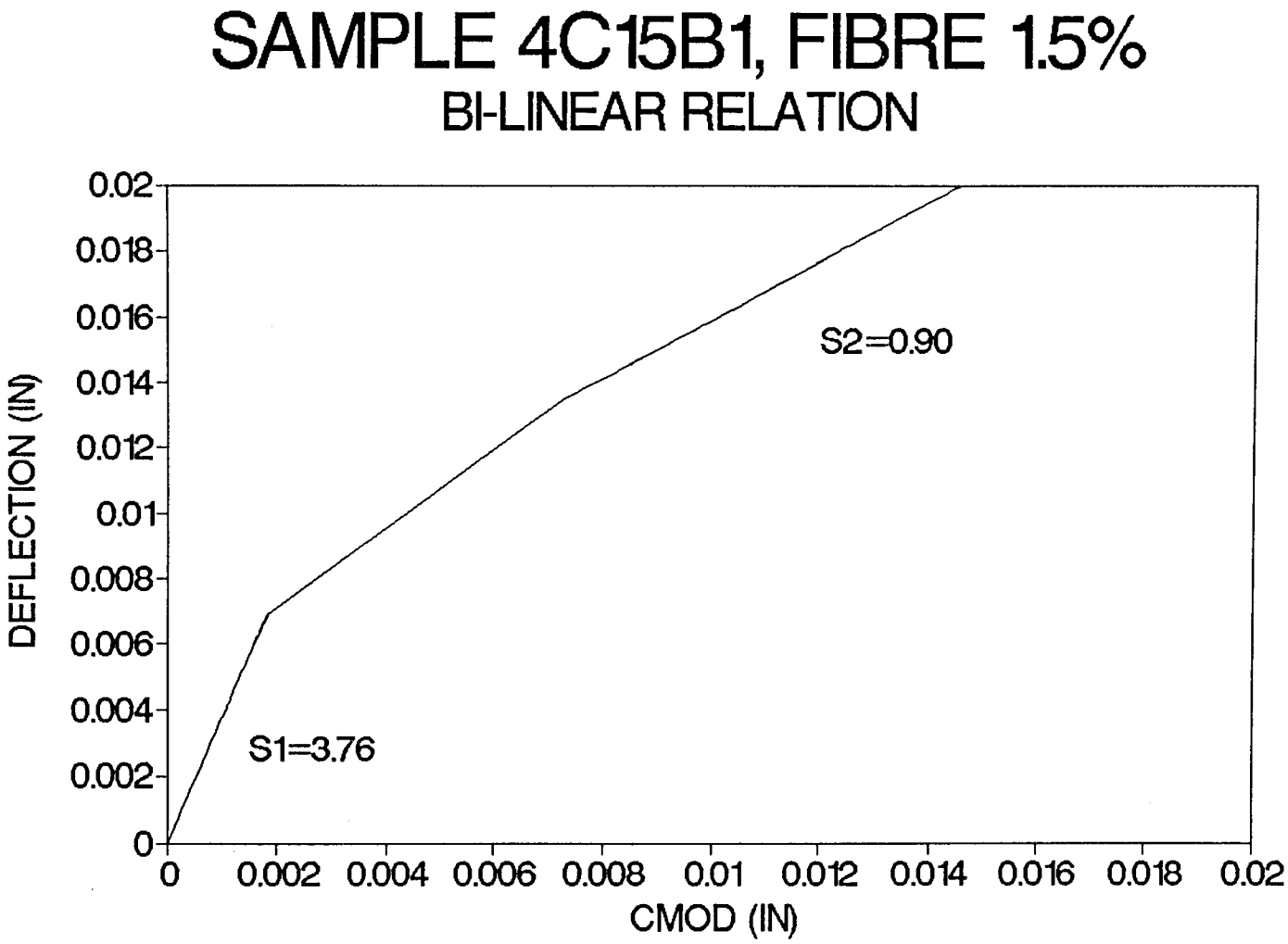

Figure A 2.4d Bilinear CMOD-Deflection Relationship

BEAM CODE	4D05B1	
CAST DATE	8-27-91	
TEST DATE	1-15-92	
LENGTH	27.4	inch
DEPTH	6.1	inch
WIDTH	3.0	inch
KNOTCH DEPTH	1.1	inch
SPAN LENGTH	24	inch
LEG SPAN	24.1	inch
FIBRE TYPE	DRAMIX	
length	1.0	inch
%	0.5	%
wt. (fibre)	3.4	lbs
MIX P CEMENT TYPEI	35.0	lbs
SAND PASSED #4 SIE	81.0	lbs
#3/8 inch AGGREGAT	81.0	lbs
WATER	16.1	lbs
MAXIMUM LOAD	1870.12	lbs
A	0.177273	
V1(A)	1.441132	
V2(A)	0.143266	
S/D	3.958442	
E	2963948	psi
S1	3.640037	
S2	1.17192	

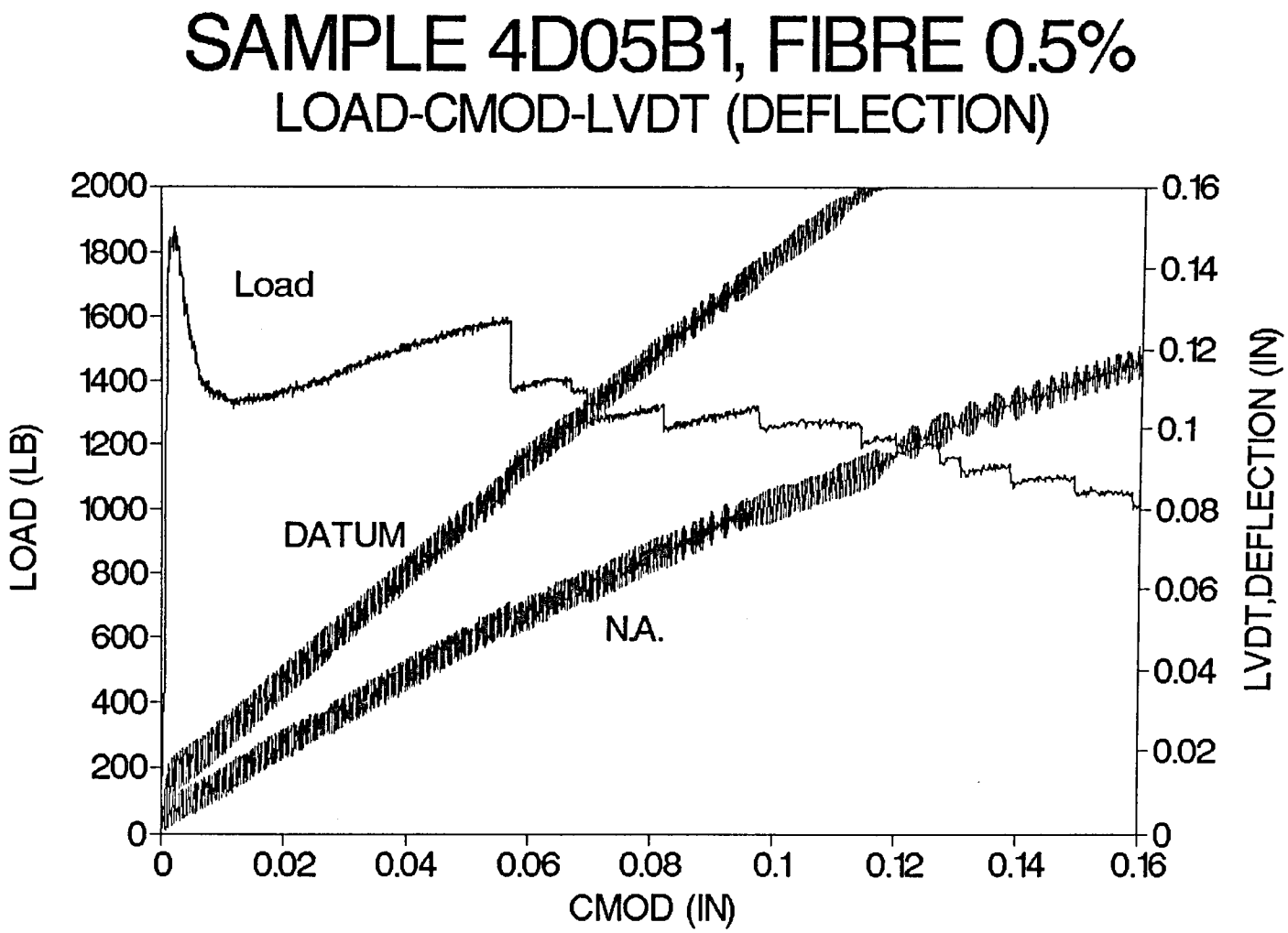

Figure A 2.5a Load-CMOD-Deflection Relationship

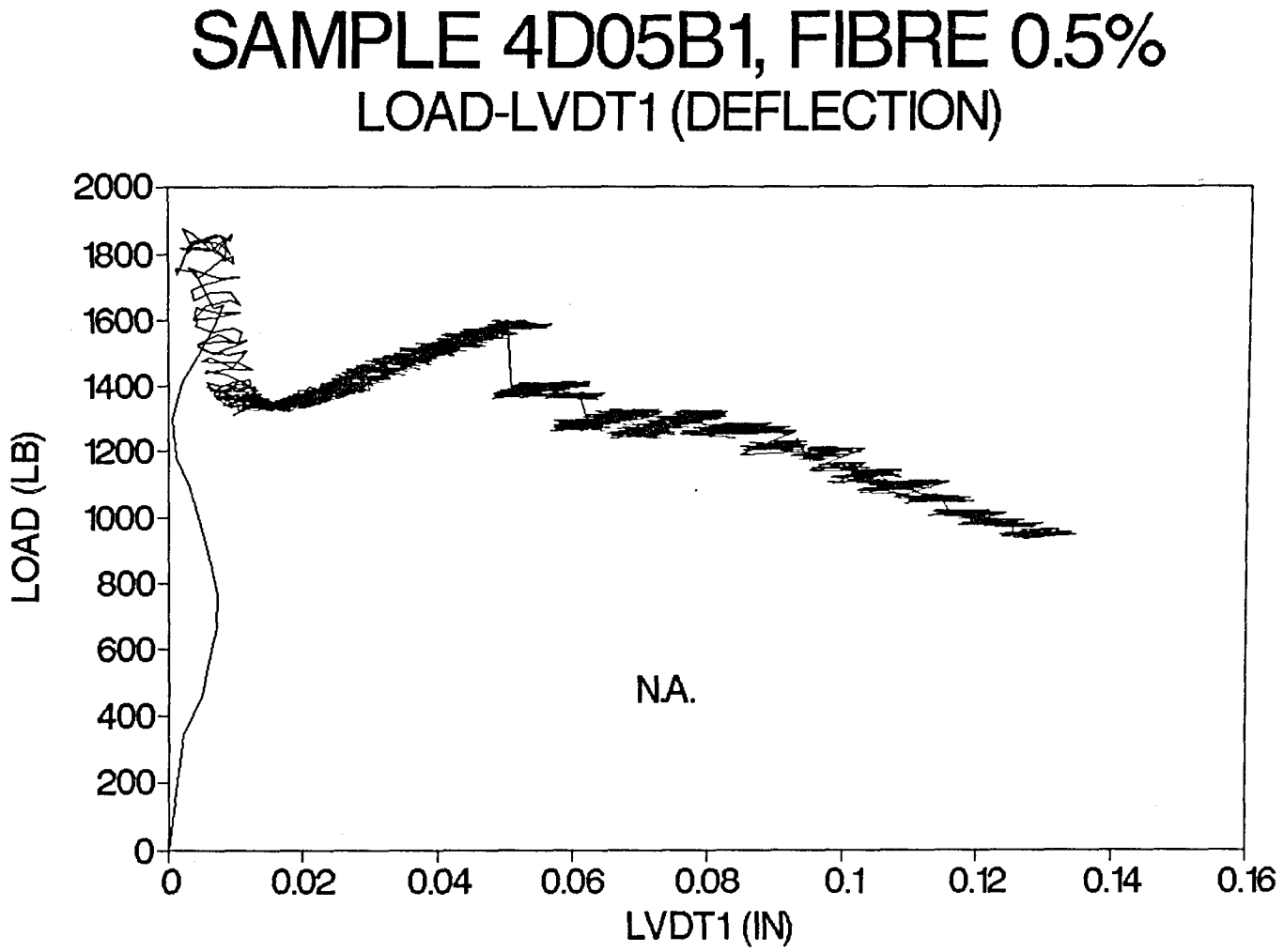

Figure A 2.5b Load-Deflection (N.A.) Relationship

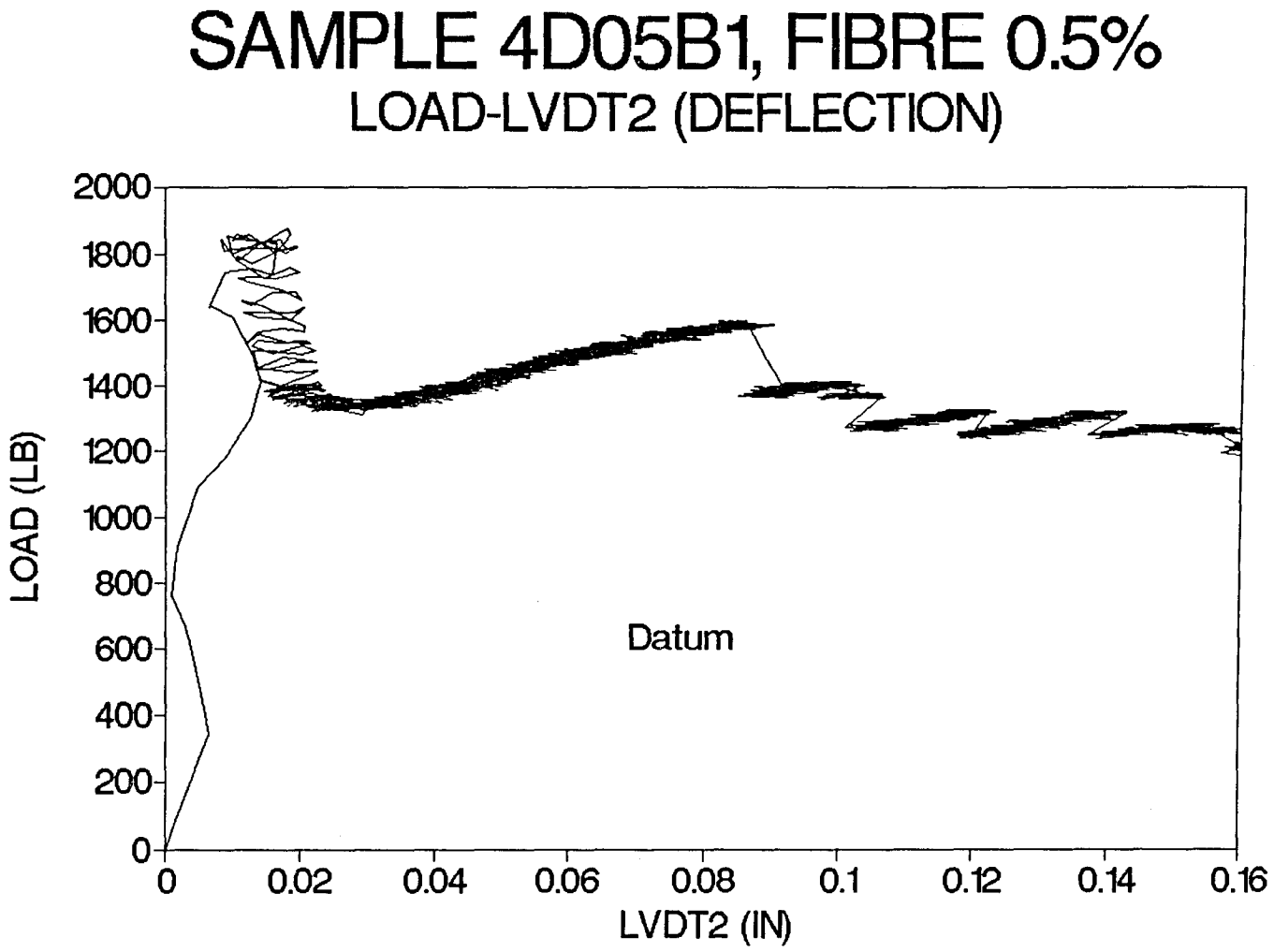

Figure A 2.5c Load-Deflection (Datum) Relationship

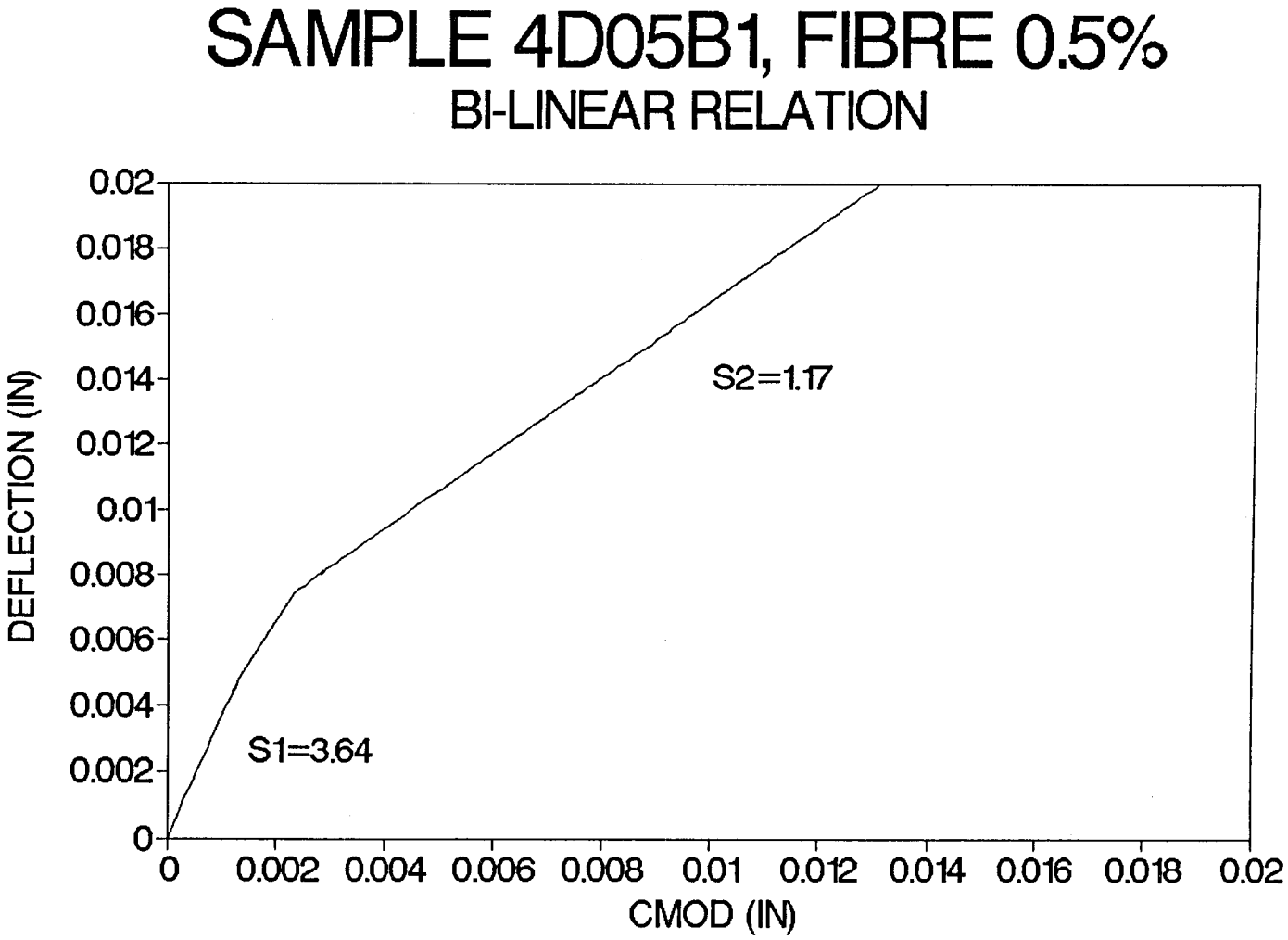

Figure A 2.5d Bilinear CMOD-Deflection Relationship

BEAM CODE		4D10B1
CAST DATE		8-30-91
TEST DATE		1-15-92
LENGTH		27.3 inch
DEPTH		6.1 inch
WIDTH		3.1 inch
KNOTCH DEPTH		1.1 inch
SPAN LENGTH		24 inch
LEG SPAN		24.0 inch
FIBRE TYPE		DRAMIX
length		1.0 inch
%		1.0 %
wt. (fibre)		6.9 lbs
MIX P	CEMENT TYPEI	34.7 lbs
	SAND PASSED #4 SIE	80.6 lbs
	#3/8 inch AGGREGAT	80.6 lbs
	WATER	16.0 lbs
MAXIMUM LOAD		2846.68 lbs
A		0.175974
V1(A)		1.439495
V2(A)		0.141296
S/D		3.958442
E		3044797 psi
S1		3.663293
S2		1.01568

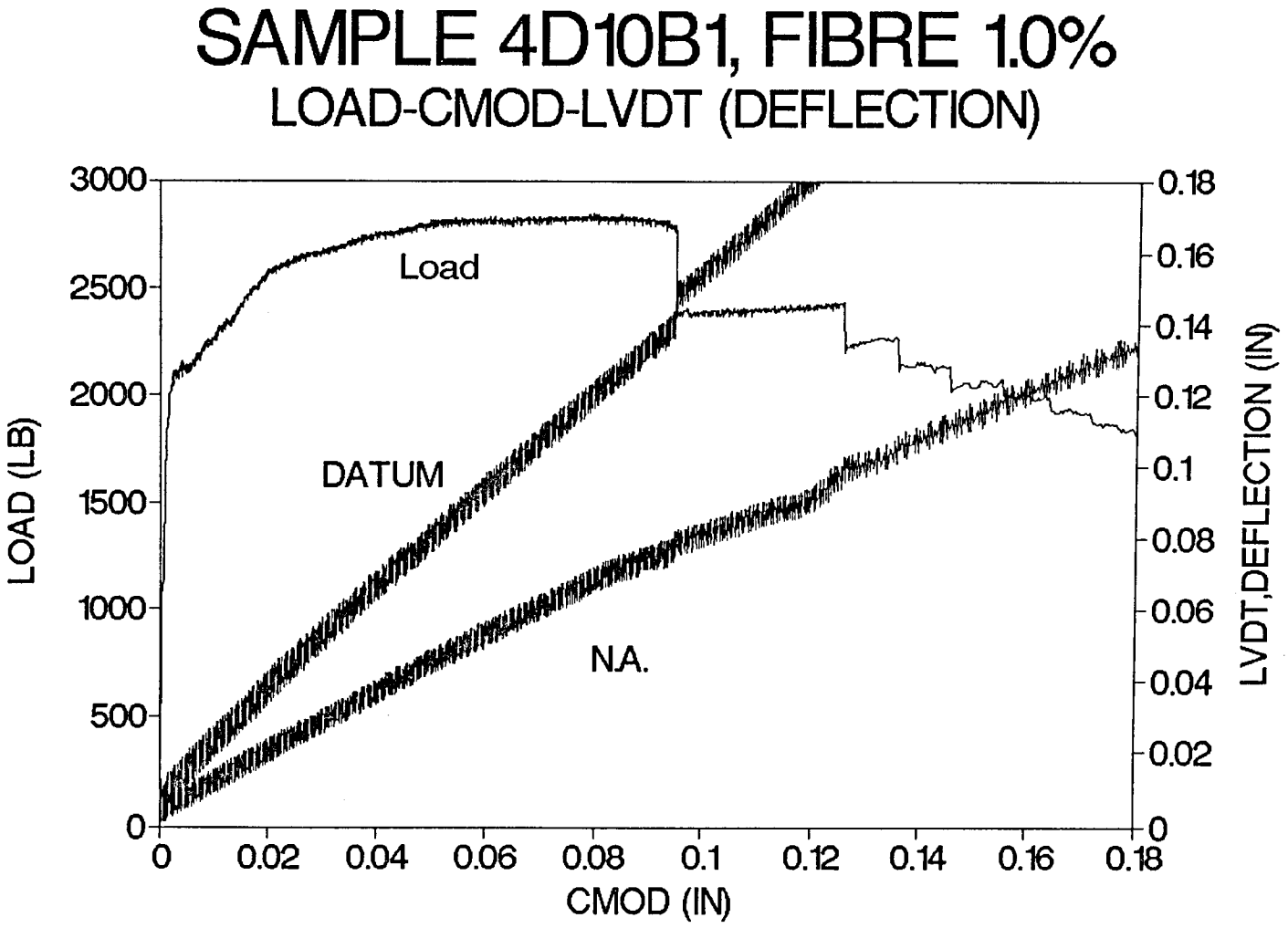

Figure A 2.6a Load-CMOD-Deflection Relationship

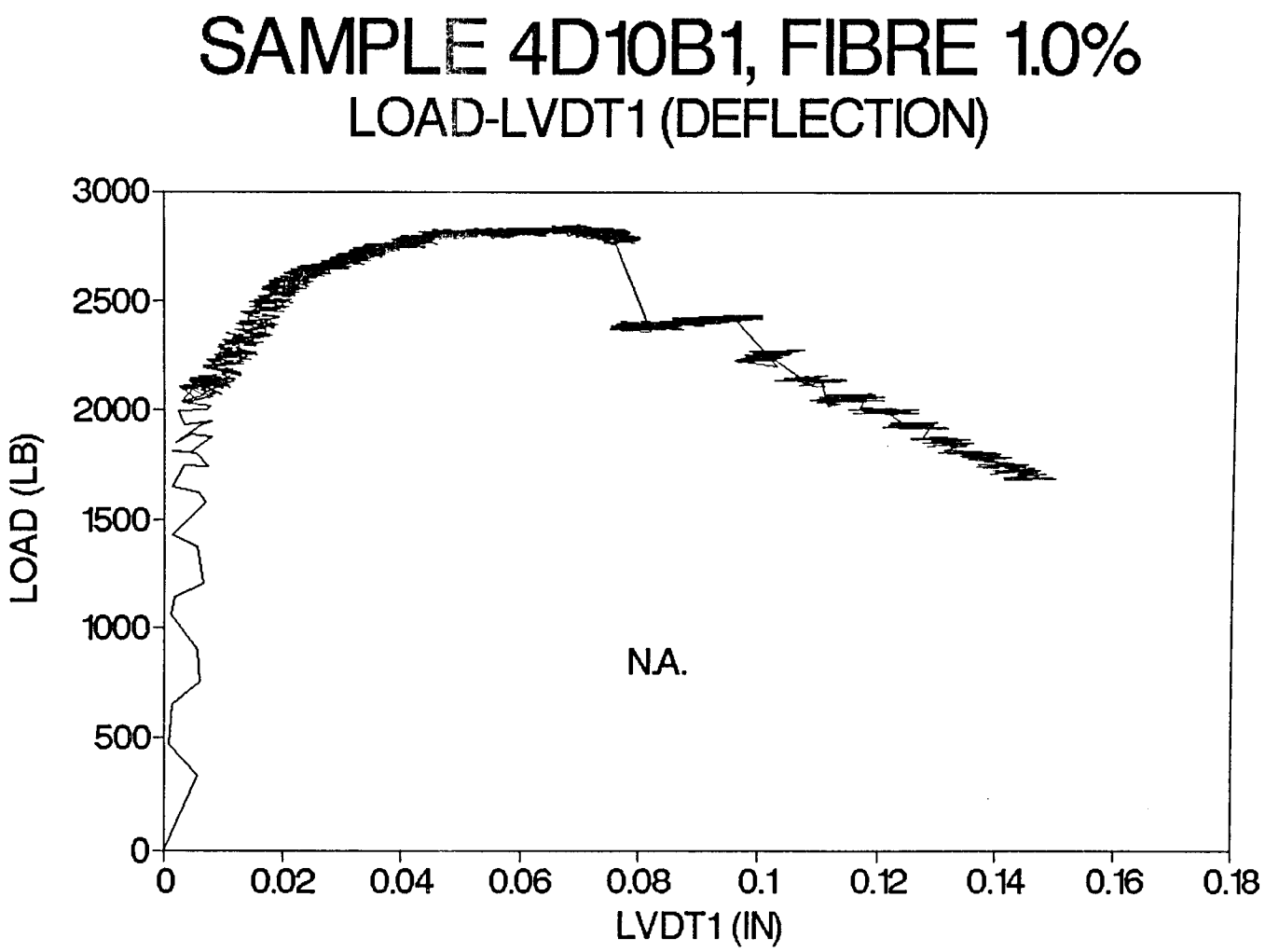

Figure A 2.6b Load-Deflection (N.A.) Relationship

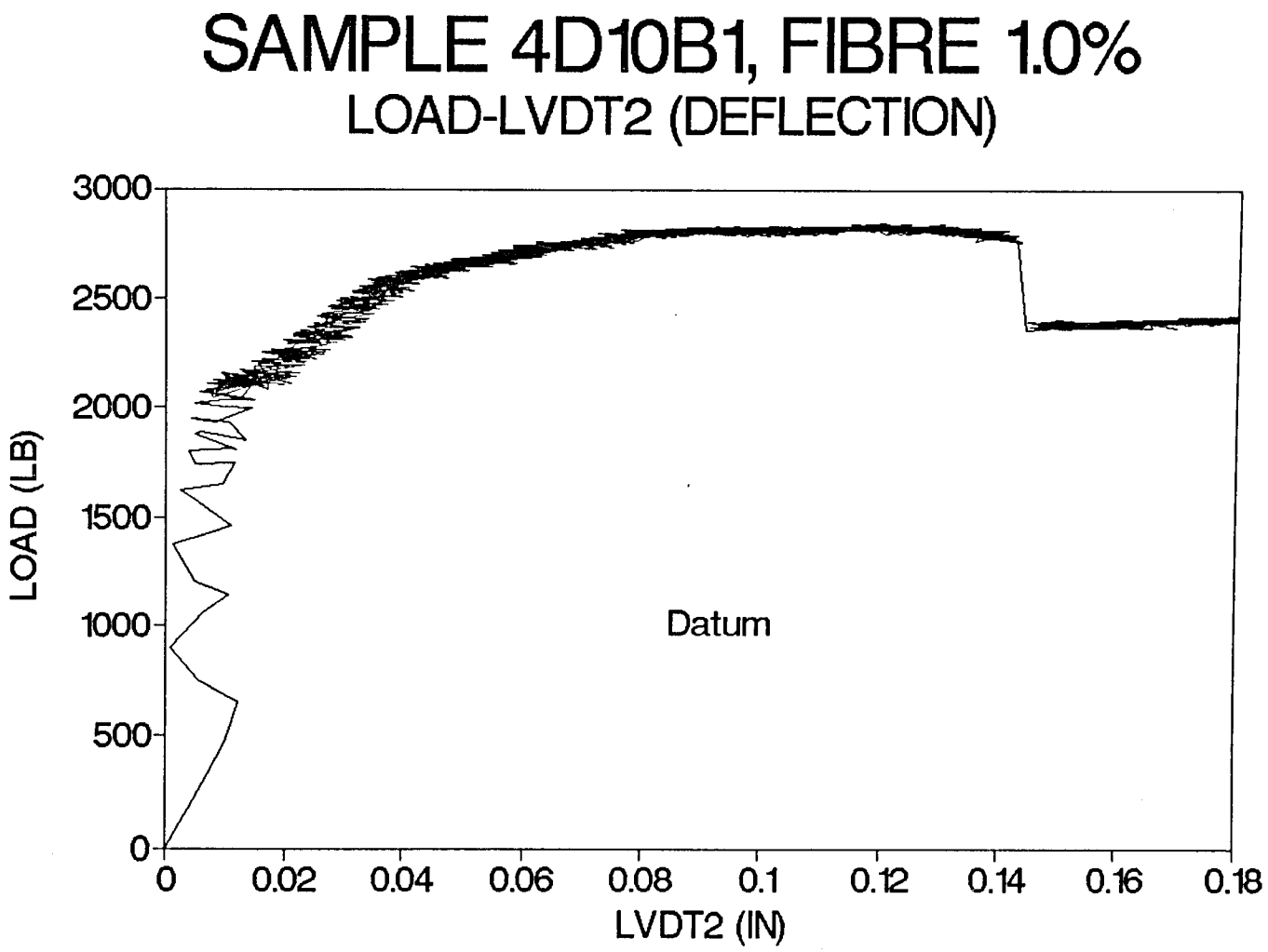

Figure A 2.6c Load-Deflection (Datum) Relationship

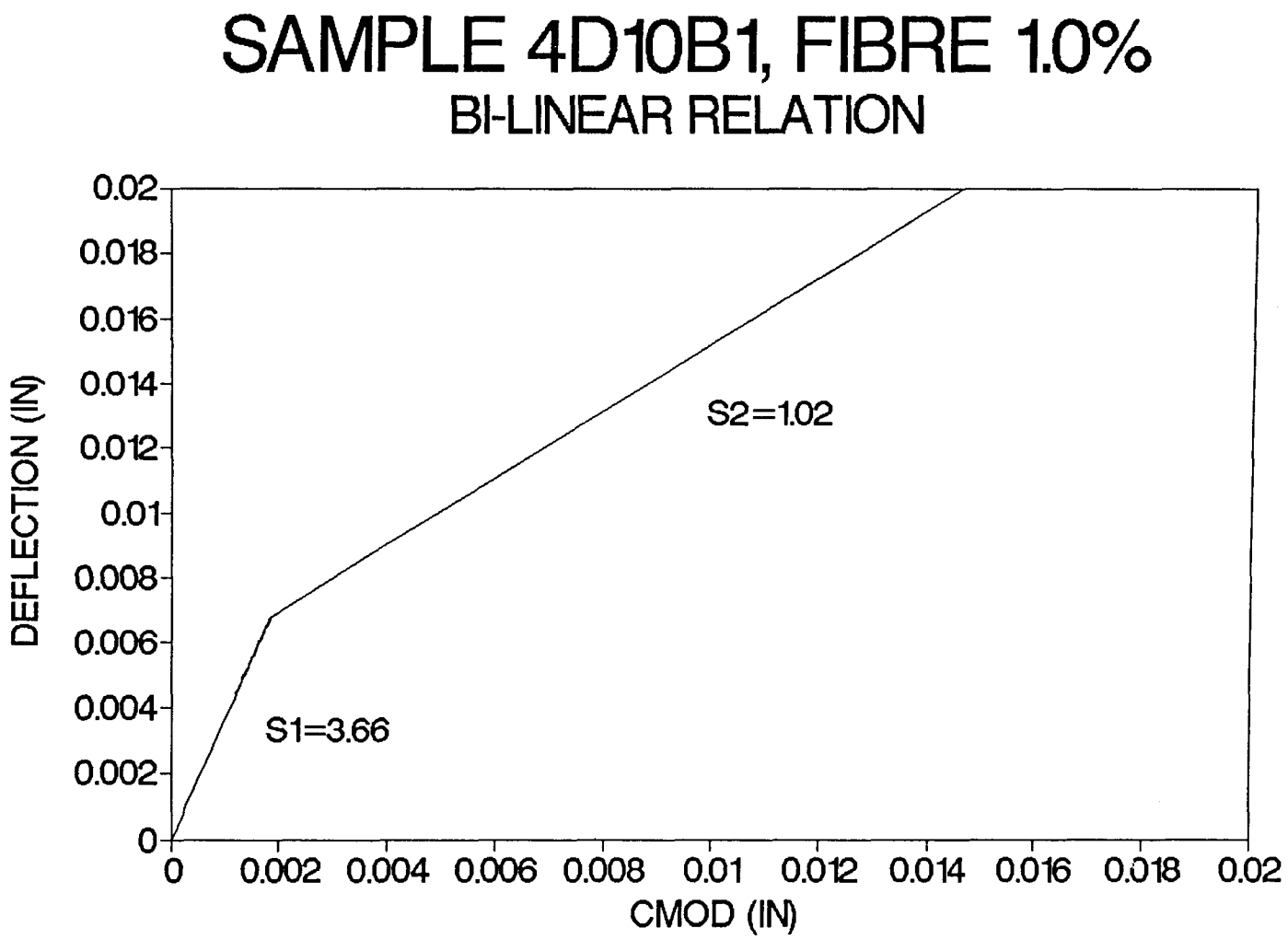

Figure A 2.6d Bilinear CMOD-Deflection Relationship

BEAM CODE	4D15B1	
CAST DATE	9-5-91	
TEST DATE	1-15-92	
LENGTH	27.1	inch
DEPTH	6.1	inch
WIDTH	3.0	inch
KNOTCH DEPTH	1.1	inch
SPAN LENGTH	24	inch
LEG SPAN	23.8	inch
FIBRE TYPE	DRAMIX	
length	1.0	inch
%	1.5	%
wt. (fibre)	10.3	lbs
MIX P CEMENT TYPEI	34.6	lbs
SAND PASSED #4 SIE	80.2	lbs
#3/8 inch AGGREGAT	80.2	lbs
WATER	15.9	lbs
MAXIMUM LOAD	3842.77	lbs
A	0.182051	
V1(A)	1.447364	
V2(A)	0.150633	
S/D	3.907692	
E	3210212	psi
S1	3.557188	
S2	0.919119	

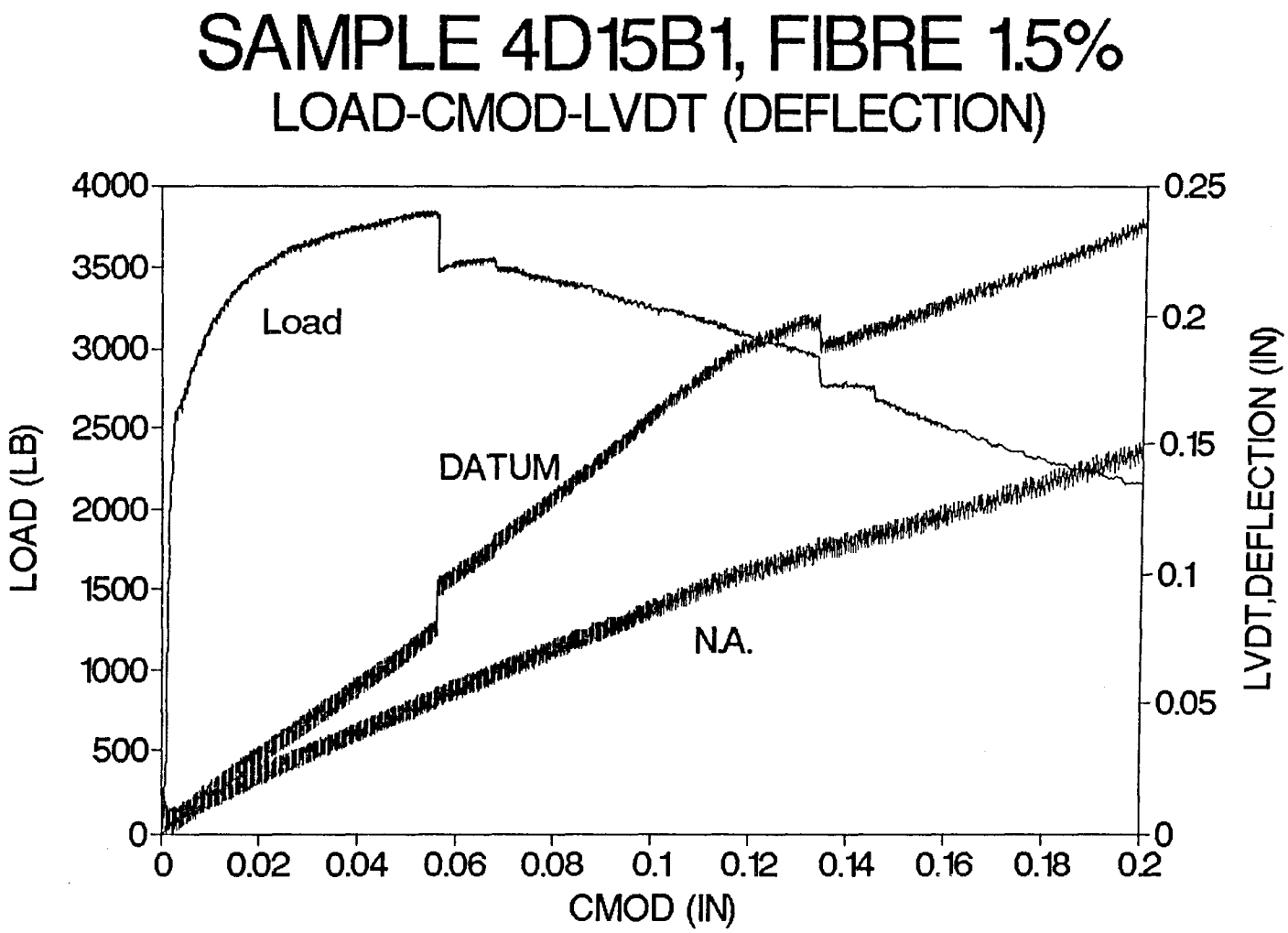

Figure A 2.7a Load-CMOD-Deflection Relationship

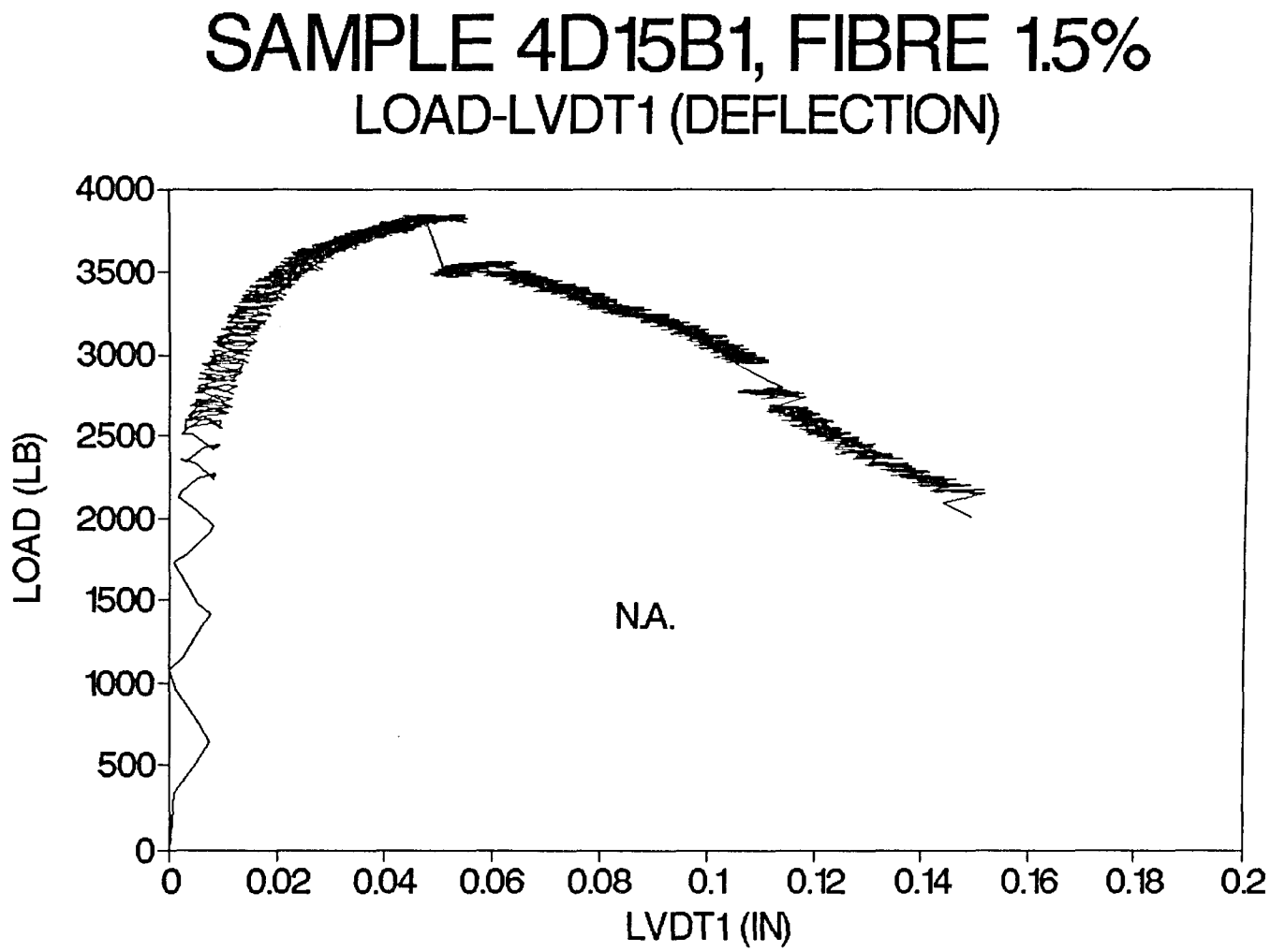

Figure A 2.7b Load-Deflection (N.A.) Relationship

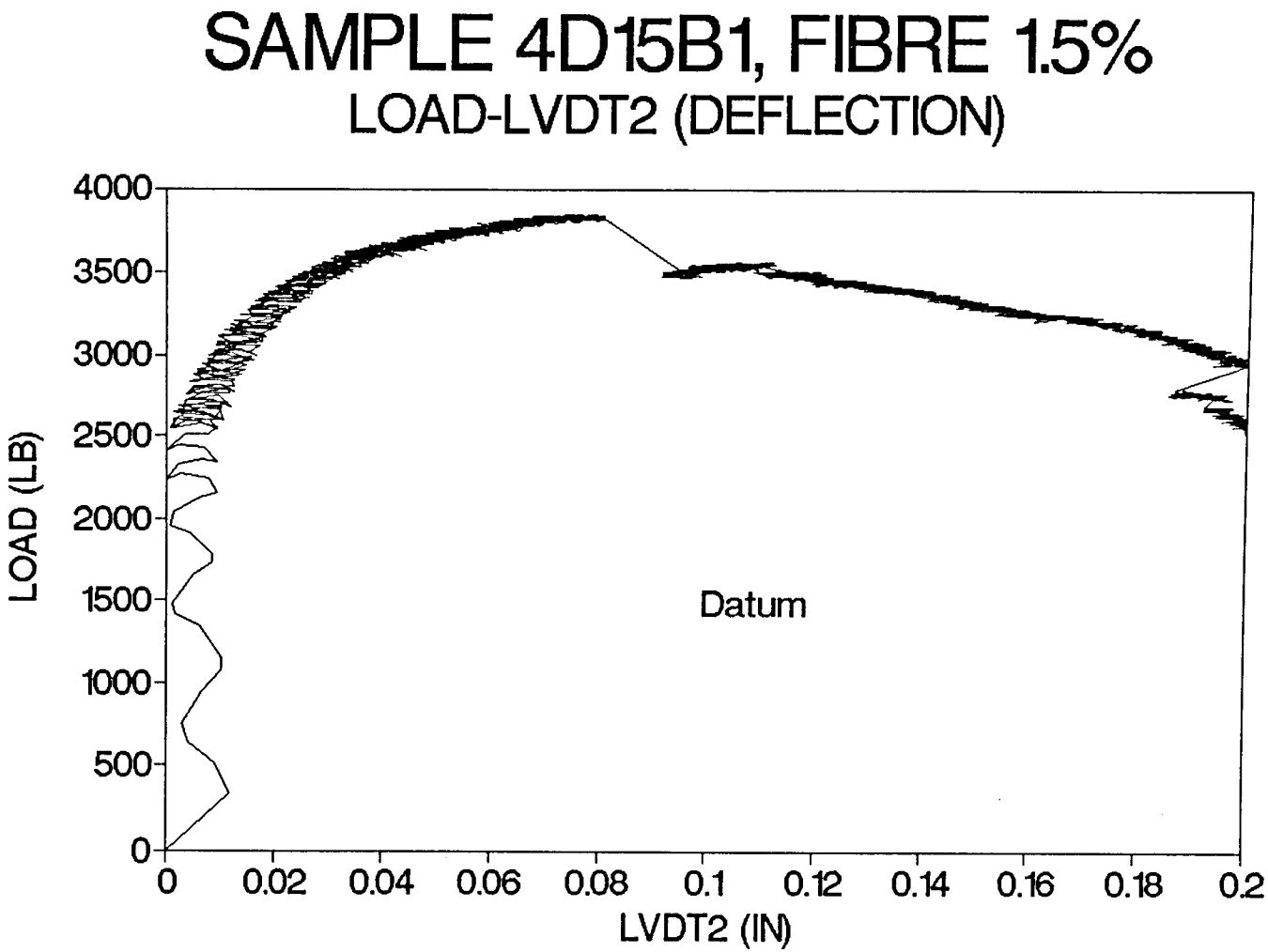

Figure A 2.7c Load-Deflection (Datum) Relationship

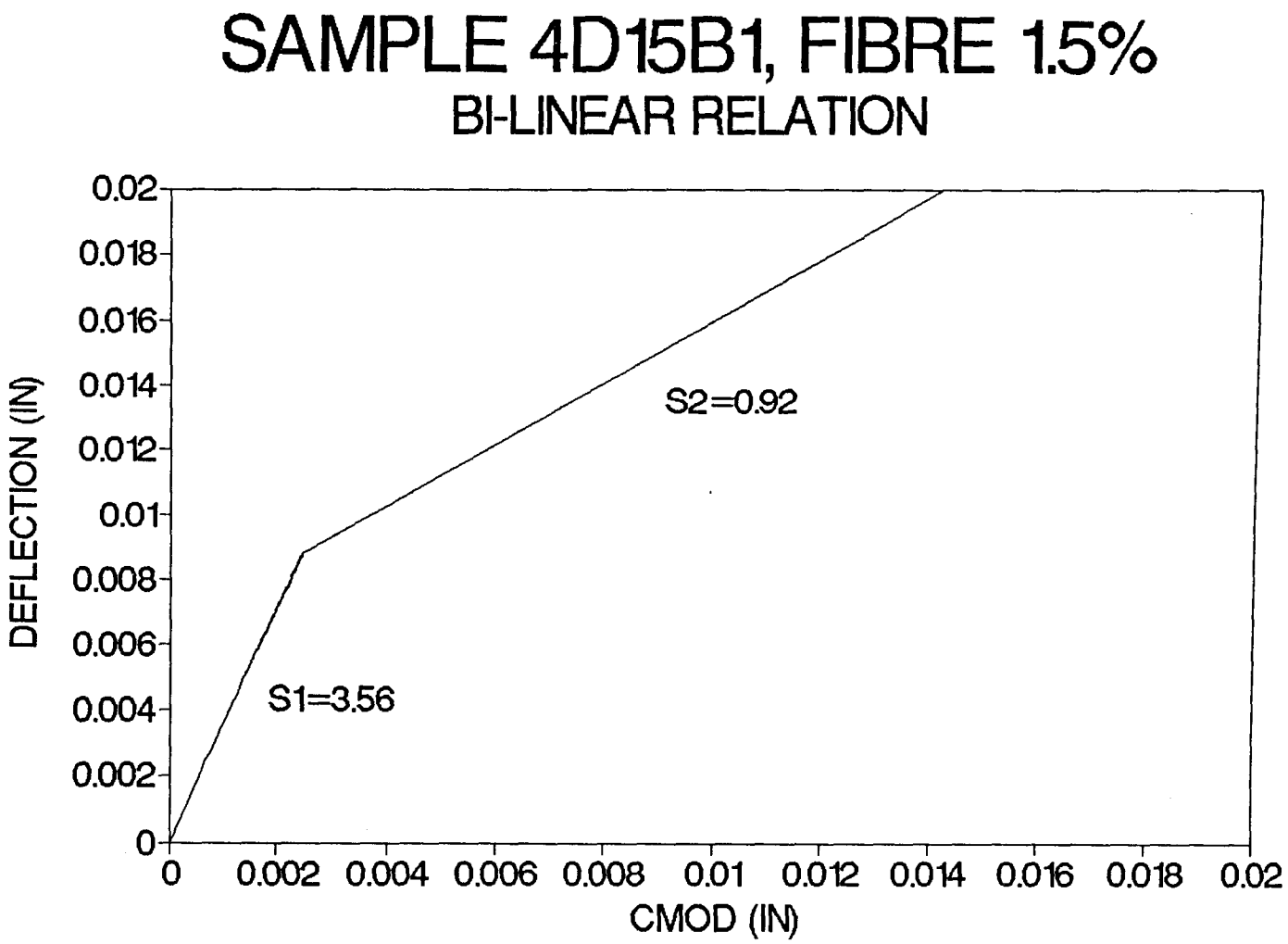

Figure A 2.7d Bilinear CMOD-Deflection Relationship

BEAM CODE		4D10B2
CAST DATE		8-31-91
TEST DATE		1-15-92
LENGTH		27.0 inch
DEPTH		6.1 inch
WIDTH		3.1 inch
KNOTCH DEPTH		1.1 inch
SPAN LENGTH		24 inch
LEG SPAN		24.01575 inch
FIBRE TYPE		DRAMIX
length		2.0 inch
%		1.0 %
wt. (fibre)		6.9 lbs
MIX P	CEMENT TYPEI	34.7 lbs
	SAND PASSED #4 SIE	80.6 lbs
	#3/8 inch AGGREGAT	80.6 lbs
	WATER	16.0 lbs
MAXIMUM LOAD		4345.7 lbs
A		0.183974
V1(A)		1.449965
V2(A)		0.15365
S/D		3.907692
E		3031313 psi
S1		3.525002
S2		0.538845

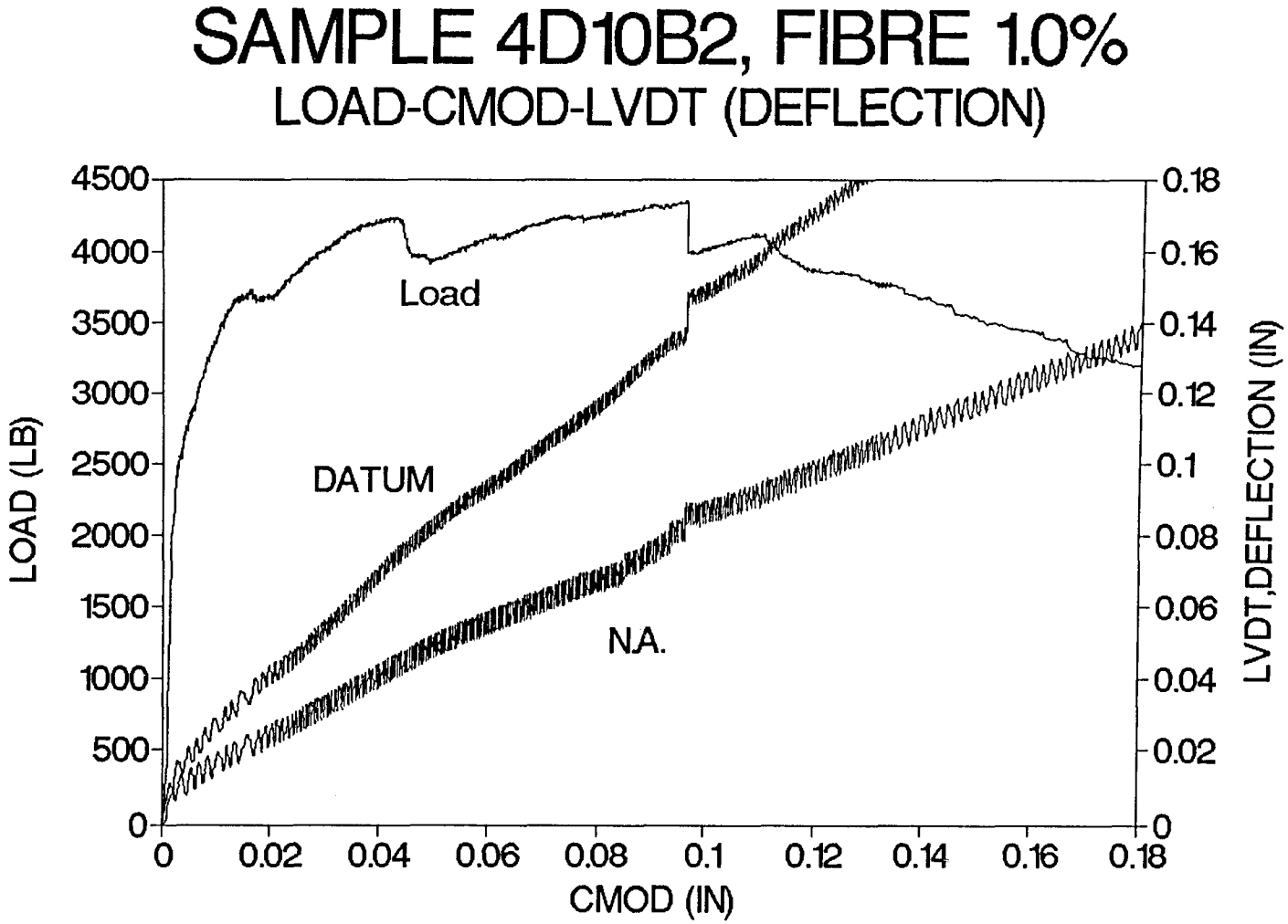

Figure A 2.8a Load-CMOD-Deflection Relationship

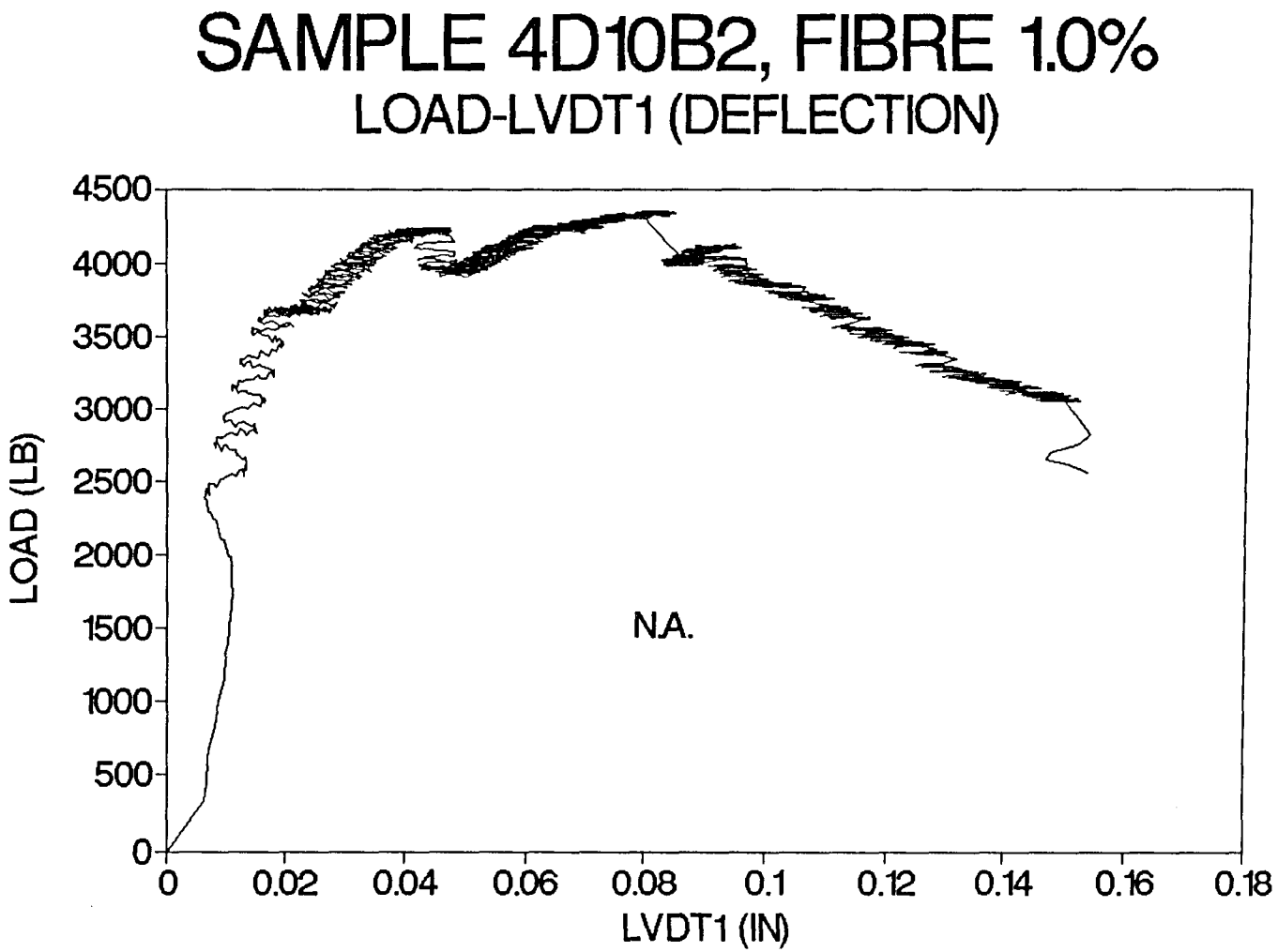

Figure A 2.8b Load-Deflection (N.A.) Relationship

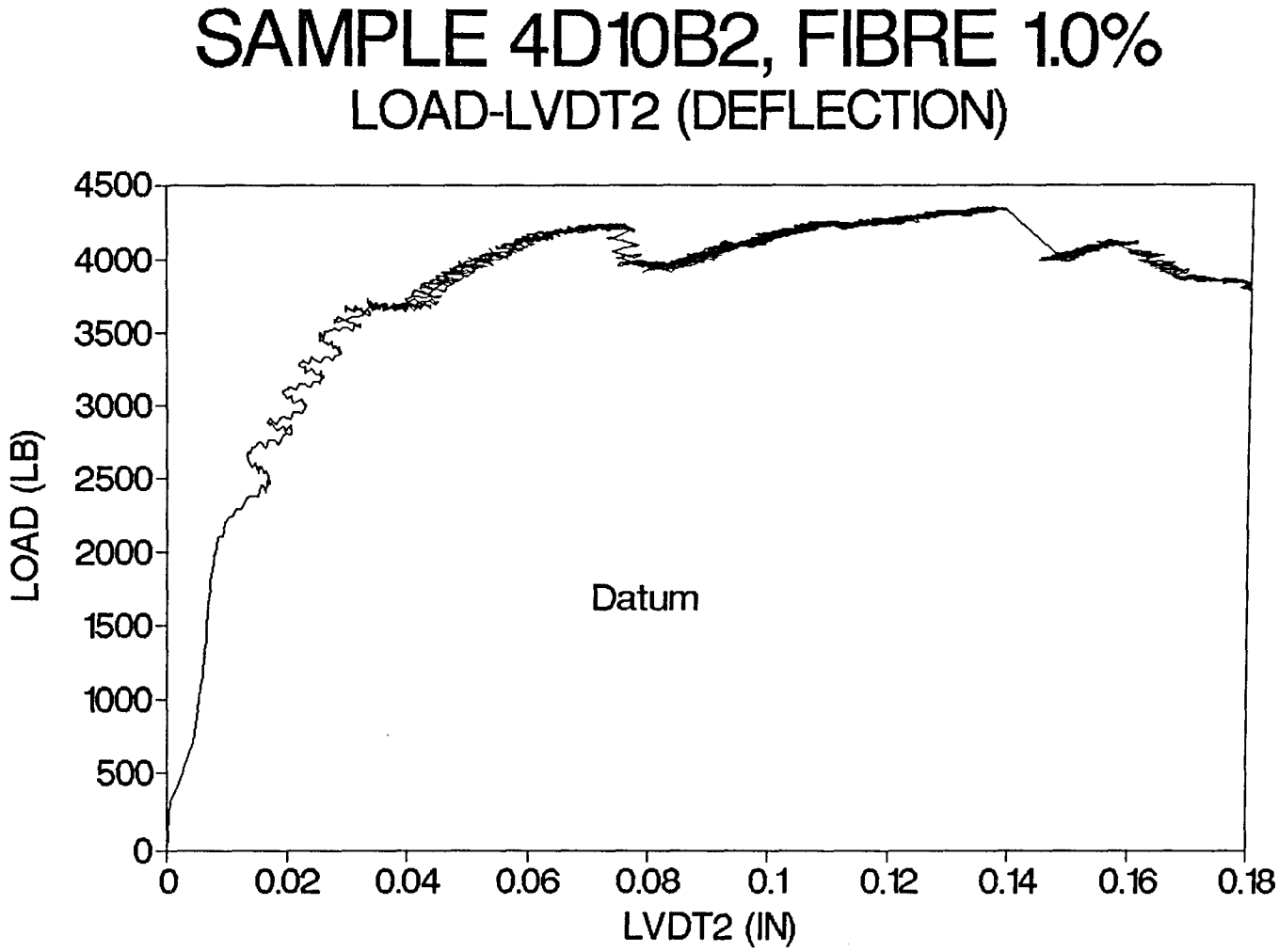

Figure A 2.8c Load-Deflection (Datum) Relationship

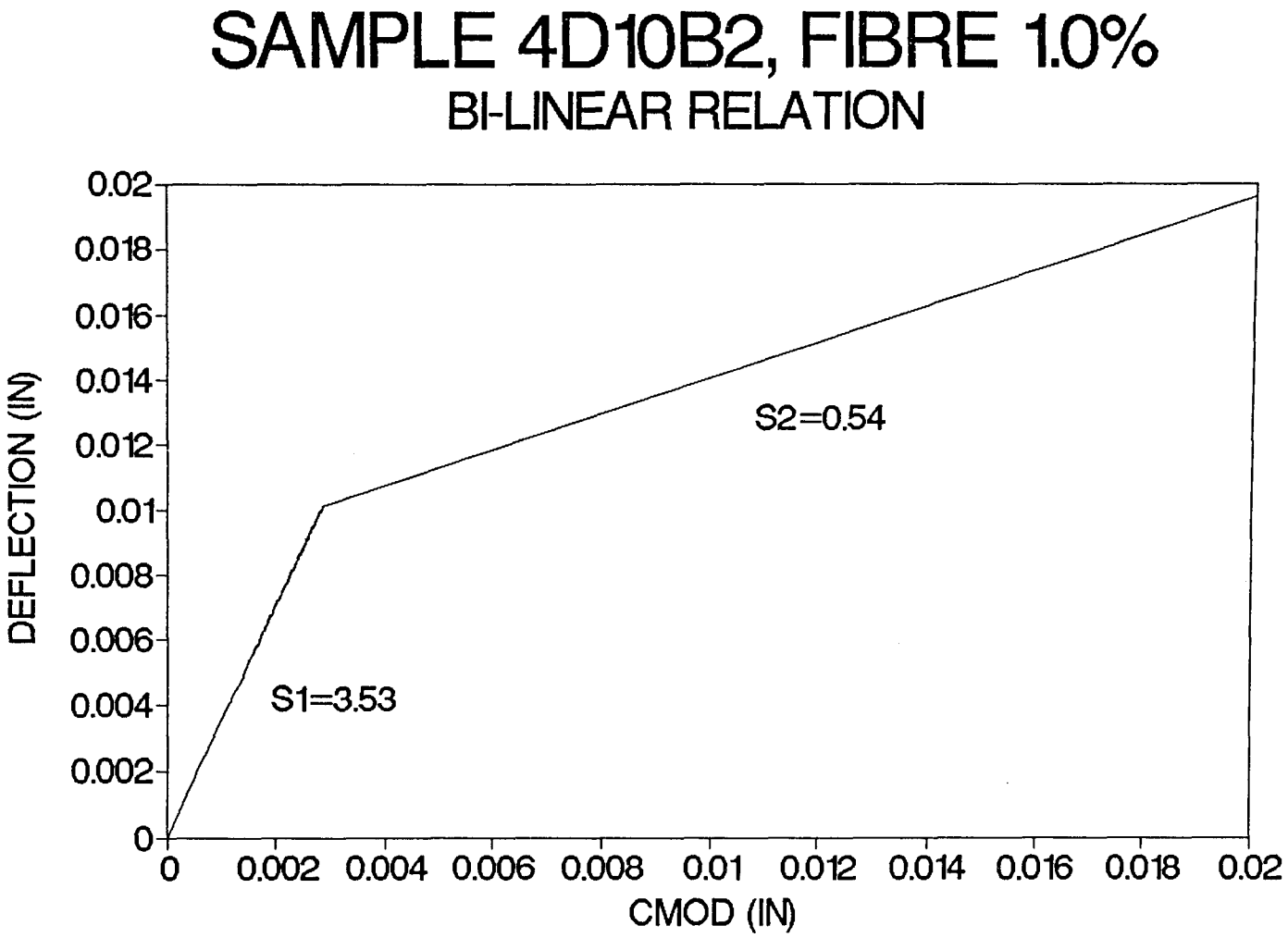

Figure A 2.8d Bilinear CMOD-Deflection Relationship

REFERENCES

1. RILEM Draft Recommendation, "Determination of the Energy of Mortar and Concrete by Means of Three-Point Bend Tests on Notched Beams", Materials and Structures, Vol. 18, No. 106, 1985, pp.285-296.

2. Tindukasiri, Sira and Wecharatana, Methi. "Fracture of Cementitious Composites." Presented in Bangkok, Thailand, November, 1992, at the *Annual Meeting of the Engineering Institute of Thailand ' 1992,* Bangkok, Thailand: pp.1235-1252.

3. Suk Ki Kim, "The Constant Fracture Angle Model for Cementitious Materials." Dissertation for the Degree of Doctor of Philosophy. New Jersey Institute of Technology. 1991.

4. Vellore S.Gopalaratnam, Surendra P. Shah, Gorkon B. Batson, Marvin E. Criswell, V. Ramakrishnan, and Methi Wecharatana, "Fracture Toughness of Fiber Reinforced Concrete", ACI Materials Journal, Vol. 88, No. 4, July-August 1991, pp.339-353.

5. Sawarng Ratanalert and Methi Wecharatana, "Evaluation of Existing Fracture Models", in Proceedings of ACI SP-118 "Fracture Mechanics : Application to concrete", 1989, pp. 113-146.

6. Zdenek P. Bazant and B. H. Oh, "Crack Band Theory for Fracture of Concrete", Material and Construction, Vol. 16, No. 93, 1983, pp. 155-177.

7. Yeoushang Jenq, Surendra P. Shah, "Two Parameter Fracture Model for Concrete", Journal of Engineering Mechanics, Vol. 111, No. 10, October, 1985, pp. 1227-1241.